Cement and Concrete Research 40 (2010) 643–675

Contents lists available at ScienceDirect

Cement and Concrete Research

journal homepage: http://ees.elsevier.com/CEMCON/default.asp

The so-called alkali-carbonate reaction (ACR) — Its mineralogical and geochemical details, with special reference to ASR

Tetsuya Katayama

Kawasaki Geological Engineering Co. Ltd., 2-11-15 Mita, Minato-ku, Tokyo, 108-8338, Japan

ARTICLE INFO

Article history:
Received 15 January 2009
Accepted 24 September 2009

Keywords:
Alkali-carbonate reaction (ACR) (C)
ASR gel (B)
Cryptocrystalline quartz (D)
Dedolomitization (C)
SEM-EDS (B)

ABSTRACT

Typical examples of so-called alkali-carbonate reaction (ACR) in the Canadian field concretes in Ontario, CSA concrete prism, RILEM concrete microbars and RILEM mortar bar containing Pittsburg aggregate, were examined petrographically based on polarizing microscopy, SEM observation and quantitative SEM-EDS analysis of the reaction products. It was revealed that ASR gel was the main product responsible for the crack formation in concretes, and that this gel had a common nature to that in the typical ASR. That is, ASR gel presented distinctive compositional trend lines, passing from low-Ca ASR gel at [Ca/Si] = 1/2–1/6, [Ca]/[Na + K] = 1.0 to the "convergent point" with [Ca/Si] = 1.3–1.8, [Ca]/[Na + K] = 100 at which chemical equilibrium is attained with CSH gel. The so-called ACR is a combination of deleteriously expansive alkali-silica reaction (ASR) of cryptocrystalline quartz, and harmless dedolomitization which produces brucite and carbonate halo. In laboratory specimens, fine dolomitic aggregate undergoes dedolomitization, and brucite and ASR gel react to form non-expansive Mg-silicate gel on the dolomite crystals. This explains why the mortar bar produces smaller expansion than the concrete microbar, and why the reaction products are so minute that they escape attention by optical microscopy. As a crystalline counterpart, mountainite is a candidate for low-Ca ASR gel, while sepiolite is one for Mg-silicate gel. Concealed ASR was detected in ACR-affected field concretes undergoing ingress of deicing salt which formed Friedel's salt and Cl-doped CSH gel. Compositions of ASR products, methods of sample preparation and analysis for correct identification of ACR, and artifacts were critically reviewed.

1. Introduction

The mechanisms of so-called alkali-carbonate reaction (ACR) have been controversial. In the early 1990s, Katayama posited that ACR is a combined reaction of deleteriously expansive ASR of cryptocrystalline quartz, and harmless dedolomitization of dolomitic aggregate [1], based on critical review of the published references on ACR, and subsequently extracted this quartz from ACR reactive Pittsburg aggregate by phosphoric acid treatment [2]. Recently, this theory was confirmed by means of polarizing microscopy, SEM observation and quantitative SEM-EDS analysis using the same polished thin sections of concretes [3–5]. The investigations revealed the key importance on the expansiveness of mortar and concrete of Mg-silicate gel formed by the interaction of ASR and dedolomitization products. However, in view of the fact that field instances of ACR have become rare even in Canada, it was decided to gather and present as much analytical data about reaction products as possible to provide the background to understand the nature of the reaction. This paper will focus on the chemical compositions of the reaction products in the ACR, as analyzed by the quantitative SEM-EDS of the materials.

2. Materials used

2.1. Sample origin

Three Austrian carbonate aggregates [5] and Canadian Pittsburg aggregate (bulk, 1st lift, MTO stockpile [6]), examined with RILEM AAR-5 concrete microbars (aggregate 4–8 mm) and AAR-2 mortar bars (aggregate 0–4 mm) at VÖZFI [7], were used here. Another batch of the Pittsburg aggregate (most reactive layer Pit-16, 1st lift, CANMET stockpile) [8], tested with AAR-5 concrete microbars in prolonged storage (NaOH or KOH added to cement: $Na_2Oeq = 1.5$ wt.%, 80 °C, 1 M NaOH, 28 days) at KGE, was also used. Of the field-deteriorated concretes that had undergone typical alkali-carbonate reaction (ACR) in the past, an old ballast wall concrete with the Pittsburg aggregate (1st lift) came from a bridge in Gananoque (MTO collection, built 1957), and from a concrete curb in Cornwall (placed 1979), both in Ontario, Canada [3,4]. These field concretes were from within 5 cm of the surface. An old CSA concrete prism prepared by MTO (38 °C, two years, 1992) was also examined for comparison. The coarse aggregates (nos.9, 10, 12 and 15) crushed for the concrete microbar and mortar bar, were suffixed C and F (originally l in [3]), respectively, in this paper. Reference specimens of opal-A_N (hyalite: Valeč, Bohemia, Czech) and opal-CT (Virgin Valley, Nevada, USA) were used for phosphoric acid treatment.

E-mail address: katayamat@kge.co.jp.

0008-8846/$ – see front matter © 2009 Elsevier Ltd. All rights reserved.
doi:10.1016/j.cemconres.2009.09.020

2.2. Terminology and notation

The number of figures in this paper is arranged according to the sample categories, not in the order of explanation. The term "gel" formally refers to amorphous, non-crystalline material, but "CSH gel" will apply to optically isotropic calcium silicate hydrates of alite and belite, which may include poorly crystalline materials. The term "CSH paste" is avoided because of the confusing resemblance with "cement paste" which contains additional non-silicate hydrates. The origin of the gel as alite or belite has been individually identified by microscopy, and not as an unspecified paste-like mixture of these. For descriptive convenience, the term "ASR gel" will be used to denote gel-like silicates formed by ASR, irrespective of the Ca/Si ratio, actually ranging from optically isotropic to often intermixed crystalline "rosettes", unless particularly mentioned. A well adjusted quantitative EDS, used for polished thin section in this study, will be noted as SEM-EDS, not an EPMA (EDS). To facilitate easy comparisons of the oxide ratio of reaction products, oxide notation is adopted rather than structural composition formulae. In XRD analysis, the conventional unit Å is kept for *d*-spacing of the materials, while nA will be used for electron beam current in SEM-EDS analysis. The name "Pittsburg" quarry in Kingston, Ontario, Canada will be used following the conventional usage by the producer, though the township is actually Pittsburgh. "Pittsburg aggregate" is confined to the bulk aggregate from the first lift of the quarry, and aggregate from a particular horizon of the same lift is distinguished, e.g. Pit-16. The term "diagenesis" will apply to progressive burial diagenesis starting from a very shallow burial of sediments with ambient temperature, i.e. >30 °C, although such a shallow geological succession had eventually been eroded out in many regions of the world. The size range of quartz follows: cryptocrystalline quartz <4 μm, while microcrystalline quartz >10 μm.

3. Methods of investigation

Thin section preparation, polarizing microscopy, SEM-EDS analyses (SEM observation, quantitative analysis, elemental mapping) and supplementary analyses (XRD analysis, phosphoric extraction of quartz, insoluble residue by HCl) will be described.

3.1. Polarizing microscopy

3.1.1. Thin section preparation

Polished thin sections (20 mm by 30 mm, thickness 15 μm) of the test specimens and field concretes were prepared for polarizing microscopy to examine the presence of reaction products in the carbonate aggregate. Since concretes consist of heterogeneous materials of varying hardness on the Mohs's scale from about 1 to 4 with ASR gel, up to 7 with quartz in the aggregate, double polishing was avoided to reduce the formation of an uneven surface and thinning-out of the soft portions.

The following procedures were taken to minimize possible preparation artifacts: before cutting, low-viscosity epoxy resin was impregnated and hardened at a room temperature to reinforce the fragile materials in the specimens. Non-polar coolant (liquid paraffin) was used as a lubricant throughout the cutting and grinding to limit surface leaching. Metal-bonded diamond disc was used to remove saw marks, but scratches formed by the disc were eliminated by grinding with abrasive powder and then smoothed (alumina: size 5 μm). Lapping debris and lubricant were cleansed by an ultrasonic vibrator with organic solvents (30 s, acetone, preferably non-polar hexane). The section was bonded to the slide glass (28 mm by 48 mm) with epoxy resin at a moderate temperature (38 °C), so as to avoid optical changes in elongation of ettringite, heat-induced shrinkage cracks within the cement paste, and thermal warping of the slide glass that leads to the circular-wearing of the section during the grinding. Thin section machine with a diamond cup wheel (diamond: size 60 μm) and a thin diamond blade were used to facilitate the thinning process, before grinding with abrasive powder (alumina: size 5 μm). Most of the thin sections were dry-polished with diamond powder (size 1.5 μm) and subjected to ultrasonic cleaning, checking their surface under the polarizing/reflecting microscope in reflected light. For SEM-EDS analysis, a cover glass was not mounted, and such polished thin sections were stored in vacuum to avoid secondary weathering.

3.1.2. Polarizing microscopy

A polarizing/reflecting microscope (Nikon Optiphot-II Pol, reflecting light apparatus, ×25–400) was used in transmitted light to examine the rock types of carbonate aggregate contained; reaction products (rims, haloes, ASR gel) and expansion cracks originating from the aggregate; hydration products (in cracks, air voids, aggregate–paste interfaces) and paste carbonation; differences in the reactions among specimens, i.e. mortar bar (Fig. 1), concrete microbar (Fig. 2), concrete prism (Fig. 4), and field concrete (Fig. 5). Supplementary point-counting was done to obtain modal distribution (vol.%) of the coarse aggregate in these specimens, using up to five thin sections (Table 1). In the selection of analytical targets for SEM-EDS analysis, reflected light was used to identify unhydrated cores of cement particles (light appearance: alite, belite) and surrounding CSH gel (dark appearance), after screening them in crossed-polar transmitted light. Examinations under reflected light also confirmed the presence of pyrite in the carbonate aggregate, the state of infilling materials within cracks, the thickness of polished thin sections with a focus micrometer, and the progress of weathering that occurred on the surface of the sections during long-term storage and repeated removal from the vacuum desiccators.

3.2. SEM-EDS analysis

3.2.1. Quantitative EDS analysis

After completing polarizing microscopy, SEM observation and quantitative SEM-EDS analyses were done on the reaction products (brucite, ASR gel, CSH gel and cement hydrates), using the same polished thin sections (JEOL JSM 5310LV/JED 2140, light element detector for B-U). It was operated at 15 kV with a beam current of 0.12 nA (occasionally 0.08 nA), mainly at magnification ×2000 (counting time 100 s, dead time 30%, vacuum 10^{-4}–10^{-3} Pa, ZAF correction). Carbon was coated as a conductive layer (thickness 15 nm) to avoid charge-up during SEM observation and analysis. Probe diameter was 0.4 μm, as checked by the beam-print on the coating, with a heat-induced halo about five times larger. Thin sections generally had a sufficient thickness for analysis (15 μm), relative to the information obtained by the electron beam (depth 1–5 μm). Standard materials used for calibration include: minerals for Si (quartz: Japan), Na (albite: Amelia Court House, Virginia, USA), K (adularia: Val Cristallina, Grisons, Switzerland) and S (chalcopyrite: Japan); synthesized oxides for Ti (rutile), Al (corundum), Fe (hematite), Mn (manganosite) and Mg (periclase); artificial materials for Ca (wollastonite glass), P ($K_2O{\cdot}TiO_2{\cdot}P_2O_5$) and Cl (halite). SEM photographs are shown in Figs. 1–6.

3.2.2. Precision of analysis

The *lower limits of detection* of elements in this EDS system are on the order of 0.02–0.05 wt.%, depending on the concentration of coexisting major elements. The analytical values in EDS have a precision about 1/10 that of WDS, because in the typical analysis of ASR gel [9], EDS yielded atomic ratios of [Ca]/[Na + K] up to 10^3, while WDS yielded nearly 10^4, keeping a similar trend. Output values to two decimal places were used for calculation of [Ca]/[Na + K] ratio of ASR gel and compositional formulae of hydrates, but Tables 2–6 will present data rounded off to overall three digits, considering the accuracy of analysis by EDS.

Results of analysis will be shown without normalizing the total to 100%, omitting minor elements (Ti, Mn, P). Compositions of reaction products will be plotted on the Si–Mg–Ca diagram (Figs. 7, 8), and on the [Ca/Si]–[Ca]/[Na + K] diagram (Fig. 9). The discrepancy of analytical sum totals from 100% is attributable primarily to water and carbon dioxide not analyzed by EDS, and secondarily to extremely thin phases (thickness <5 μm) in thin section including over-thinned soft gel and hydrates; minute flakes and needles in the porous matrix; and edge-like phases underlain by epoxy resin. Conversely, larger total values than the ideal are caused by partial dehydration of hydrous phases in the vacuum process. Summing up these counter-factors, most particularly influenced by the variations in the thickness of target phases, the overall *relative error range* of analysis possibly reaches 30%.

3.2.3. Mapping of elements

Elemental mapping was performed with the same SEM-EDS at magnifications ×350–1500 (15 kV, 0.12 nA, beam diameter 0.6 μm, pitch 0.9–1.8 μm, dwell time 0.1 ms/pixel, dead time 40%, sweep time ×400, image 256 by 256 pixels). From those elements simultaneously mapped, several species (Si, Al, Mg and Na) were selected for illustration of the reaction products (Fig. 3): carbonate halo in cement paste; ASR gel, Mg-silicate gel and cryptocrystalline quartz in reacted aggregate. Supplementary elemental mapping and spot analysis were conducted for powder samples extracted with phosphoric acid to check if the rinsing of phosphoric acid was successful and quartz was free from artifacts, e.g. formation of silicon phosphate ($SiO_2 \cdot P_2O_5$) and phosphorus oxide (P_2O_5) that cause overestimation of the residue.

3.3. XRD analysis

As a supplementary measure to identify secondary alteration of cement hydrates, XRD analysis was done on a powdered sliced chip of field concretes, whose counterpart was used for thin sectioning. To examine possible ingress of chloride ions (<5 cm from surface) in the field-deteriorated concretes undergoing ACR, X-ray powder diffraction analysis was done as a supplementary measure to identify cement hydrates (AFt and AFm phases) and salts. Concrete chips that were counterparts to thin sections (20 mm by 30 mm by 5 mm, epoxy-coated, stored within a polyethylene envelope since 1988) were, essentially removing coarse aggregate, crushed and sieved into size <0.15 mm, then dry-pulverized with agate mortar and pestles for analysis. Powdered specimens set on the glass holder were analyzed by older equipment (Rigaku Geiger Flex CN2013: radiation CuKα, λ = 1.541 Å, Ni filter, 30 kV, 10 mA, diffraction angle 2–60°2θ, time constant chiefly 1 s (= 0.03°2θ), scanning speed 2°/min, divergent slit 1°, scattering slit 1°, receiving slit 0.15 mm).

Diffractograms were identified for cement hydrates based on the basal spacings between 8 and 12°2θ, with reference to collected data [10] and ICDD files for phase [11]: ettringite (no.41–1451), tricarboaluminate (no.41–215), monosulfate (no.18–275), Kuzel's salt (no.19–203), hemicarboaluminate (no.41–221), hydrocalumite (no.16–333), sulfate variety of hemicarboaluminate (no.41–476), Friedel's salt (no.35–105), monocarboaluminate (no.41–219), plus main peaks of halite (no.5–628) and sylvite (no.41–1476). For laboratory concrete microbars (NaOH or KOH immersion for 28 days), dolomitic limestone coarse aggregate from the Pittsburg quarry were separated from the mortar portion by crushing, and both portions were analyzed for reaction products sepiolite (no.13–595), brucite (no.7–239) and hydrotalcite (no.41–1428). Minerals of the aggregate origin, illite (8.8–8.9°2θ) and hornblende (10.4°2θ), were distinguished from the above cement hydrates by the help of polarizing microscopy. Opal specimens before and after the phosphoric acid treatment, as well as the acid insoluble residue (HCl) of the Pittsburg aggregate were, also subjected to XRD analysis.

3.4. Extraction of quartz

3.4.1. Phosphoric acid

To liberate silica minerals from carbonate aggregates for SEM observation to examine the size and morphology [3], phosphoric acid treatment was performed based on the Japanese standard JCAS I-31 [12] which was developed from the method of Talvitie [13]. This technique completely dissolves carbonate minerals, feldspars and clay minerals, and extracts silica minerals undetectable by polarizing microscopy in thin section. Aggregate was comminuted by the vibratory disc mill to pass through a 75 μm sieve, avoiding over-pulverization by cyclic crushing of larger blocks left on the sieve. Powder sample was dissolved by hot concentrated phosphoric acid (H_3PO_4 85 wt.%, size <75 μm, sample 0.3 g/25 ml), set to start boiling after 90 s on the heater (300 W) and continue boiling for 12 min. The solution was filtrated with powder pulp, rinsed with a dilute hydrochloric acid (1:9), then with hot water. Because quartz is dissolved slightly in this condition (e.g. 2 wt.% at 12 min, 4 wt.% at 14 min for the Ottawa sand [14]), the standard procedure prescribes a correction for the difference in the dissolution between 12 min and 14 min [i.e. quartz (wt.%) = residue (wt.%) at 14 min + 2.0 × (residue wt.% at 12 min − residue wt.% at 14 min); where 2.0 is an experimentally determined coefficient [12,14]]. However, because the author's experience with carbonate aggregates containing crypto- to microcrystalline quartz indicates that a measurement with 12 min boiling gives a value within an acceptable range of underestimation (relative error <10%), results with only 12 min boiling will be presented.

As an optional procedure adopted by the author, the extracted residue was ignited at 800 °C for 1 h to incinerate the filter paper, with minimum transformation of the silica minerals, to visualize the morphology of quartz for SEM observations (chalcedony, cryptocrystalline quartz, microcrystalline quartz, fragments of detrital large quartz). Although opaline silica has long been believed to be completely dissolved in this test [14], two representative mineral specimens of opal (Opal-A_N, opal-CT) were examined for comparison. This method has been successfully used by the author since the 1980s for quantitative XRD analysis of cristobalite, tridymite and quartz in the volcanic aggregates in Japan, New Zealand and Iceland [15,16].

3.4.2. Insoluble residue

The amount of acid insoluble residue of the carbonate aggregates was measured with hydrochloric acid after JIS R5202 [17], using the same powder as that for the phosphoric acid extraction (size <75 μm, sample 1 g/10 ml of 1:1 concentrated HCl, hot water added to 50 ml, heating 5 min over a water bath). For XRD and SEM observation, moderate condition was applied (size <150 μm, sample 10 g/100 ml of 1:1 concentrated HCl, room temperature, storage 30 min, filtration with aspirator). These procedures completely dissolve dolomite and calcite, but quartz, feldspar and clay minerals are retained.

4. Results

Petrographic examination is useful in directly identifying the loci of chemical reactions, e.g. from what mineral constituents and in what manner reaction products had formed, and on what portion of surrounding cement paste and to what extent deterioration had resulted, thence in hypothesizing divergent behaviors on the chemical reactions versus expansion of the test specimens, including the mortar bar, concrete microbar, concrete prism and field concretes.

4.1. Polarizing microscopy

4.1.1. Austrian aggregates

Carbonate aggregates came from Jurassic formations in different areas of Austria. For reference, carbonate mineral compositions were estimated from the chemical analytical data by VÖZFI [7], because

Table 1
Lithofacies of carbonate aggregates in concrete (vol.%) and extracted quartz by phosphoric acid treatment of coarse aggregate (wt.%).

	Concrete microbar RILEM AAR-5					Concrete prism CSA	Field concrete in Ontario	
	9C	10C	12C	15C	Na28	CR1[a]	Bridge Gananoque[b]	Curb Cornwall[c]
Aggregate	Austria	Austria (gravel)		Kingston, Canada (Pittsburg 1st lift)				Cornwall
	Bulk	Bulk	Bulk	Bulk	Pit-16	Bulk	Bulk	Bulk
Limestone								
Oolitic, pelletoidal		3						15[d]
Biosparitic	26[d]	2	2[d]	3[d]			4	10
Micritic	19[d]	5[d]	8[d]	20[d]	12[d]	27[d]	35[d]	12[d]
Argillaceous, shaley		5[d]	7[d]		3[d]	9[d]	21[d]	9[d]
Sandy				3[d]	12[d]		8	5
Spicular, siliceous	30[d]		3[d]					
Dolomitic limestone								
Micritic	8[d,e]	11[d]		17[d]	6[d,e]	9[e]	4[e]	5[e]
Mosaic, massive			13[e]	12[e]		9[e]	3[e]	9[d,e]
Argillaceous, shaley	8[d,e]	3[e]	7[d,e]	23[d,e]	58[d,e]	45[d,e]	13[d,e]	24[d,e]
Sandy					9[e]		4[d,e]	2[e]
Dolostone								
Micritic, massive		5[e]	20[e]					
Mosaic, massive		61[d,e]	40[e]	17[e]		1[e]	8[e]	5[e]
Argillaceous		5		5[d,e]				2[e]
Sandy								2[e]
Chert	9[d]							
Extracted Qz (insol.)	14.3[f]	10.0[f]	6.7[f]	3.2[f]	4.8[f] (16.8)			
Sample origin	VÖZFI 2001	VÖZFI 2001	VÖZFI 2001	VÖZFI 2001	KGE	MTO 1992	MTO 1992	TK 1986
Storage/construction	14 days	14 days	14 days	14 days	28 days	2 years	1957	1979
Aggregate stockpile	VÖZFI	VÖZFI	VÖZFI	MTO	CANMET	MTO		

[a] 38 °C, stored 2 years.
[b] 1000 Island Parkway Bridge (ballast wall built in 1957 and later replaced: MTO collection).
[c] Water Street (placed in 1979).
[d] Contains ASR gel.
[e] Contains reaction rims and carbonate haloes formed by dedolomitization.
[f] Quartz: extracted by phosphoric acid treatment [3], insoluble residue: extracted by HCl.

accurate modal analysis was not feasible due to the fine texture of dolomite crystals, often micritic (a few μm across). Cryptocrystalline quartz disseminated in the carbonate matrix [3] was not detected by the optical microscopy, otherwise it was concentrated as a patch of chert.

Siliceous limestone aggregate (no.9C) is highly heterogeneous, comprising of calcite (60 wt.%) and dolomite (7 wt.%) with total SiO_2 (33 wt.%). Limestones, both micritic and biosparitic rich in fossil fragments (50–150 μm), are predominant (45 vol.%) (Table 1). Spicular limestone is subordinately contained (30 vol.%). This is rich in parallel-oriented sponge spiculae (diameter 50–100 μm) composed of chalcedony, embedded within fine-grained matrix of calcite (<10 μm) and dolomite rhombs (10–40 μm) that grades into chert. Minor lithofacies include: chert composed of crypto- to microcrystalline quartz originating from spiculae; micritic dolomitic limestone (dolomite, calcite <10 μm); and stratified argillaceous dolomitic limestone containing dolomite rhombs (10–30 μm), fossil fragments (50–200 μm) and laminations with pyrite spots. Veins of coarse-grained calcite (<1 mm) and microcrystalline quarts, cut these lithologies.

Dolostone aggregate (no.10C) from a gravel-pit (maximum size: 3 cm as received) has a calculated composition of dolomite (81 wt.%) and calcite (15 wt.%) with SiO_2 (4 wt.%). Argillaceous matter is rarely contained. Dominant lithology is massive and less argillaceous, medium (10–30 μm) to coarse-grained (60–100 μm) dolostone composed of mosaic crystals of dolomite, comprising 60 vol.% of the aggregate. Minor rock types include: micritic dolostone, argillaceous dolomitic limestone with fine-grained dolomite (10 μm) and detrital grains of well-crystallized quartz (20–60 μm), stratified argillaceous limestone with stylolite seams, and sparitic limestone with rounded fossil fragments.

Dolomitic limestone aggregate (no.12C) from another gravel-pit contains dolostones similar to no.10 but more limestone: dolomite (53 wt.%) and calcite (42 wt.%) with total SiO_2 (4 wt.%). The aggregate is dominated (40 vol.%) by massive, less argillaceous, medium (20–50 μm) to coarse-grained (60–150 μm) dolostone, composed of mosaic dolomite. Subordinate rock types are, massive micritic dolostone (5–10 μm), argillaceous dolomitic limestone, micritic limestone with argillaceous seams and fossil fragments, micritic limestone with sponge spiculae (diameter 50–100 μm, chalcedony rimming the core of microcrystalline quartz), and shaley limestone.

4.1.2. Canadian aggregates

The Pittsburg aggregate (bulk, 1st lift) in Kingston came from the Ordovician Gull River Formation, which was used for the AAR-5 concrete microbar (no.15C) and AAR-2 mortar bar tests (no.15F). This is a dense rock containing, by calculation, calcite (62 wt.%) and dolomite (25 wt.%) with total SiO_2 (7 wt.%) and illite, but ranges widely in lithology. Under the microscope, major rock types were: micritic limestone, slightly dolomitic micritic limestone, argillaceous dolomitic limestone, and dolostone, each comprising 20 vol.% and making up 80 vol.% of the aggregate (Table 1). Argillaceous dolomitic limestone, which came from well stratified thin beds, contains silt-sized dolomite rhombs (15–50 μm) scattered within a micritic matrix of calcite and within an argillaceous matrix, often interlayerd with argillaceous laminations rich in illite and pyrite grains. This is a typical deleteriously reactive lithology. Slightly dolomitic micritic limestone contains sporadic dolomite rhombs (10–30 μm) and argillaceous seams with pyrite grains. Massive dolostone consists of a mosaic aggregation of medium-grained dolomite crystals (20–50 μm) and is poor in argillaceous impurity. As a minor lithology, massive dolomitic limestone with a medium-grained mosaic texture of dolomite has a matrix of micritic calcite. Sandy to silty limestone contains detrital grains (20–60 μm) of quartz, with minor amounts of plagioclase and K-feldspar. Cryptocrystalline quartz was not visible in thin section, but authigenic quartz with idiomorphic hexagonal outlines was rarely seen.

The most reactive horizon in the same quarry (Pit-16, 1st lift) used for the prolonged tests (Na28, K28) consisted essentially of argillaceous dolomitic limestone with silt-sized dolomite rhombs (15–50 μm) scattered within an argillaceous matrix, although about

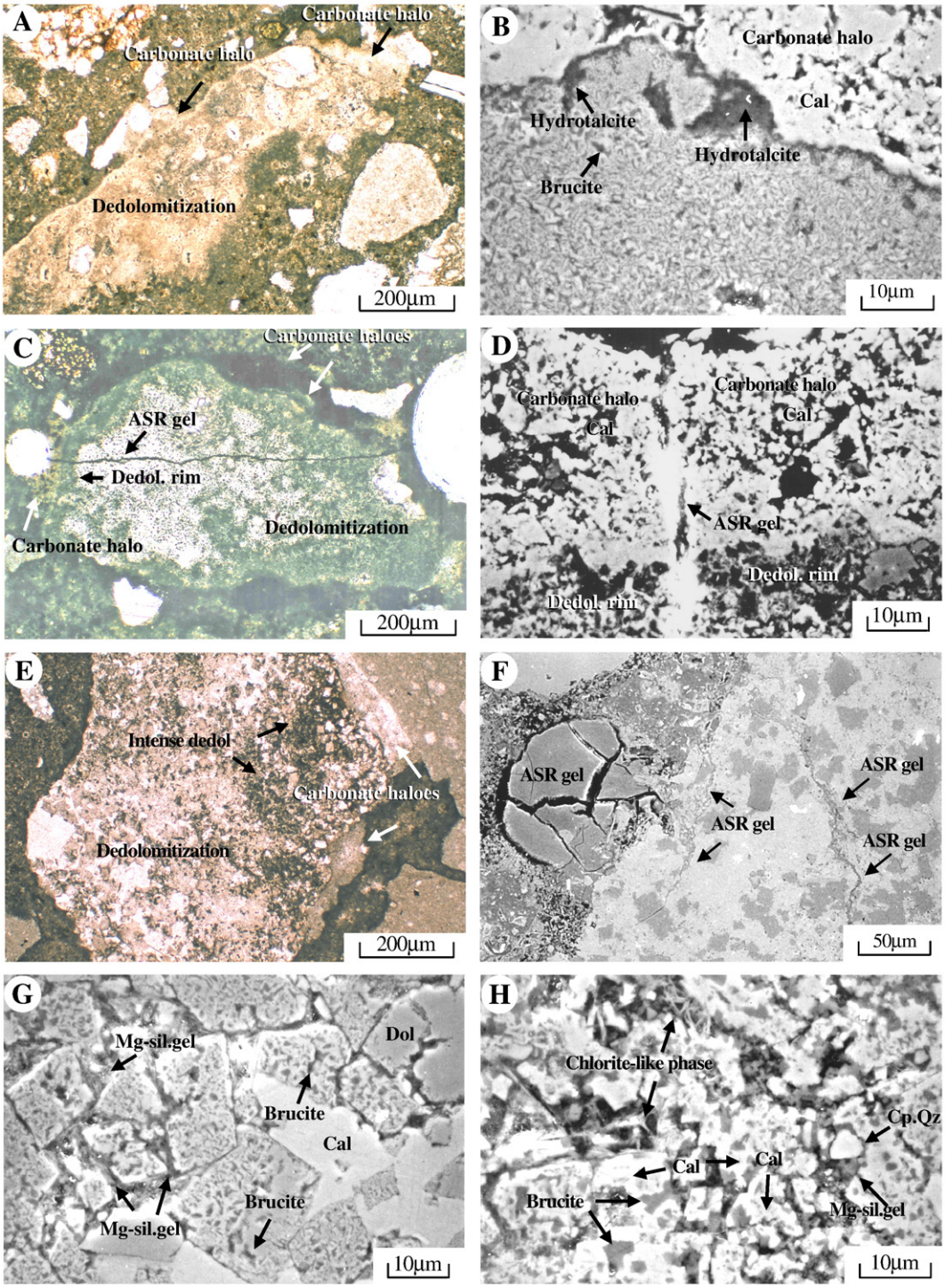

Fig. 1. RILEM AAR-2 mortar bar (aggregate <4 mm). (A)–(F): *Austrian dolostones.* (A) Entirely dedolomitized particle of dolostone no.10F, producing carbonate halo without cracking, (B) hydrotalcite rim on dolomite crystals, and brucite spots within the aggregate; (C) intensely decomposed dolostone no.12F, forming a faint crack (D) with ASR gel cutting through the carbonate halo. (E)–(H): *Bulk Pittsburg aggregate* no.15F. (E) Intense dedolomitization of dolomitic limestone, forming carbonate haloes without cracking, (F) ASR gel in argillaceous dolomitic limestone exuding along cracks into air void. Dolomitic limestone with (G) moderately dedolomitized portion leaving pseudomorphs of dolomite rhombs and interstitial Mg-silicate gel, and (H) intensely dedolomitized portion with spots of coarse-grained brucite (dark), calcite (bright), Mg-silicate gel around cryptocrystalline quartz, and flakes of a chlorite-like phase.

40 vol.% consisted of other carbonate lithologies. This typical reactive lithology was dominant in the CSA concrete prism that developed crack-lining gel in early 1990s at MTO, as well as in the ACR-affected concrete curb that contained a similar aggregate from a different quarry in Cornwall. However, this rock type was less abundant in the ACR-affected bridge in Gananoque made with the Pittsburg aggregate (1st lift).

4.1.3. RILEM mortar bar

The Pittsburg aggregate (no.15, bulk, 1st lift) produced smaller expansion in the mortar bar than in the concrete microbar, presenting a typical behavior of so-called alkali-carbonate reaction [5,7]. Dolomitic aggregates near the mortar surface (depth <5 mm) exhibited pronounced dedolomitization, due to good penetration of NaOH solution into small particles. Under transmitted light, entirely reacted

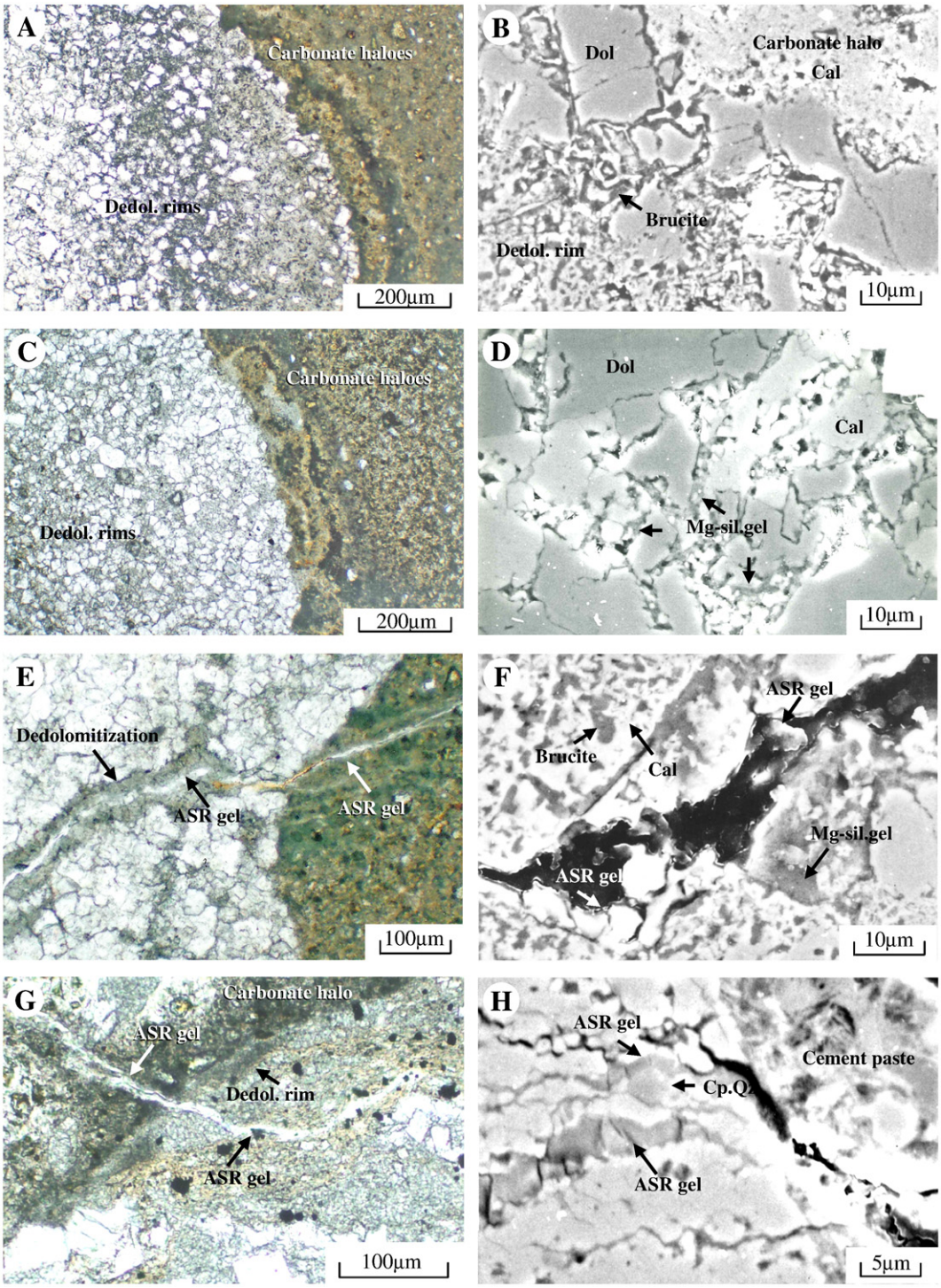

Fig. 2. RILEM AAR-5 concrete microbar (aggregate 4–8 mm). (A)–(D) *Dedolomitization without cracking:* (A) Austrian dolostone no.12C, forming pronounced reaction rims, carbonate haloes free from expansion cracks in the cement paste, (B) brucite spots in the reaction rim and calcite crust in the halo; (C) Dolomitic limestone in the Pittsburg aggregate no.15C (bulk, 1st lift, MTO stockpile), Ontario, Canada, producing reaction rims, carbonate haloes, and (D) spots of Mg-silicate gel. (E)–(H) *Cracking due to ASR*: (E) Austrian dolostone no.10C, producing crack-lining ASR gel and (F) reaction zone (dedolomitization) along the crack, composed of brucite spots (dark) and secondary calcite distant from the crack, and Mg-silicate gel (dark) near ASR gel; (G) Argillaceous dolomitic limestone in the bulk Pittsburg aggregate no.15 C, forming crack-filling ASR gel, faint reaction rim and diffuse carbonate halo; (H) Veins of ASR gel being formed from cryptocrystalline quartz within slightly dolomitic limestone [3,5].

aggregate particles presented dark to light brownish color, along with conspicuous *carbonate halo*, composed mainly of secondary calcite, in the embedding cement paste without cracking (Fig. 1A,E).

Occasionally, a *reaction zone* had formed along pre-existing cracks within aggregate particles (no.10F: Fig. 1C). The carbonate halo was optically dense where it was developed in a confined space between two aggregate particles (no.15F: Fig. 1E). Aggregate inside the mortar bar (depth >5 mm) often formed a *reaction rim* indicative of partial dedolomitization. Except for a typical ASR-reactive siliceous limestone including a chert (no.9F: [3,7]), cracks were generally less evident in the mortar bar and confined within aggregate particles. A fine crack was filled with ASR gel, only identifiable by SEM observation with EDS analysis (no.12F: Fig. 1D). ASR gel was identified filling air voids near the argillaceous dolomitic limestone in the Pittsburg aggregate, without

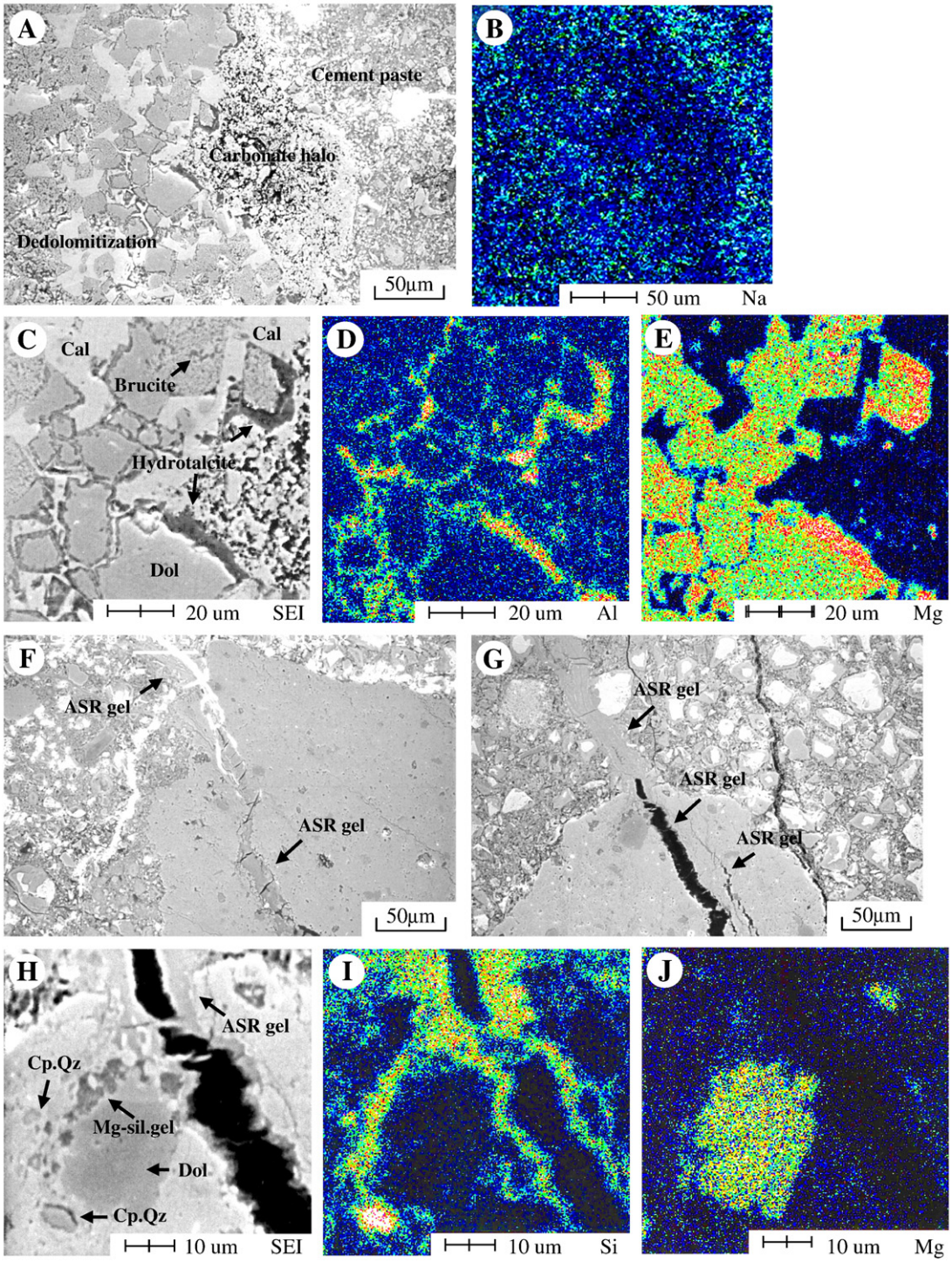

Fig. 3. Mapping of elements. (A)–(E): *RILEM AAR-2 mortar bar* made with the bulk Pittsburg aggregate (1st lift, MTO stockpile). (A) Dolomitic limestone producing a porous calcitic carbonate halo, (B) surrounded by the outer halo enriched in Na. (C) Cement–aggregate interface forming a dark hydrotalcite rim on the dolomite rhombs, shown by (D) Al and (E) Mg images. (F)–(J): *RILEM AAR-5 concrete microbar* made with the most reactive layer in the Pittsburg quarry (Pit-16, 1st lift, CANMET stockpile) with added (F) NaOH (Na28) or (G) (H) KOH (K28) [5]. Argillaceous dolomitic limestone developed wide cracks filled with ASR gel through prolonged reaction (28 days). (H) (I) ASR gel (Si image) with concentration gradient, suggestive of migration from cryptocrystalline quartz into crack, and (J) Mg-silicate gel (Mg image) surrounding dolomite rhombs.

producing cracks in the surrounding cement paste (no.15F: Fig. 1F, see SEM photograph).

4.1.4. RILEM concrete microbar

In the concrete microbar prepared by VÖZFI, dedolomitization was pronounced in Austrian dolostone aggregate (no.12C: Fig. 2A) and in dolomitic limestone from Kingston (no.15C: Fig. 2C), forming conspicuous internal reaction rims limited by the periphery of the aggregate, as well as *dedolomitized zones* along pre-existing cracks formed by the process of crushing aggregate or preceded by ASR (no.10C: Fig. 2E) [3,5]. Dedolomitization also developed carbonate halo, composed of fan-shaped aggregation of secondary calcite in the surrounding cement paste. Occasionally, the carbonate halo presented multiple zoning in transmitted light, composed of calcite crust (bright) and outer zone (dark) that grades outward into normal cement paste (Fig. 2A,C). Argillaceous dolomitic limestone (no.15C:

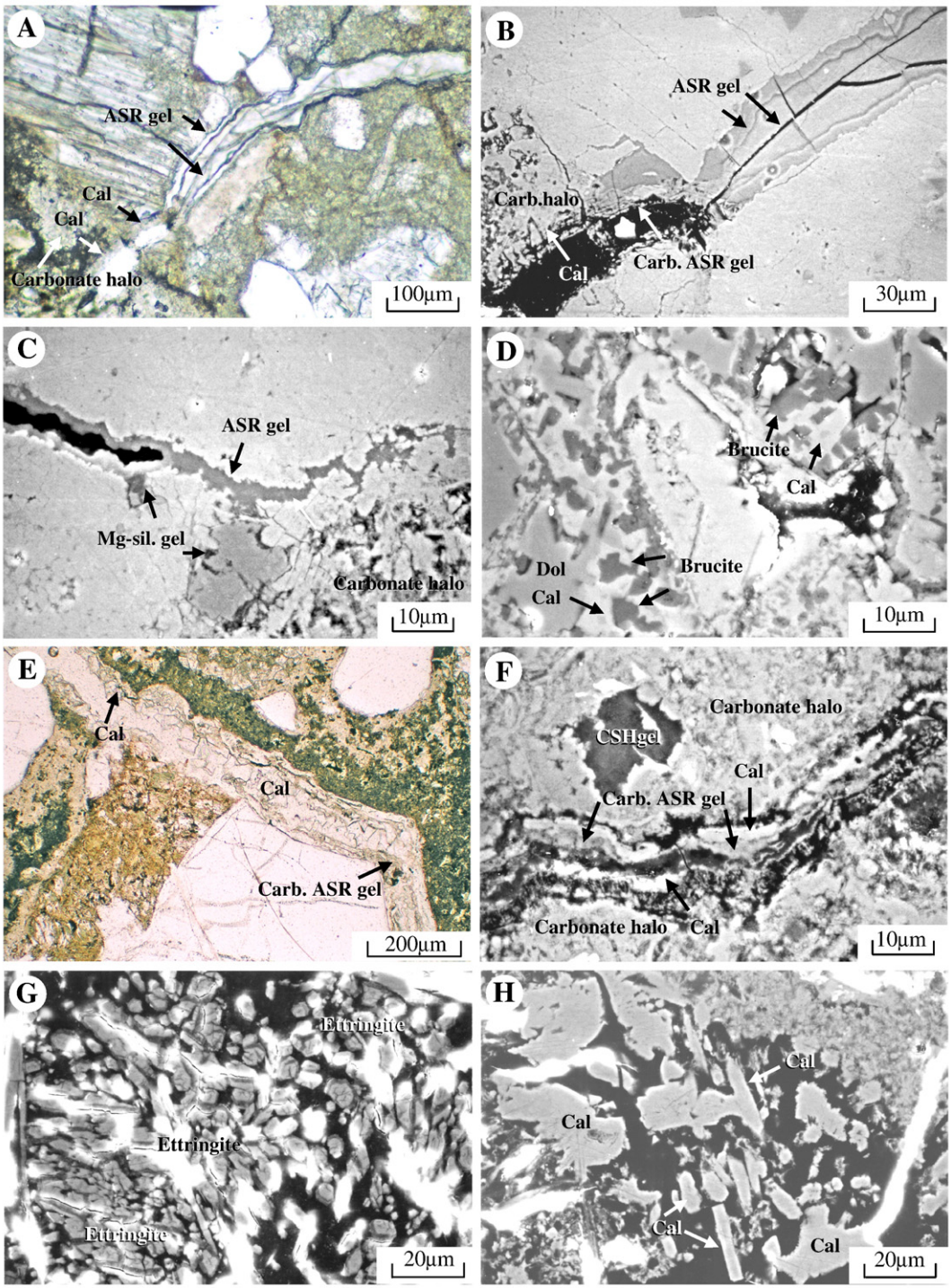

Fig. 4. CSA concrete prism made with the Pittsburg aggregate (bulk, 1st lift, MTO stockpile: 2 years): (A) (B) Composite vein of ASR gel within slightly dolomitic argillaceous limestone, grading into the calcite lining within cement paste, (C) thin vein of ASR gel, and spots of Mg-silicate gel (dark) around dolomite rhombs in slightly dolomitic limestone, (D) spots of brucite (dark) formed in dolostone aggregate, (E) wide crack filled with calcite spars within cement paste, (F) composite vein of calcite and carbonated ASR gel, cutting though the carbonate halo on the dolomitic limestone (outside of image) within cement paste. (G) Bundle of ettringite needles cut at a right angle with hexagonal outlines filling wide crack within cement paste, (H) pseudomorphs of calcite replacing the ettringite needles within crack in cement paste.

Fig. 2G) exhibited less marked dedolomitization than the dolostone and dolostone aggregates. Unless ASR was involved, dedolomitization of coarse aggregate did not induce any expansion cracks in the surrounding cement paste, in contrast to the Austrian dolostone (no.12C:Fig. 2A) and dolomitic limestone in the Pittsburg aggregate (bulk 1st lift) (no.15C: Fig. 2C) [3,4].

Cracks extending from the reacted aggregate into the cement paste suggesting expansion occurred only associated with ASR (Fig. 2E,G). These cracks were filled or lined with ASR gel, irrespective of lithology whether dolostone, dolomitic limestone, or siliceous limestone (Table 1, [3]). Stratified aggregate produced gel-filled cracks, arranged in parallel with argillaceous interlayers (no.15C: Fig. 2G). Concrete microbar made with the most reactive layer of the Pittsburg quarry (P-16, 1st lift, CANMET stockpile) with added NaOH (Fig. 3F) or KOH (Fig. 3G) at KGE, produced larger expansion than the bulk Pittsburg aggregate [5,7]. Upon extended exposure to testing conditions

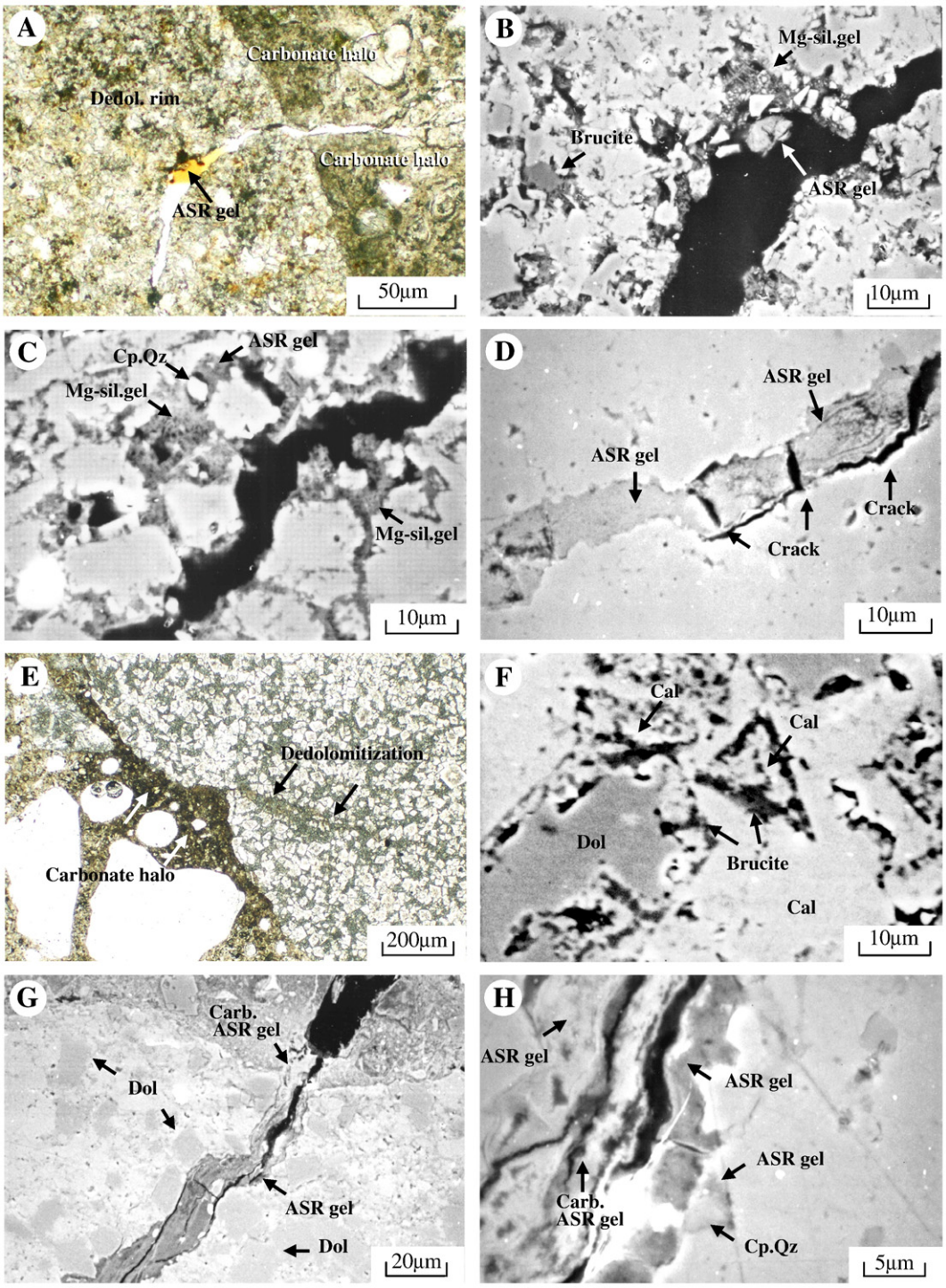

Fig. 5. Field-deteriorated concretes in Ontario, Canada. (A)–(D): *Bridge in Gananoque* (built 1957, old ballast wall). (A) Argillaceous dolomitic limestone with a reaction rim cut by open crack, (B) originally filled with ASR gel that was almost lost during the cutting and polishing. Dedolomitization forming brucite on dolomite rhombs, and Mg-silicate gel pseudomorphic after dolomite; (C) dolomitic limestone with a dedolomitized zone along the crack, containing ASR gel around cryptocrystalline quartz and Mg-silicate gel; (D) crack-filling ASR gel wearing off from limestone aggregate. (E)–(H): *Concrete curb in Cornwall* (placed 1979). (E) Dolomitic limestone, forming a dedolomitized zone along pre-existing crack, and a carbonate halo without cracking cement paste, and (F) pseudomorphic texture composed of brucite spots (dark) and calcite after dolomite rhombs; (G) argillaceous dolomitic limestone filled with layered ASR gel, (H) originated from cryptocrystalline quartz but partly carbonated due to later weathering [3,4].

(28 days), argillaceous dolomitic limestone created wider gel-filled cracks (see SEM, Fig. 3F,G), about 5 times wider than cracks in concrete microbars exposed for 14 days [4].

4.1.5. CSA concrete prism

The concrete prism made with the Pittsburg aggregate and stored 2 years at MTO (bulk 1st lift, MTO stockpile) contained wide expansion cracks (width 15–150 μm), and most resembled field-deteriorated concretes in that it produced calcite veins during the long storage of the prism. In the early 1990s, Rogers noted crack-lining materials in this specimen consisted of calcite, ettringite and gel-like materials, and suspected that some of crack-lining "gel" might contain brucite [18]. To verify this, polished thin sections were prepared in 1994 from a sliced concrete block whose counterpart had already been petrographically

examined at MTO. The formation of ASR gel in the Pittsburg aggregate was first confirmed in this concrete prism at that time, and some of compositions analyzed with WDS have been published in 1998 [19]. The same thin sections having been stored in the vacuum desiccator were again examined here. As a result, 15–20 years time delay between Rogers's original and the author's recent observations did not allow for the changes or reactions noticed to take place.

Cracks formed by the expansion of concrete prism were either open or filled with ASR gel, ettringite, or calcite. The concrete contained wide cracks lined with alternating layers of sparry calcite (Fig. 4E) or intruded by ettringite needles or both. ASR gel was identified in varying forms. Within slightly dolomitic argillaceous limestone, ASR gel occurred as a composite vein of two generations, i.e. the earlier lining, and later filling in the crack (Fig. 4A), but, inside the aggregate, it graded into an anisotropic vein of crystalline mosaic, suggestive of a carbonated gel phase. In the cement paste, the same crack from the ASR gel was lined with secondary calcite on one side (Fig. 4A), while it was filled with ettringite on the other side of the aggregate.

4.1.6. Field concretes

All the features of chemical reactions found in the laboratory specimens were also present in field concretes. ASR gel occurred in various lithologies of coarse aggregate, including limestone, shaley limestone, dolomitic limestone and argillaceous dolomitic limestone [3,4]. In Gananoque concrete, dedolomitization rim was visible on the inner periphery of argillaceous dolomitic limestone aggregate, along with sporadic carbonate haloes in the surrounding cement paste, both showing a dark appearance in transmitted light (Fig. 5A). A crack was noted along the boundary between the dedolomitization rim and the interior of the aggregate, radially extending into the cement paste. In concrete from Cornwall, dolomitic limestone was dedolomitized along pre-existing cracks in the coarse aggregate (Fig. 5E), formed in the crushing of the aggregate, as well as carbonate haloes (dark in transmitted light) in the cement paste, without producing cracks. However, in both localities of ACR, crack-filling ASR gel, particularly in the cement paste, was often carbonated due to weathering and later forming carbonate haloes, and was obscured by high-birefringent calcites within carbonated cement paste and carbonate aggregate.

4.2. SEM observation

Combined examination of SEM and mapping of elements by SEM-EDS on the same polished thin section was very effective in identifying the details of products in the carbonate aggregate and in the cement paste. Although weathered ASR gel tended to be worn off during the sample preparation, small fragments of ASR gel in concrete could still be identified by SEM. In this paper, secondary electron images (SEI) showing surface topography and morphology were presented (Figs. 1–6).

4.2.1. Dedolomitization

Optically entirely dedolomitized aggregate particles in the mortar bar contained fine- (Fig. 1B,G) to coarse-grained brucite (no.15F: Fig. 1H), depending on the degree of dedolomitization in each particle. The darker the reaction zones appear in transmitted light in thin section, the more brucite can be identified in SEM. Dolomite crystals in reaction rims (no.12C: Fig. 2B) and dedolomitized zones along cracks (no.10C: Fig. 2F) had decomposed into a combination of dark spots of brucite (<3 μm) and secondary calcite, leaving a mottled texture, pseudomorphic after dolomite rhombs. Carbonate halo was a porous crust of secondary calcite replacing the cement paste (Figs. 1D,E, 3A), while the surrounding outer halo was cement paste enriched in Na (Fig. 3B), e.g. alkali carbonates [3].

Among other phases identified associated with dedolomitization, *Mg-silicate gel* was the most common that occurred replacing brucite after dolomite rhombs within aggregate (no.10C: Fig. 2F), or surrounding dolomite rhombs interstitially (no.15F: Fig. 1G; no.15C: Fig. 2D), or altering ASR gel around cryptocrystalline quartz (no.15F: Fig. 1H) [4]. On the surface of dolostone aggregate, a narrow rim (possibly *hydrotalcite*) appeared replacing brucite (no.10F: Fig. 1B, no.15F: Fig. 3C), which presented a substantial amount of Al and Mg, as indicated by the mapping of elements by SEM-EDS (Fig. 3D,E). In zones of advanced dedolomitization, a platy *chlorite-like phase* occurred within decomposed dolomite crystals (no.15F: Fig. 1H), intimately associated with brucite, secondary calcite and Mg-silicate gel.

In the concrete prism made with the Pittsburg aggregate at MTO (bulk, 1st lift, stored in 2 years), dolostone particles developed coarsely grained spots of brucite and calcite within patchy reaction rims on the periphery of the aggregate (Fig. 4D), whereas dolomite rhombohedra within the argillaceous dolomitic limestone aggregate are surrounded by Mg-silicate gel. In old concrete from Gananoque, dedolomitization had proceeded intensely in the Pittsburg aggregate, and here again a chlorite-like phase has been found from the reaction rim of argillaceous dolomitic limestone aggregate [4]. Mg-silicate gel appeared replacing dolomite rhombs, ASR gel and brucite along the crack, while brucite was confined to the areas distant from the crack-filling ASR gel (Fig. 5B,C). In the concrete curb in Cornwall, pseudomorphs of spotted brucite and calcite replace dolomite rhombs along pre-existing cracks within dolomitic limestone, precipitating carbonate haloes in the cement paste without accompanying expansion cracks (Fig. 5E,F).

4.2.2. Alkali-silica reaction

When used as fine aggregate, dolomitic limestone in the Pittsburg aggregate only displayed evidence of dedolomitization (no.15F: Fig. 1F,G), whereas larger sand particles (size 4 mm) of argillaceous dolomitic limestone occasionally produced ASR gel, filling minute cracks within the aggregate and adjacent air void without accompanying cracks in the cement paste (no.15F: Fig. 1F). In the concrete microbar (size 4–8 mm), very thin ASR gel (width <5 μm) filled or lined cracks in the aggregate extending into cement paste (no.10C: Fig. 2F), and cryptocrystalline quartz was altering to ASR gel (no.15C: Fig. 2H). The most reactive layer in the Pittsburg quarry (Pit-16, 1st lift), with added NaOH (Fig. 3F) or KOH (Fig. 3G,H), produced wider cracks upon extended exposure (28 days) [4,6]. Mapping of elements by SEM-EDS clearly showed a concentration gradient within ASR gel veins extending from the reacted aggregate into cement paste. In the Si image (Fig. 3H,I), a concentration gradient implying a path of migration of ASR gel can be seen that had originated from the cryptocrystalline quartz into crack-lining ASR gel within the reacted aggregate. Separately, dark spots of Mg-silicate gel had formed, replacing the rim on the reacted dolomite rhombs (Fig. 3H,J).

SEM observation of the polished thin section of concrete prism was useful in characterizing the composite vein of crack-filling ASR gel within aggregate (Fig. 4B). It graded into an anisotropic gel, possibly a mixture of calcium carbonate and ASR gel, as suggested by SEM-EDS analysis (Table 3) with a well-defined carbon peak. SEM observation was also essential in tracing very thin veins of ASR gel, with widths down to 0.5 μm or less, that grades into crack-lining ASR gel in argillaceous dolomitic limestone (Fig. 4C).

In field concretes, crack-filling ASR gel was less evident. This was because the fragility of the texture, composed of carbonated gel and dedolomitization products, left the products in the cement paste susceptible to abrasion during grinding and polishing of thin sections, leaving only open cracks. Nevertheless, in Gananoque, small patches of ASR gel were detected by the SEM observation from open cracks (average width 10 μm) within argillaceous dolomitic limestone (Fig. 5B) and around cryptocrystalline quartz in reacted dolomitic limestone (Fig. 5C). The ASR gel in Fig. 5B had a habit of rosette, implicating an old product, but other examples appeared to be less crystalline, essentially amorphous as observed on the polished thin section by SEM. By contrast, ASR gel was relatively well preserved in less dolomitic limestone aggregate with similar crack width (10 μm)

(Fig. 5D). In the concrete curb in Cornwall, cracks in argillaceous dolomitic limestone were filled with ASR gel, but its extension in the cement paste was worn away during sample preparation (Fig. 5G).

4.2.3. Carbonation of ASR gel

ASR gel has been partly carbonated in both laboratory concrete prism and field concretes, showing evidence of weathering and forming calcite veins. Cracks in the concrete prism were filled with multilayered veins, composed of secondary calcite and variously carbonated ASR gel. They cut through the carbonate halo around the reacted dolomitic aggregate, often enclosing spots of CSH gel pseudomorphic after original cement grains (Fig. 4F).

The concrete prism also contained long needles of ettringite with hexagonal cross-section (Fig. 4G, 20–50 μm) in cracks and in air voids along cracks, which were often replaced by secondary calcite pseudomorphic after ettringite needles (Fig. 4H) but grading into veins of sparry calcite (Fig. 4E). Dolomitic limestone aggregate from the Pittsburg quarry contained sporadic minute grains of pyrite. However, no relationship could be seen between the occurrence of pyrite and the precipitation of secondary ettringite. The formation of the ettringite is the result of re-precipitation from the cement paste, which had undergone leaching and carbonation along the cracks formed by ASR, and hence was not the cause of the expansion of these concretes, nor delayed ettringite formation (DEF). Calcite replacing ettringite is indicative of precipitation from entrapped water in cracks with low ion concentrations.

Field concretes had undergone more intense and complicated weathering including replacement of ASR gel by calcium carbonate, leaching of cement paste by humidity and rain water along cracks, carbonation of cement paste along cracks and by dedolomitization around the dolomitic aggregate, and ingress of chloride ions from deicing salt. The ballast wall concrete from Gananoque contained cracks with linings of calcite with rhombic outlines, some grading into the carbonate halo around dedolomitized coarse aggregate particles. The concrete curb in Cornwall contained crack-filling ASR gel, often inter-layered with carbonated ASR gel and calcite veins of later generations (Fig. 5G,H), and rosette-like aggregation of platy calcium carbonate, suggestive of vaterite within cracks in the cement paste. Secondary carbonation of ASR gel along cracks has also been reported from Newfoundland, Canada, where late-expansive ASR of argillaceous aggregate is combined with freeze–thaw weathering [9].

In highly carbonated portions near the dolomitic aggregate and within interstices along the aggregate–paste interface, were porous pseudomorphs of platy hydrates (5–20 μm) being replaced by calcium carbonate. In Gananoque, tuffaceous sandstone in the sand occasionally contained rosette-like aggregations of large tabular crystals (10–50 μm), resembling a habit considered typical for hydrocalumite-carboaluminate minerals.

4.2.4. Extracts from the aggregate

SEM observation of the liberated silica minerals in the phosphoric acid residue identified several forms of quartz in the carbonate aggregates, but cryptocrystalline quartz was the most common form of silica (Table 1). Austrian siliceous limestone contained fragments of microcrystalline quartz and chalcedony both in sponge spiculae (no.9: Fig. 6A). In addition to these, dolomitic gravels contained cryptocrystalline quartz (no.10: Fig. 6B) and fragments of chert with mosaic aggregation of distinctively crystallized cryptocrystalline quartz with polygonal outlines (no.12: Fig. 6C). No overgrowth of siliceous material, implying secondary opal or secondary quartz, was detected on the polygonal quartz grains. Canadian Pittsburg aggregate (no.15C: Fig. 6E) contained cryptocrystalline quartz, which was more abundant in the most reactive layer (Pit-16: Fig. 6D) that is rich in argillaceous dolomitic limestone. Aggregates from this quarry invariably contained idiomorphic cryptocrystalline to microcrystalline quartz with well-defined faces with pseudohexagonal prismatic habit, which had formed through a coalescent grain growth, i.e. recrystallization of cryptocrystalline quartz during diagenesis [3]. No overgrowth or interstitial filling of siliceous material, implying secondary opal or secondary quartz, was detected on the quartz grains.

Untreated reference opal-An had a dense texture with a conchoidal fracture resembling a glass or large quartz (Fig. 6F). Reference opal-CT was generally dense with only partly granular texture resembling cryptocrystalline quartz (Fig. 6G), and did not present the lepisphere texture characteristic of this phase. Extracts from phosphoric acid of these opals after heating also exhibited a smooth or granular surface under SEM, resembling the textures as before. Thus, in a strict meaning, when opal with the above habits is present as an independent phase, it cannot be distinguished from cryptocrystalline quartz and large quartz by means of SEM observation with EDS analysis.

The acid insoluble residue of the most reactive layer of the Pittsburg quarry (Pit-16) by HCl abounded in the minute flakes of illite (Fig. 6H), sporadically associated with tiny plates of chlorite.

4.3. SEM-EDS analysis

Results of mortar bar (Table 2), concrete microbar (Table 3), concrete prism (Table 4), and field concretes from Gananoque (Table 5) and Cornwall (Table 6) in Canada were presented. Compositions of reaction products, including brucite $Mg(OH)_2$, Mg-silicate gel, hydrotalcite-like phase, chlorite-like phase, ASR gel and reacted quartz, were plotted in atomic ratios on the Si–Mg–Ca triangular diagram (Figs. 7, 8). Brucite occupies the Mg-corner of the diagram, while cryptocrystalline quartz represents the Si-corner when it has not been altered. Carbonate minerals: dolomite, calcite, and carbonated products of dedolomitization and secondary precipitation in cracks, as well as carbonated ASR gel, were omitted from this diagram.

To clarify the chemical characteristics of the ASR gel in detail, reaction products with essential amounts of Si and Ca will be examined hereafter on the [Ca/Si]–[Ca]/[Na + K] diagram developed by the author in the 1990s. This diagram has a format to distinguish five gel-like materials in concrete, indicating the position of ASR gel in concrete and reflecting the stage of ASR and cement hydration [9,19–22]: 1) crack-filling ASR gel in aggregate, 2) crack-filling ASR gel in cement paste, 3) air void-filling ASR gel in cement paste, 4) CSH gel after alite, and 5) CSH gel after belite (Fig. 9). Crystalline form of rosette is also plotted as ASR gel. Cement hydrates (AFm and AFt phases) were analyzed to obtain rough compositional formulae for identification (Tables 5, 6). The analytical sum totals varied considerably by location, due to varying thickness and porosity of reaction products in thin section, as well as partial dehydration in the low-pressure conditions encountered in carbon coating, storage of thin sections, and SEM observation with SEM-EDS analysis. However, the data obtained were considered reliable enough to allow compositional diagrams and reproducing compositional formulae. Katayama demonstrated by the mapping of elements that the outer zone of the carbonate halo is enriched in alkali-carbonate released by dedolomitization [3].

For reference, additional analysis was performed of dolomite crystals in the aggregate. Dolomite in the Pittsburg aggregate in the Gananoque concrete presented compositions of 57–60 mol% $CaCO_3$ and 40–43 mol% $MgCO_3$, corresponding to *high-Ca calcian dolomite* (>55 mol% $CaCO_3$). In contrast, dolomite in the Austrian aggregates in the concrete microbar (nos.10C, 12C) ranged 53–56 mol% $CaCO_3$, indicating the common presence of *low-Ca calcian dolomite* (<55 mol% $CaCO_3$). In the calculation of carbonate compositions of the aggregate, stoichiometric composition of dolomite (50 mol% $CaCO_3$) was used for convenience.

4.3.1. Brucite and Mg-silicate gel

Brucite has been found in the concrete microbar, made with the Austrian dolostone aggregate (no.10C, Fig. 7B, Table 3) or the Pittsburg aggregate (bulk, 1st lift) stored for a normal period (14 days) (no.15C, Fig. 7D, Table 3), as well as in the field-deteriorated concretes from Gananoque (Fig. 8C,D, Table 5) and Cornwall (Fig. 8E, Table 6). Brucite

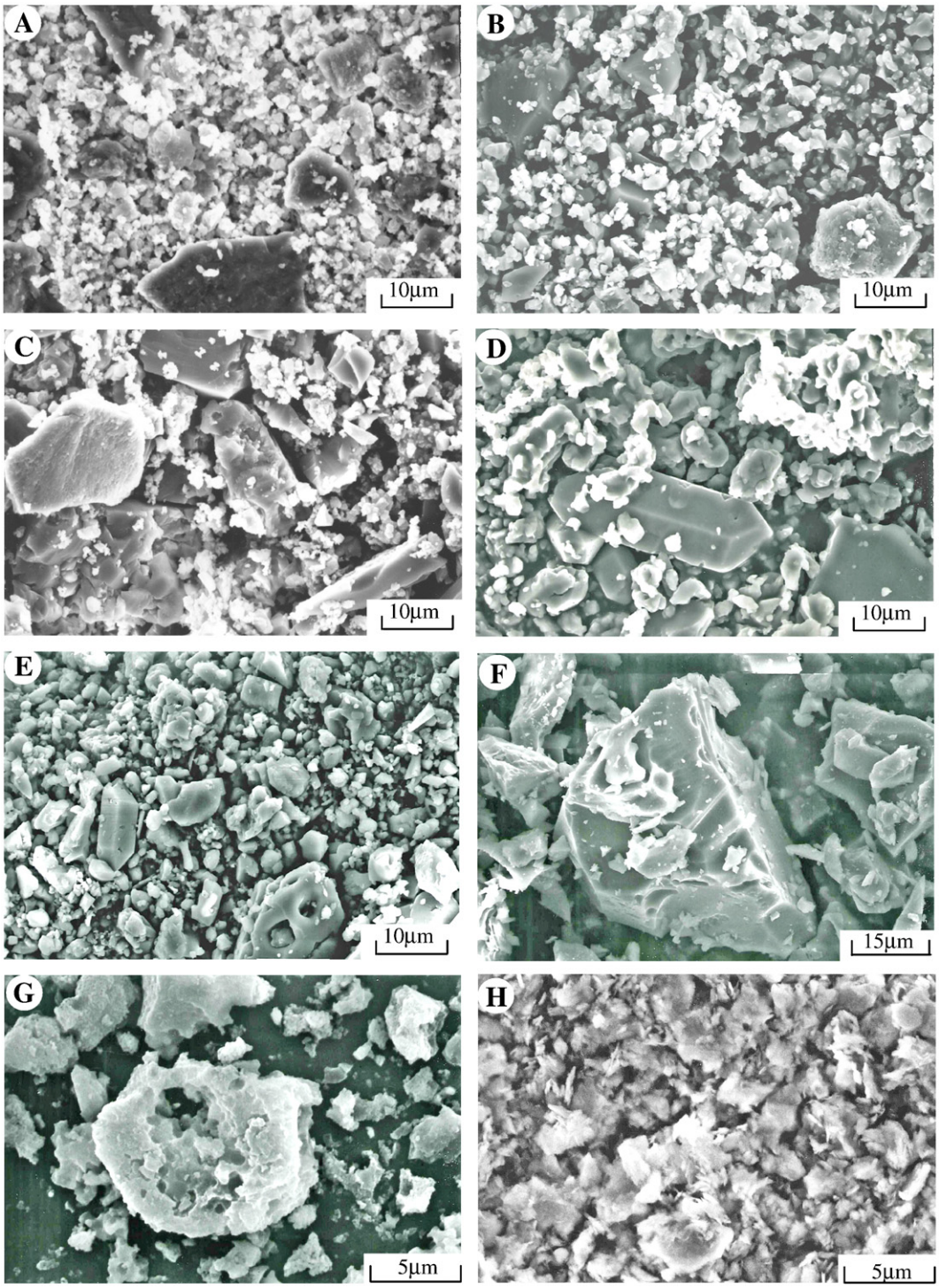

Fig. 6. SEM photographs of free-silica extracted by phosphoric acid. (A) Austrian siliceous limestone no.9 with microcrystalline quartz and chalcedony, (B) Austrian dolostone no.10, rich in cryptocrystalline quartz, and (C) Austrian dolomitic limestone no.12, with crypto- to microcrystalline quartz, chalcedony and mosaic of cryptocrystalline quartz indicative of a chert inclusion. (D) Pittsburg aggregate no.15 (bulk, 1st lift, MTO stockpile) with idiomorphic prismatic crypto- to microcrystalline quartz; and (E) the most reactive layer in the Pittsburg quarry, Ontario, Canada (P-16, 1st lift, CANMET stockpile), rich in polygonal to prismatic cryptocrystalline quartz; reference opal after phosphoric treatment with (F) dense texture preserved in opal-A_N from Bohemia, and (G) granular texture left within opal-CT from Nevada; (H) HCl-insoluble residue, showing illite flakes with the most reactive layer in the Pittsburg quarry (P-16, 1st lift).

was absent in the concrete microbars (Na28, K28: Fig. 8A,B) made using a highly reactive layer in the Pittsburg quarry (Pit-16, 1st lift) and stored for a prolonged period (28 days), but was rare in the fine fraction of the mortar bar (no.15F: Fig. 7F, Table 2).

Mg-silicate gel occupies wide areas in the triangular diagram and was collectively shown as "dolomite rim", together with precursor brucite and associated chlorite-like phase (Figs. 7, 8). With the Austrian siliceous limestone aggregate rich in ASR gel, Mg-silicate gel present as gel veins that graded into ASR gel veins was also plotted as dolomite rim for convenience (no.9C, Fig. 7A, Table 3). Mg-silicate gel was dominant in the coarse aggregate (no.12C, Fig. 7C) whereas it was intermixed with Ca and Al through the entire cross-section of the particle of fine aggregate

Table 2
Representative compositions of ASR gel (wt.%) in the carbonate aggregates in RILEM AAR-2 mortar bars as determined by SEM-EDS analysis on polished thin sections.

	10F			12F			15F					
	Austria (gravel) Dolostone			Austria (gravel) Dolostone			Kingston, Canada (Pittsburg, bulk, 1st lift) Argil. dol. ls		Dolomitic limestone			
	Mg-sil. gel Spot	Brucite Spot	Hydrotalcite Rim	ASR gel[a] Paste crack	Mg-sil. gel Spot	Al-sil. gel Spot	ASR gel[a] Aggr. crack	ASR gel[a,b] Void	Mg-sil. gel Matrix	Chlorite-like[c] Flake	Brucite Spot	Hydrotalcite Rim
SiO_2	38.4	1.50	2.16	31.6	24.8	31.8	37.2	30.2	23.2	24.5	2.07	1.98
Al_2O_3	13.5	0.00	10.7	7.06	0.17	14.1	0.82	1.05	6.98	12.6	1.21	9.62
Fe_2O_3	1.96	0.55	0.52	1.64	0.68	4.63	0.00	0.00	4.38	9.83	1.86	0.46
MgO	16.7	58.4	24.1	5.42	30.6	6.19	0.00	0.00	18.7	17.5	46.7	23.8
CaO	8.52	1.55	3.74	47.2	16.1	9.90	20.2	25.7	3.49	6.23	4.59	2.39
Na_2O	0.60	0.72	0.00	3.08	0.45	0.52	4.19	4.10	0.20	0.02	0.00	0.00
K_2O	1.72	0.30	0.00	1.38	0.11	4.19	3.30	1.13	1.71	0.22	0.01	0.00
SO_3	0.15	0.00	0.37	1.13	0.00	0.26	0.19	0.20	0.42	0.31	0.20	0.43
Total	81.6	63.1	41.6	100.0[d]	72.9	71.6	65.9	62.4	59.1	71.2	56.5	38.7
I				1.60			0.58	0.91				
II				6.54			1.76	2.92				
III	0.39				0.65				0.55	0.52		

I: atomic ratio [Ca]/[Si], II: atomic ratio [Ca]/([Na]+[K]), III: atomic ratio [Mg]/([Mg]+[Si]).
[a] Optically isotropic.
[b] As published in [4].
[c] $5(Mg_{0.64},Fe_{0.18},Ca_{0.16})O\cdot(Al_{0.91})_2O_3\cdot 3SiO_2\cdot nH_2O$.
[d] Total normalized to 100% because of low total amount (35 wt.%) by exposed resin.

(<4 mm) (no.12F, Fig. 7C) that had undergone dedolomitization. With the Pittsburg aggregate, Mg-silicate gel was found from the interior of the aggregate (e.g. size 4 mm) (no.15F, Fig. 7E), but, on the surface of the aggregate, it had modified compositions rich in Ca and Al (no.15F, Fig. 7F) (Table 2) [5]. Mg-silicate gel is very common in concretes that have undergone advanced reaction, such as the concrete microbars stored for a prolonged period (Fig. 8A,B, Table 3) and the field concretes from Gananoque (Fig. 8C,D, Table 5) and Cornwall (Fig. 8E, Table 6). Mg-silicate gel varies widely in composition depending on the distance from ASR gel and brucite. On the Si–Mg tie-line in the triangular diagram, several examples of Mg-silicate gel have [Mg/Si] atomic ratios nearly corresponding to 4/6, i.e. [Mg]/[Mg+si]=0.4 typically with concrete microbar specimens Na28 and K28, suggestive of sepiolite ($4MgO\cdot 6SiO_2\cdot 7H_2O$) (Fig. 8A,B, Table 3).

4.3.2. Hydrotalcite and chlorite-like phase

The hydrotalcite-like phase, with [Mg/Al] atomic ratios near 3.0, suggestive of hydrotalcite $6MgO\cdot Al_2O_3\cdot CO_2\cdot 12H_2O$, always gave a total amount of analysis around 40 wt.% (Table 2), which was smaller than that of its ideal amount of 57 wt.%, excluding volatile species H_2O and CO_2 that cannot be measured by SEM-EDS. This was probably due to a gel-form or a very porous thin form of this substance [20]. Compositions of the hydrotalcite-like phase formed on the surface of dolomitic limestone aggregate in the AAR-2 mortar bar (size 4 mm: Pittsburg 15F) were plotted as "dolomite interface" omitting Al, which are located close to brucite (Fig. 7E,F).

The platy chlorite-like phase found within highly dedolomitized aggregates in the mortar bar (Fig. 7E) and field concrete (Fig. 8C), both made with the Pittsburg aggregate, had compositions closely

Table 3
Representative compositions of ASR gel (wt.%) in the carbonate aggregates in RILEM AAR-5 concrete microbars as determined by SEM-EDS analysis on polished thin sections.

	9C		10C			12C		15C		Na28			K28	
	Austria (quarry)		Austria (gravel)			Austria (gravel)		Pittsburg, bulk 1st lift		Kingston, Canada (Pittsburg, P-16, 1st lift)				
	Argil. dol. ls		Dolostone		Dolostone	Dolostone	Dolostone	Argl.d.l	Argl.d.l	Argil. dol. ls			Argil. dol. ls	
	ASR gel[a]	Mg-sil. gel[b]	ASR gel[a]	Mg-sil. gel[b]	Brucite[b]	Calcite[b]	Brucite	ASR gel[c]	Brucite[d]	ASR gel[a]	ASR gel[a]	Mg-sil. gel[e]	ASR gel[a]	Mg-sil. gel[e]
	Vein in aggregate	Vein in aggregate	Vein in aggregate	Rim of dolomite	Dedol. spot	Dedol. spot	Dedol. spot	Vein in aggregate	Dedol. spot	Vein in paste	Vein in aggregate	Rim of dolomite	Vein in aggregate	Rim of dolomite
SiO_2	41.6	42.4	45.1	19.7	1.93	0.65	1.18	41.4	7.66	30.1	47.9	44.8	52.1	50.9
Al_2O_3	2.66	0.87	0.79	4.78	1.42	0.07	0.00	1.15	1.02	2.46	1.13	2.56	0.98	1.11
Fe_2O_3	0.81	0.44	0.00	4.29	0.32	0.00	0.34	0.71	1.02	0.30	0.00	2.27	0.00	1.03
MgO	0.58	12.6	0.00	16.3	50.3	7.90	56.6	0.00	57.6	0.01	0.03	17.6	0.13	19.6
CaO	11.1	1.92	16.2	4.61	2.56	46.5	2.54	10.4	8.58	36.8	23.2	3.93	16.5	3.08
Na_2O	2.46	2.55	4.35	5.98	0.96	0.35	0.68	2.07	2.04	0.50	2.55	0.87	1.51	1.22
K_2O	6.31	3.28	8.58	3.10	0.52	0.25	0.00	4.38	0.88	0.28	4.33	1.34	4.72	2.25
SO_3	0.00	0.12	0.00	0.12	0.06	0.13	0.00	0.87	0.09	1.74	0.00	0.00	0.08	0.00
Total	65.5	64.2	75.0	58.8	58.2	56.2	61.3	60.9	77.9	72.2	79.1	73.4	75.9	79.1
I	0.29		0.38					0.27		1.31	0.52		0.34	
II	0.93		0.89					1.15		30.0	2.37		1.97	
III		0.31		0.55								0.37		0.36

I: atomic ratio[Ca]/[Si], II: atomic ratio [Ca]/([Na]+[K]), III: atomic ratio [Mg]/([Mg]+[Si]).
[a] Optically isotropic.
[b] As published in [3].
[c] Rosette-like.
[d] Originally described as Mg-silicate gel in [3].
[e] As published in [4].

Table 4
Representative compositions of ASR gel (wt.%) in the carbonate aggregate and cement hydrates in CSA concrete prism as determined by SEM-EDS analysis on polished thin sections.

	Coarse aggregate (Pittsburg, bulk 1st lift)							Cement paste						
	CR1-1			CR1-2				CR1-1					CR1-2	
	Argil. dol. ls		Dolostone	Slightly dolomitic argil. ls				Carbonate halo			Less carb.	Carb.	Non-carb.	Carb.
	Rim of dolomite	Vein	Dedol. crack	Pseud. dolomite	Composite vein Inside wall			Pseudomorph After alite	Crust	Composite vein	Vein	Vein	Crack-filling	Vein
	Mg-sil. gel	ASR gel[a]	Brucite spot	Mg-sil. gel	ASR gel[a]	ASR gel[a]	Carbonated ASR gel[b]	CSH gel	Calcite petal-like	Carbonated ASR gel[a]	Ettringite[c] prism	Calcite spar	Ettringite[d] needle	Calcite after ettr.
SiO_2	26.7	44.3	0.96	30.3	40.7	42.6	23.6	38.1	4.16	36.0	0.70	1.35	0.56	1.02
Al_2O_3	0.00	0.00	0.35	1.84	0.00	0.00	0.00	1.85	0.31	1.68	10.5	0.22	10.5	0.12
Fe_2O_3	1.71	0.26	0.73	2.17	0.00	0.08	0.00	1.23	0.50	0.38	0.00	0.00	0.17	0.06
MgO	17.9	0.00	52.1	20.7	0.00	0.00	0.00	1.97	0.00	0.00	0.00	0.00	0.00	0.00
CaO	12.0	21.8	3.03	8.41	36.6	25.7	25.8	11.7	49.6	9.92	35.4	53.5	33.5	52.1
Na_2O	0.00	0.30	0.00	0.00	0.13	0.11	0.17	0.17	0.09	0.21	0.00	0.06	0.06	0.26
K_2O	0.71	0.37	0.00	0.43	0.10	0.25	0.18	0.29	0.34	0.57	0.00	0.07	0.01	0.14
SO_3	0.00	0.35	0.17	0.10	0.14	0.00	0.50	0.98	0.19	0.51	22.8	0.47	24.6	0.11
Total	62.9	67.4	57.3	63.9	77.7	68.7	50.3	56.2	55.2	49.3	69.4	55.7	69.4	53.8
I		0.53			0.97	0.64	1.17	0.33		0.29				
II		22.2			101	51.1	42.1	18.0		9.38				
III	0.50			0.51										

I: atomic ratio [Ca]/[Si], II: atomic ratio [Ca]/([Na]+[K]), III: atomic ratio [Mg]/([Mg]+[Si]).
[a] Optically isotropic.
[b] Contains irregular patches.
[c] $3CaO(Al_{0.98}, Si_{0.04})_2O_3 \cdot 3Ca[(SO_4)_{0.90}, (X)_{0.10}] \cdot nH_2O$ X: 2OH or CO_3.
[d] $3CaO(Al_{1.03}, Fe_{0.01}, Si_{0.04})_2O_3 \cdot 3Ca(SO_4)_{1.03} \cdot nH_2O$.

resembling clinochlore $5(Mg,Fe)O \cdot Al_2O_3 \cdot 3SiO_2 \cdot 4H_2O$. It was almost always associated with Mg-silicate gel, and contained either excess Mg or Ca, probably derived from closely associated brucite or secondary calcite in SEM-EDS analysis (Tables 2, 5) [4]. One example of analysis shows that this chlorite (clinochlore) contains substantial Fe, partly substituting Mg ($5 \times [Mg/Fe] = 3.65:1.35$ [4]) (Table 5, footnote c), which corresponds to 55 at.% of Mg on the Si–Mg tie-line [$= 3.65 \times 100/(3.00 + 3.65)$] (= 58 at.% inclusive of excess Mg) on the triangular diagram (e.g. Fig. 8C).

4.3.3. CSH gel

The compositions of ASR gel and calcium silicate hydrates formed on alite and belite (CSH gel) were plotted on the [Ca/Si]–[Ca]/[Na+K] diagram, excluding the Mg-silicate gel (>5 wt.% MgO, Fig. 9). In the

Table 5
Representative compositions of ASR gel (wt.%) in the carbonate aggregate and cement hydrates in the ballast wall concrete from Gananoque as determined by SEM-EDS analysis on polished thin sections.

	Coarse aggregate (Pittsburg, bulk 1st lift)							Fine aggregate		Cement paste				
	K4					K0		K3(2)		K0 Less carbonated		K2(1) Carbonated	K4 Carbonated	K0 Less carbonated
	Dolomitic limestone					Argil. dol. ls.		Tuffaceous sandstone void		After alite	After belite	Interspace	Around cement	Around cement
	Crypt. quartz[a]	ASR gel[b]	Mg-sil. gel	Chlorite-like[a,c]	Chlorite-like[a,d]	ASR gel[e]	Brucite spot	Hydro-calumite[f]	Hydro-calumite[g]	CSH gel	CSH gel	Tricarbo-aluminate[h]	Monocarbo-aluminate[i]	Friedel's salt[j]
SiO_2	94.0	40.4	20.2	24.4	21.9	50.5	1.15	1.29	0.42	21.1	25.4	1.10	5.19	3.33
Al_2O_3	0.88	1.21	0.46	12.5	16.9	0.20	0.00	11.5	14.1	1.29	1.14	8.86	12.1	14.4
Fe_2O_3	0.08	1.29	0.91	13.2	17.5	0.36	0.74	3.18	2.55	0.72	1.47	1.76	1.54	0.38
MgO	1.86	11.3	22.1	23.1	15.4	0.00	66.1	0.00	0.00	1.22	0.21	0.00	0.67	0.25
CaO	1.25	4.17	5.00	0.42	2.42	11.5	0.85	31.2	36.1	33.1	36.4	36.5	34.5	39.2
Na_2O	0.28	0.13	0.15	0.43	0.08	0.20	0.75	0.00	0.00	0.02	0.12	0.00	0.00	0.21
K_2O	0.00	0.62	0.23	0.44	0.25	6.04	0.00	0.20	0.20	0.16	0.18	0.01	0.00	0.58
SO_3	0.00	0.12	0.61	0.19	0.18	0.22	0.19	3.81	1.78	0.21	1.39	0.32	1.71	0.74
Cl								0.13	0.31	3.34	2.81	0.84	0.41	11.1
Total	98.4	59.2	49.7	74.6	74.6	69.0	69.8	51.3	55.4	61.2	69.1	49.4	56.1	70.2
I		0.10				0.24				1.68	1.54			
II		5.56				1.53				151	85.5			
III			0.62	0.58	0.51									

I: atomic ratio[Ca]/[Si], II: atomic ratio [Ca]/([Na]+[K]), III: atomic ratio [Mg]/([Mg]+[Si]).
[a] As published in [4].
[b] Optically isotropic.
[c] $5(Mg_{0.73}, Fe_{0.27})O \cdot Al_2O_3 \cdot 3SiO_2 \cdot nH_2O + (Mg_{1.00}, Si_{0.31})O \cdot mH_2O$.
[d] $5(Mg_{0.60}, Fe_{0.34}, Ca_{0.07})O \cdot (Al_{1.20})_2O_3 \cdot 3(Si_{0.94}, Al_{0.06})O_2 \cdot nH_2O$.
[e] Rosette-like.
[f] $3CaO(Al_{0.81}, Fe_{0.14}, Si_{0.07})_2O_3 \cdot Ca[(X)_{0.65}, (SO_4)_{0.34}, (Cl_2)_{0.01}] \cdot nH_2O$ X: 2OH or CO_3.
[g] $3CaO(Al_{0.86}, Fe_{0.10}, Si_{0.02})_2O_3 \cdot Ca[(X)_{0.81}, (SO_4)_{0.14}, (Cl_2)_{0.05}] \cdot nH_2O$ X: 2OH or CO_3.
[h] $3CaO(Al_{0.80}, Fe_{0.10}, Si_{0.09})_2O_3 \cdot 3Ca[(X)_{0.85}, (SO_4)_{0.04}, (Cl_2)_{0.11}] \cdot nH_2O$ X: CO_3.
[i] $3CaO(Al_{0.77}, Fe_{0.06}, Si_{0.28})_2O_3 \cdot Ca[(X)_{0.82}, (SO_4)_{0.14}, (Cl_2)_{0.04}] \cdot nH_2O$ X: CO_3.
[j] $3CaO(Al_{0.81}, Fe_{0.01}, Si_{0.16})_2O_3 \cdot Ca[(Cl_2)_{0.88}, (SO_4)_{0.05}, (X)_{0.07}] \cdot nH_2O$ X: 2OH.

Table 6
Representative compositions of ASR gel (wt.%) in the carbonate aggregate and cement hydrates in the concrete curb from Cornwall as determined by SEM-EDS analysis on polished thin sections.

	Coarse aggregate							Cement paste						
	C1(4)				C0		C1(4)	C1(4) Non-carbonated		C6 Non-carb.	CC Non-carb.	CD(2) Carb. crack	C1(4) Non-carbonated	
	Argillaceous dolomitic limestone				Dol.ls.		Dol.ls.	After alite	After belite	Void	Void	Aligned void	Around cement	Around cement
	Composite gel vein				Dedol		Dedol							
	Crypt quartz	ASR gel[a]	Leached ASR gel[a]	Carbonated ASR gel	Calcite Carb.halo	Brucite spot[b]	Calcite spot	CSH gel	CSH gel	NaCl-CSH	Ettringite[c]	Ettringite[d]	Friedel's salt[e]	Friedel's salt[f]
SiO_2	89.6	66.4	61.5	20.6	1.99	5.42	0.35	17.7	21.0	10.2	0.79	0.34	3.58	1.56
Al_2O_3	0.89	3.73	0.00	0.44	0.30	0.86	0.30	1.56	2.27	1.24	7.20	8.94	15.0	12.4
Fe_2O_3	0.24	0.66	0.00	0.00	0.35	5.71	0.49	0.31	1.31	0.65	0.59	0.32	0.66	1.27
MgO	0.00	0.00	0.00	0.00	0.00	47.4	3.34	0.72	1.19	0.47	0.36	0.00	0.28	0.94
CaO	0.85	8.38	3.71	36.6	49.5	5.52	50.3	31.9	31.7	15.1	27.2	31.6	39.9	33.4
Na_2O	0.16	0.05	0.14	0.21	0.29	0.51	0.19	0.06	0.00	11.7	0.13	0.05	0.00	0.00
K_2O	0.10	1.85	0.00	0.24	0.79	0.35	0.42	0.10	0.15	0.92	0.17	0.00	0.35	0.37
SO_3	0.18	0.36	0.00	0.39	0.34	0.06	0.09	0.91	0.83	1.57	19.6	19.4	0.80	0.59
Cl								1.31	1.08	12.5			8.93	10.3
Total	92.0	81.4	65.4	58.5	53.6	65.8	55.5	54.6	59.6	54.5	56.0	60.7	69.5	60.8
I		0.14	0.06	1.91				1.93	1.62					
II		0.38	13.7	54.3				149	176					

I: atomic ratio[Ca]/[Si], II: atomic ratio [Ca]/([Na]+[K]).
[a] Optically isotropic.
[b] As published in [4].
[c] $3CaO(Al_{0.88}, Fe_{0.04}, Si_{0.08})_2O_3 \cdot 3Ca(SO_4)_{1.01} \cdot nH_2O$.
[d] $3CaO(Al_{0.93}, Fe_{0.02}, Si_{0.04})_2O_3 \cdot 3Ca[(SO_4)_{0.86}, (X)_{0.14}] \cdot nH_2O$ X: 2OH or CO_3.
[e] $3CaO(Al_{0.83}, Fe_{0.02}, Si_{0.16})_2O_3 \cdot Ca[(Cl_2)_{0.69}, (SO_4)_{0.06}, (X)_{0.25}] \cdot nH_2O$ X: 2OH.
[f] $3CaO(Al_{0.82}, Fe_{0.05}, Si_{0.09})_2O_3 \cdot Ca[(Cl_2)_{0.95}, (SO_4)_{0.05}] \cdot nH_2O$.

concrete microbar (15C: Fig. 9C), calcium silicates alite and belite hydrated to CSH gel with a [Ca/Si] atomic ratio down to 2.0, corresponding to hydration products in mature paste. This [Ca/Si] ratio was even higher than that of ordinary concretes not subjected to immersion in NaOH solution. Abundant portlandite [$Ca(OH)_2$] surrounded the CSH gel, implicating co-precipitation from a pore solution saturated with OH ions.

In contrast, the Canadian field concretes contained CSH gel with the lowest [Ca/Si] ratios and chloride, i.e. Gananoque with [Ca/Si] down to 1.5, Cl 1.9–3.5 wt.% (Fig. 9G, Table 5), and Cornwall with [Ca/Si] down to 1.3, Cl 0.4–2.2 wt.% (Fig. 9H, Table 6). The concrete microbar (Na28: Fig. 9E) stored for a prolonged period (28 days), presented [Ca/Si] ratio of CSH gel of 1.8, being intermediate between the field concretes and the concrete microbars stored in two weeks. These field concretes came from within 5 cm of the concrete surface. In one case with the concrete curb in Cornwall, relatively large amounts of Na and Cl with an atomic ratio of about 1.1, implicating the presence of halite (NaCl), were identified in close relationship with CSH gel (Table 6). The presence of chloride could possibly originate from deicing salt. In other cases, chloride ions are assumed to be adsorbed to CSH gel, as discussed later. According to the author's experience in Japan, both halite and sylvite (KCl) have been identified on the fracture surface (depth 2 cm) within deteriorated concrete deck that had formed pot-holes on the corroded reinforcing steel bars due to the ingress of deicing salt. In other case with a pop-out phenomenon appeared on the bridge pier, veins of halite that fill cracks formed by the pop-out (depth 5 mm) have been identified in the thin section cleansed with acetone.

4.3.4. Aluminate and sulfoaluminate hydrates

The total number of atoms Al + Fe + Si was found to be very close to 2.0, if Ca was normalized to 4.0 in AFm phases, or to 6.0 in AFt phases (Tables 4–6). With SEM-EDS analysis, CO_3 and 2OH cannot be determined and are expressed here as X, and their total fraction in Ca[(X), (SO_4), (Cl_2)] of the AFm phases and in 3Ca[(X), (SO_4), (Cl_2)] of the AFt phases was calculated by balance of $SO_4 + 2Cl$ from 1.0 exactly. In the empirical formulae thus obtained for the cement hydrates, the number of anions (actually OH) necessary for balancing the difference in the valence between Al^{3+} and Si^{4+} was ignored for convenience, and the total of (OH) and H_2O was simply expressed as nH_2O.

In the Gananoque concrete, small tabular crystals of *Friedel's salt* in less carbonated cement paste had a composition of $3CaO(Al_{0.81}, Fe_{0.01}, Si_{0.16})_2O_3 \cdot Ca[(Cl_2)_{0.88}, (SO_4)_{0.05}, (X)_{0.07}] \cdot nH_2O$, where X is possibly 2OH (Table 5). Small platelets or flakes in carbonated cement paste had a composition of $3CaO(Al_{0.77}, Fe_{0.06}, Si_{0.28})_2O_3 \cdot Ca[(X)_{0.82}, (SO_4)_{0.14}, (Cl_2)_{0.04}] \cdot nH_2O$, along with a well-defined carbon peak indicating they consist of *monocarboaluminate*. Large tabular hydrates in voids within tuffaceous sandstone lack chloride and ranged in composition from $3CaO(Al_{0.86}, Fe_{0.10}, Si_{0.02})_2O_3 \cdot Ca[(X)_{0.81}, (SO_4)_{0.14}, (Cl_2)_{0.05}] \cdot nH_2O$ to $3CaO(Al_{0.81}, Fe_{0.14}, Si_{0.07})_2O_3 \cdot Ca[(X)_{0.65}, (SO_4)_{0.34}, (Cl_2)_{0.01}] \cdot nH_2O$ (Table 5). The minor carbon peaks in the EDS spectrum are indicative of minerals with a low carbonate content, e.g. *hydrocalumite* $3CaOAl_2O_3 \cdot Ca(OH)_2 \cdot 12H_2O$ (11.0°2θ peak), hemicarboaluminate $3CaOAl_2O_3 \cdot Ca[(CO_3)_{0.5}, (2OH)_{0.5}] \cdot 11.5H_2O$ (10.8°2θ peak) or its sulfate variety $3CaOAl_2O_3 \cdot Ca[(CO_3)_{0.67}, (SO_4)_{0.33}] \cdot 11H_2O$ (11.3°2θ peak). Hydrocalumite has been identified filling cracks in the argillaceous interlayers of the slightly dolomitic limestone in this concrete [3]. Again, hydrate corresponding to Kuzel's salt $3CaOAl_2O_3 \cdot Ca[(SO_4)_{0.5}, (Cl_2)_{0.5}] \cdot 12H_2O$ was not detected. Prisms within the interstices on the aggregate–paste interface presented a composition of $3CaO(Al_{0.80}, Fe_{0.10}, Si_{0.09})_2O_3 \cdot 3Ca[(X)_{0.85}, (SO_4)_{0.04}, (Cl_2)_{0.11}] \cdot nH_2O$ with a well-defined carbon spectrum, suggestive of *tricarboaluminate*.

The Cornwall concrete contained a wide range of solid solution between hydrocalumite and Friedel's salt, from $3CaO(Al_{0.83}, Fe_{0.02}, Si_{0.16})_2O_3 \cdot Ca[(Cl_2)_{0.69}, (SO_4)_{0.06}, (X)_{0.25}] \cdot nH_2O$ to $3CaO(Al_{0.82}, Fe_{0.05}, Si_{0.09})_2O_3 \cdot Ca[(Cl_2)_{0.95}, (SO_4)_{0.05}] \cdot nH_2O$, near the end member, where X is likely 2OH (Table 6). Ettringite in the air voids had normal compositions ranging from $3CaO(Al_{0.88}, Fe_{0.04}, Si_{0.08})_2O_3 \cdot 3Ca(SO_4)_{1.01} \cdot nH_2O$ to $3CaO(Al_{0.93}, Fe_{0.02}, Si_{0.04})_2O_3 \cdot 3Ca[(SO_4)_{0.86}, (X)_{0.14}] \cdot nH_2O$, and occasionally showed evidence of alteration (decrease of S and Al) in cracks with signs of carbonation and leaching. The occurrence of the Friedel's salt, Cl-doped CSH gel and occasional NaCl within the typical concretes undergoing ACR in Ontario implies infiltration of substantial NaCl salt deicer into the concrete.

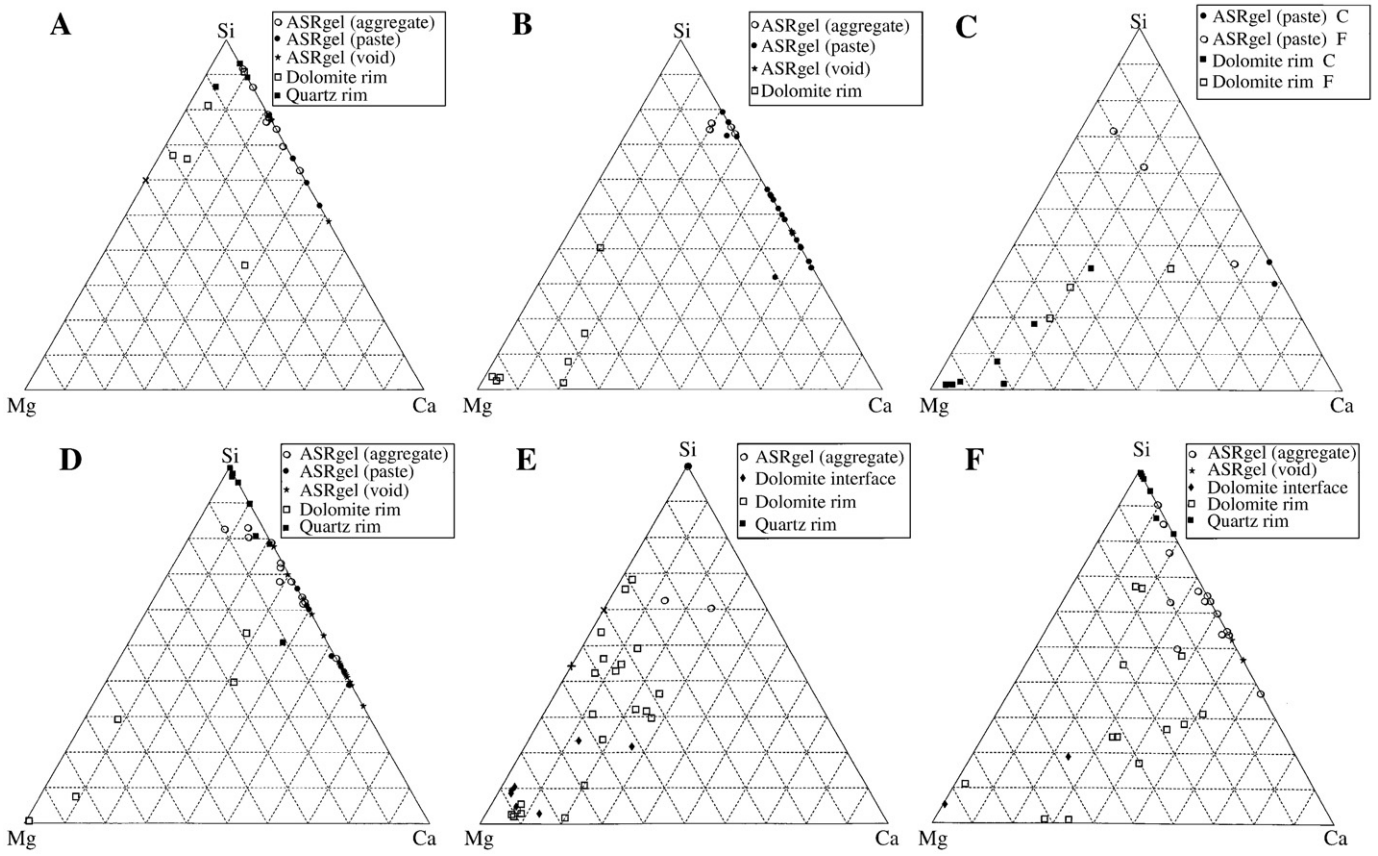

Fig. 7. Compositions of reaction products in laboratory mortar and concrete specimens as determined by SEM-EDS analysis on polished thin sections (in atomic ratios). RILEM AAR-5 concrete microbar with Austrian siliceous limestone (A) (no.9C) and dolostone (B) (no.10C). AAR-5 concrete microbar and AAR-2 mortar bar with Austrian dolomitic limestone (C) (nos.12C,12F). RILEM AAR-5 concrete microbar (D) (no.15C) and AAR-2 mortar bar (E) (F) (no.15F), both with the Pittsburg aggregate (bulk, 1st lift, MTO stockpile). (E): Aggregate surface (size: 4 mm) with hydrotalcite rim (as dolomite interface) and the interior with brucite, chlorite-like phase and Mg-silicate gel (as dolomite rim). (F): Aggregate surface (<4 mm) with Mg–Ca–Al silicate gel (as dolomite rim) and the interior of aggregate (size: 4 mm) with ASR gel. × Sepiolite with [Mg]:[Si] = 4:6, + chlorite (clinochlore) with [Mg]:[Fe]:[Si] = 3.65:1.35:3.0.

4.3.5. ASR gel

Upon transformation to ASR gel, the original habit of the cryptocrystalline quartz precursor was retained. This material is plotted as "quartz rim" in Figs. 7, 8. It also reacted with brucite to form Mg-silicate gel. Crack-filling ASR gel in carbonate aggregate occupies the Si–Ca tie-line (Figs. 7, 8). On the [Ca/Si]–[Ca]/[Na + K] diagram (Fig. 9), ASR gel exhibits a narrow range of compositional lines, directed toward the CSH gel with a distinct compositional break (Fig. 9). This tendency was common to the Austrian siliceous limestone (Fig. 9A) and dolostone (Fig. 9B) aggregates, and the Canadian argillaceous dolomitic aggregate. The Pittsburg aggregate (bulk) presents the same inclined lines in both mortar bar (no.15F: Fig. 9D) and concrete microbar (no.15C: Fig. 9C), with a wider range in the former. However, prolonged storage (28 days) (Pit-16, most reactive) resulted in less inclined lines (Na28: Fig. 9E, K28: Fig. 9F), with a "convergent point" between ASR gel and CSH gel at around [Ca/Si] = 1.8, [Ca]/[Na + K] = 100. This type of evolution of ASR gel, i.e. the single compositional line representing a typical trend of ASR, was called *type I evolution* by Katayama [9].

Field concretes presented a scatter of ASR gel compositions, but these are generally continuous with the CSH gel, with a "convergent point" at around [Ca/Si] = 1.5, [Ca]/[Na + K] = 100 for Gananoque (Fig. 9G), and at around [Ca/Si] = 1.3, [Ca]/[Na + K] = 100 for Cornwall (Fig. 8H). The compositional lines of ASR gel sloped more gently than those of the laboratory concrete microbars. With these field concretes, a short compositional line of ASR gel parallels the main line. This type of evolution of ASR gel, represented by parallel trend lines, was defined as *type II evolution* by Katayama, which has been known from deteriorated field concretes in Newfoundland undergoing combined deterioration from ASR, freeze–thaw, and carbonation along cracks [9]. The *type II* ASR gel is an advanced variety of *type I*, superimposed by intense leaching of alkalies in the particular areas (e.g. along large open cracks) within concrete.

4.3.6. Compositional lines of ASR gel in ACR concretes

The atomic ratios [Ca/Si] of ASR gel at which compositional lines intersect [Ca]/[Na + K] = 1.0 on the [Ca/Si]–[Ca]/[Na + K] diagram range between 1/2 and 1/6 (Fig. 9). These are closely similar to published results of WDS analysis for typical ASR gel: 1/5 for the bulk data of 7 field concretes from Newfoundland, Canada [21]; EDS analysis for typical ASR gel: e.g. 1/4–1/6 with 4 laboratory and 6 field concretes from Newfoundland [9], 1/4–1/6 with 4 highway structures in Okinawa, Japan [21], and 1/3 with three concrete members from two headwork structures, Japan [22].

On this diagram, near the alkali-rich corner of the compositional lines of ASR gel represents *low-Ca ASR gel*, with composition of $(Na,K)_2O{\cdot}2CaO{\cdot}6SiO_2{\cdot}nH_2O$ corresponding to mountainite, $1.5\times[2(Ca,Na_2,K_2)O{\cdot}4SiO_2{\cdot}3H_2O]$, if a mean value of [Ca/Si] ratio (1/3) is taken, although more alkali-rich gel is present. In contrast, the calcium-rich corner of the trend lines presenting the "convergent point" has variable [Ca/Si] ratios 1.3–1.8, depending on the environment to which concrete specimens had been exposed. However, with most field concretes including Gananoque and other reported localities [9,20,22], the convergent point fell near [Ca/Si] = 1.5, [Ca]/[Na + K] = 100, which corresponds to traditionally accepted CSH gel ($3CaO{\cdot}2SiO_2{\cdot}3H_2O$) [23], only if a small amount of detected alkalies {[Ca]/[Na + K] = 100, i.e. [CaO/$(Na,K)_2O$] = 200} is ignored. If the

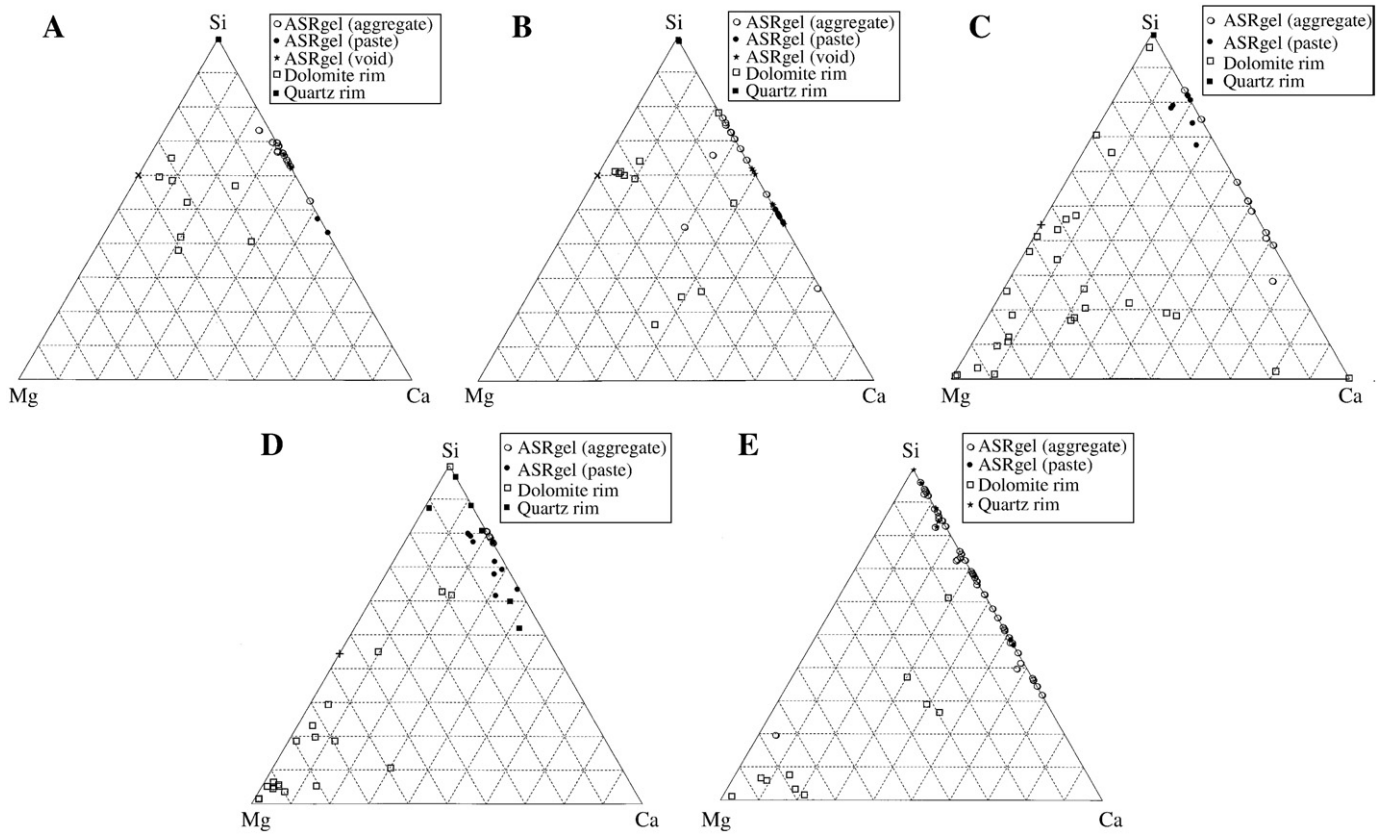

Fig. 8. Compositions of reaction products in laboratory concrete specimens and field-deteriorated concretes as determined by SEM-EDS analysis on polished thin sections (in atomic ratios). RILEM AAR-5 concrete microbar made with the most reactive layer in the Pittsburg quarry (Pit-16, 1st lift, CANMET stockpile), with added NaOH (Na28) (A) or KOH (K28) (B) to cement and stored for a prolonged period (28 days). Field concretes from ballast wall of a bridge in Gananoque (C: no.K4 mainly with dolomitic limestone; D: no.K0 with argillaceous dolomitic limestone), and from a concrete curb in Cornwall (E: no.C1(4) chiefly with argillaceous dolomitic limestone, plus no.C0 with dolomitic limestone), both in Ontario, Canada. × sepiolite with [Mg]:[Si] = 4:6, + chlorite (clinochlore) with [Mg]:[Fe]:[Si] = 3.65:1.35:3.0.

structure of the material is ignored, this composition corresponds to afwillite (or foshallasite, $3CaO{\cdot}2SiO_2{\cdot}3H_2O$) and jennite [$Ca_9Si_6O_{18}(OH)_6{\cdot}8H_2O$ or $3\times(3CaO{\cdot}2SiO_2{\cdot}11/3H_2O)$], and does not resemble the tobermorite group minerals (riversideite $5CaO{\cdot}6SiO_2{\cdot}3H_2O$, 11 Å tobermorite $5CaO{\cdot}6SiO_2{\cdot}5H_2O$, plombierite $5CaO{\cdot}6SiO_2{\cdot}7H_2O$, 14 Å tobermorite $5CaO{\cdot}6SiO_2{\cdot}9H_2O$).

On the other hand, ASR gel with [Ca]/[Na + K] = 10, on the midpoint between low-Ca ASR gel and CSH gel, is represented by *high-Ca ASR gel* with [Ca/Si] ranging 0.75–1.5, when an example of intense surface leaching of concrete (Cornwall: 0.6) is omitted. This is close to the composition of tobermorite, because a substitution of 1/4 molecule of $(Na,K)_2O = CaO$ produces a hypothetical compound $0.25(Na,K)_2O{\cdot}4.75CaO{\cdot}6SiO_2{\cdot}5H_2O$ with [Ca/Si] = 0.79, [Ca]/[Na + K] = 9.5, which is within the observed range of the trend lines.

4.3.7. ASR gel in ACR concretes and crystalline natural analogues

To find and relate crystalline counterparts to ASR gel, a series of silicate hydrate minerals containing Na, K and Ca reported from evaporate deposits and altered rocks will be examined.

Minerals with [Ca]/[Na + K] = 1.0 are discussed here. Beginning with [Ca/Si] = 1/2, ASR gel corresponds to $(Na,K)_2O{\cdot}2CaO{\cdot}SiO_2{\cdot}nH_2O$, but there is no equivalent mineral or compound to the substitution $(Na,K)_2O = CaO$ keeping the cation valence, e.g. $3(Na,K)_2O{\cdot}SiO_2{\cdot}nH_2O$ and $2(Na,K)_2O{\cdot}CaO{\cdot}SiO_2{\cdot}nH_2O$. A ratio of [Ca/Si] = 1/2.25 can be derived from gyrolite ($2CaO{\cdot}3SiO_2{\cdot}2H_2O$) if a substitution $2/3(Na,K)_2O = 2/3CaO$, is possible to produce a compound $2/3(Na,K)_2O{\cdot}4/3CaO{\cdot}3SiO_2{\cdot}2H_2O$. With [Ca/Si] = 1/3, as already mentioned, mountainite [$(Ca, Na_2, K_2)_2Si_4O_{10}{\cdot}3H_2O$ or $2(Ca,Na_2,K_2)O{\cdot}4SiO_2{\cdot}3H_2O$] is one of best candidates because of a wide range of solid solutions including a composition $2/3(Na,K)_2O{\cdot}4/3CaO{\cdot}4SiO_2{\cdot}3H_2O$ by partial substitution between 2Na, 2K and Ca. Okenite (simplified formula: $CaO{\cdot}2SiO_2{\cdot}2H_2O$) and revdite ($Na_2O{\cdot}2SiO_2{\cdot}5H_2O$) can give [Ca/Si] = 1/3, if a partial substitution of $(Na,K)_2O = CaO$ is possible to produce 1/3 $(Na,K)_2O{\cdot}2/3CaO{\cdot}2SiO_2{\cdot}2H_2O$ and $1/3(Na,K)_2O{\cdot}2/3CaO{\cdot}2SiO_2{\cdot}5H_2O$, respectively.

On the other hand, compounds with [Ca/Si] = 1/4 and 1/5, corresponding to $(Na,K)_2O{\cdot}2CaO{\cdot}8SiO_2{\cdot}nH_2O$ and $(Na,K)_2O{\cdot}2CaO{\cdot}10SiO_2{\cdot}nH_2O$, respectively, are the missing link, along with their hypothetical derivatives by cation replacement: e.g. $3CaO{\cdot}8SiO_2{\cdot}nH_2O$, $3CaO{\cdot}10SiO_2{\cdot}nH_2O$, $2Na_2O{\cdot}CaO{\cdot}8SiO_2{\cdot}nH_2O$, $2Na_2O{\cdot}CaO{\cdot}10SiO_2{\cdot}nH_2O$, etc. The ratio [Ca/Si] = 1/4 is also given by fedorite [$KNa_4Ca_4Si_{16}O_{36}(OH)_4{\cdot}6H_2O$ or $2(1/4K_2O{\cdot}Na_2O{\cdot}2CaO{\cdot}8SiO_2{\cdot}4H_2O)$] but its [Ca]/[(Na + K] ratio is 1/1.25, not 1.0. Finally, at [Ca/Si] = 1/6, ASR gel in Gananoque concrete (Fig. 9G) is assignable to a compound $(Na,K)_2O{\cdot}2CaO{\cdot}12SiO_2{\cdot}nH_2O$. This can be transformed to $3(Na,K)_2O{\cdot}12SiO_2{\cdot}nH_2O$ by cation replacement and simplified as $Na_2O{\cdot}4SiO_2{\cdot}xH_2O$, i.e. equivalent to makatite ($Na_2O{\cdot}4SiO_2{\cdot}5H_2O$) and kanemite [$NaHSi_2O_5{\cdot}3H_2O$ or 1/2 $(Na_2O{\cdot}4SiO_2{\cdot}7H_2O)$].

4.3.8. Extracts from the aggregate

A rough SEM-EDS analysis of the extracted powders by phosphoric acid indicated that crypto- to microcrystalline quartz with fine porosity yielded 98 wt.% SiO_2, while fragments of large quartz had 99 wt.% SiO_2, thus confirming that they were actually free-silica, all belonging to the varieties of quartz [3]. Phosphorus was not detected from the residue, suggesting that the rinsing of phosphoric acid was

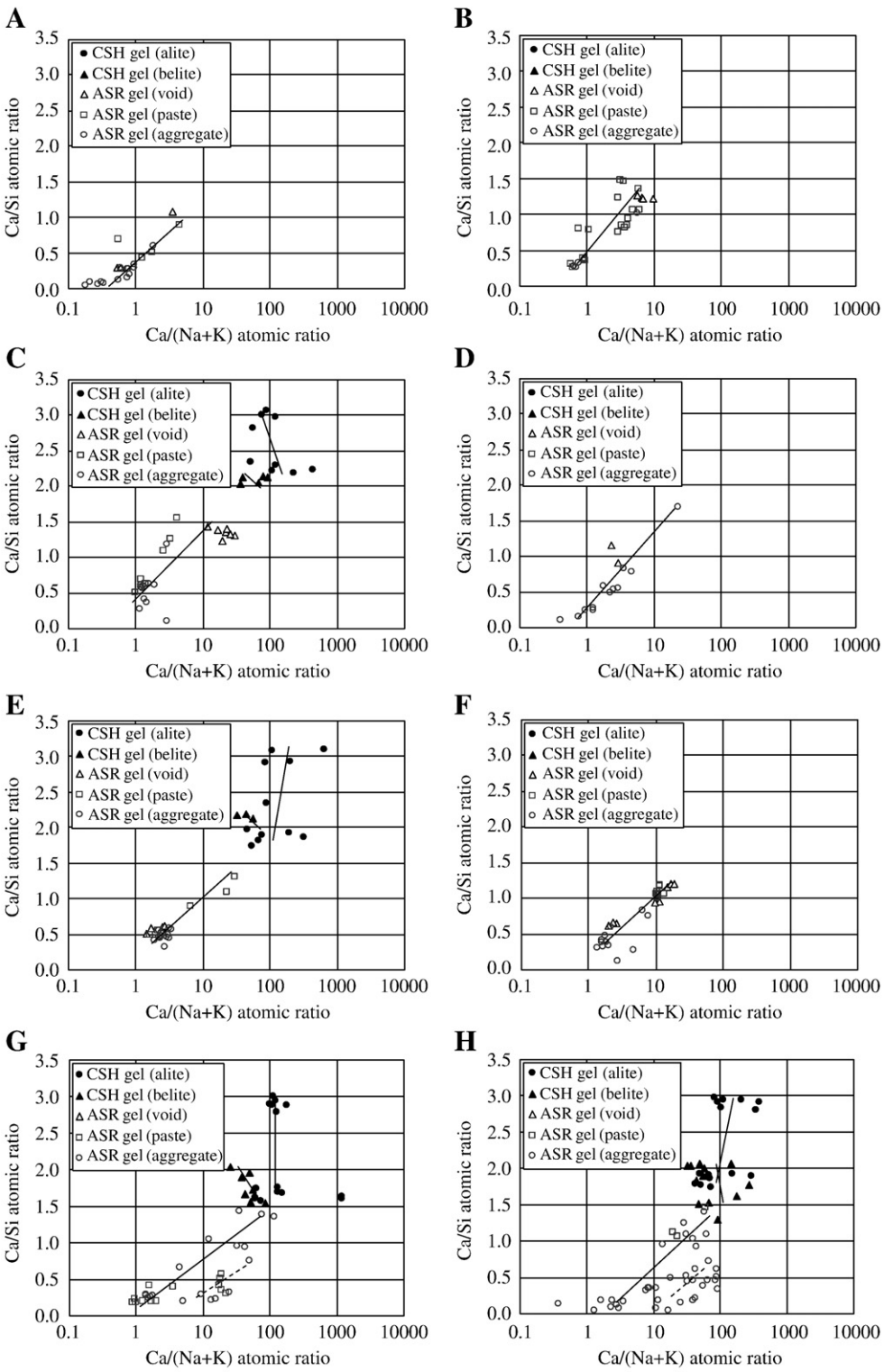

Fig. 9. Compositional trends of ASR gel as determined by SEM-EDS analysis on polished thin sections. RILEM AAR-5 concrete microbars with (A) Austrian siliceous limestone no.9C and (B) dolostone aggregates no.10C; (C) RILEM AAR-5 concrete microbar no.15C and (D) AAR-2 mortar bar no.15F with the Pittsburg aggregate (bulk, MTO stockpile); AAR-5 concrete microbars with the most reactive Pittsburg aggregate (Pit-16, CANMET stockpile) stored in a prolonged period, (E) Na28, and (F) K28; field-deteriorated concretes from Gananoque (G) and Cornwall (H), Ontario. Hydration trends of alite and belite into CSH gel are also shown.

successful. The minute flakes dominating the acid insoluble residue in the Kingston rock (Pit-16, most reactive layer) by hydrochloric acid, had a typical composition of illite: $1/2(K_{0.69}, Na_{0.04}, Ca_{0.02})_2O\cdot(Al_{0.78}, Mg_{0.16}, Fe_{0.06})_2O_3\cdot 4(Si_{0.93}, Al_{0.07})O_2\cdot nH_2O$ or $(K_{0.69}, Na_{0.04}, Ca_{0.01}, X_{0.25})(Al_{1.55}, Mg_{0.32}, Fe_{0.13})(Si_{3.71}, Al_{0.27})O_{10}\cdot(OH)_2\cdot H_2O$, where $X = H_3O$ by balance of $K + Na + (1/2)Ca$ from 1.0. This implies that the influence of leaching by HCl solution was relatively small on this mineral. However, sporadically detected

chlorite in the acid insoluble residue did not yield a good analysis: in one case, the number of (Mg,Fe)O molecule in the compositional formula $5(Mg, Fe)O \cdot Al_2O_3 \cdot 3SiO_2 \cdot 4H_2O$ only attained 3, indicative of the leaching by the acid, while bulk XRD analysis indicated the presence of chlorite.

4.4. XRD analysis

4.4.1. Alteration of cement hydrates

XRD analysis of field concretes from depths 5 cm of the surface gave several diffraction peaks of the basal spacing of cement hydrates at 11.0–11.3°2θ and 11.6°2θ, with occasional peaks at 9.4°2θ in Gananoque, while at 9.1°2θ and 10.8°2θ in Cornwall.

Of the AFm phases, monosulfate and Kuzel's salt were absent. Instead, within less carbonated cement paste, clusters of small tabular crystals (3–5 μm) were visible, belonging to the solid solution between *hydrocalumite* $3CaOAl_2O_3 \cdot Ca(OH)_2 \cdot 12H_2O$ and *Friedel's salt* $3CaOAl_2O_3 \cdot CaCl_2 \cdot 10H_2O$, which was responsible for the peak between 11.0 and 11.3°2θ. Around cement particles in the carbonated areas, irregular-shaped platelet stacks (3–5 μm) were present, which were partly carbonated, hence possibly corresponding to *monocarboaluminate* $3CaOAl_2O_3 \cdot CaCO_3 \cdot 11H_2O$ (11.6°2θ peak).

Among the AFt phases, ettringite (9.1°2θ peak) was limited to non- to less carbonated cement paste, occurring as prisms (5–30 μm) lining air voids or filling cracks in the Cornwall concrete. Highly carbonated cement paste in the Gananoque concrete contained prismatic hydrate (5–10 μm), mostly being replaced by calcium carbonate within interstices between aggregate particles and carbonated cement paste. This is suggestive of carbonate ettringite (9.4°2θ peak), i.e. *tricarboaluminate* $3CaOAl_2O_3 \cdot 3CaCO_3 \cdot 32H_2O$, rather than carboaluminates. Halite and sylvite were absent, and hydrotalcite (11.5 °2θ, 5.5 °2θ peaks) was not positively identified.

4.4.2. Reaction products

With the concrete microbar immersed in NaOH solution until 28 days (Na28), a small diffraction peak at 7.3°2θ suggestive of sepiolite ($4MgO \cdot 6SiO_2 \cdot 7H_2O$) was identified within dolomitic limestone aggregate from the Pittsburg quarry (Pit-16, most reactive layer), while it was absent in the cement paste. Old field concrete in Gananoque made with the Pittsburg aggregate (bulk, 1st lift) also presented this phase (7.2°2θ). Brucite (18.6°2θ) was not positively identified from the mortar bar (no.15F), concrete microbars (Na28, K28) and field concrete using the Pittsburg aggregate, as well as from the field concrete from Cornwall.

4.2.3. Extracts from the aggregate

Reference material opal-A_N (hyalite) from Bohemia presented a diffuse inflated halo at around 18–25°2θ showing the amorphous to poorly-ordered nature to X-ray, both before and after heating at 800 °C. Reference opal-CT specimen from Virgin Valley, Nevada had diffuse peaks (20.6°2θ, 21.6°2θ, 35.6°2θ) with a traceable amount of quartz (20.8°2θ). After heating the phosphoric acid residue, the 21.6°2θ peak (4.11 Å) contracted to 21.9°2θ (4.06 Å) typical of α cristobalite, whereas the quartz peak remained unchanged. Quite similar contraction of the *d*-spacing of opal-CT from $d = 4.10$ Å to $d = 4.06$ Å has been known from long-term burial diagenesis of siliceous sedimentary rocks in the temperature range of 30–55 °C [24]. The result shows that the heat treatment adopted for the silica residue after extraction by phosphoric acid (800 °C, 1 h), causes little problem in the phase transition that interferes the identification of the silica minerals, such as from quartz to cristobalite, or quartz to tridymite.

Acid insoluble residue of the dolomitic limestone from Pittsburg quarry (Pit-16, most reactive layer) consisted of illite (diffuse 8.7–8.8°2θ, 17.6°2θ, 19.7°2θ), chlorite (6.0°2θ, 12.4°2θ), quartz (26.6°2θ), K-feldspar (27.4°2θ) and albite (27.8°2θ). A diffuse peak of the basal reflection indicates that the illite was hydrated or slightly affected by the hydrochloric acid used.

4.5. Extraction of quartz

4.5.1. Phosphoric acid

The Canadian Pittsburg aggregate contained liberated silica minerals ranging from 3.2 wt.% in the bulk aggregate (no.15: 1st lift), used for the AAR-5 concrete microbar and AAR-2 mortar bar tests, to 4.8 wt.% in the most reactive layer (Pit-16). With the Austrian aggregates liberated silica minerals ranged from 6.7–10.0 wt.% in the dolostones (nos.10,12) to 14.3 wt.% in the siliceous limestone containing chert inclusions (no.9: Table 1) [3].

As a reference material, opal-A_N (hyalite) from Bohemia, which presented a diffuse inflated halo because of its X-ray amorphous nature, gave 41.0 wt.% of residue which still remained amorphous even after the heating, while opal-CT from Nevada gave 5.1 wt.% of residue consisting of cristobalite, according to XRD analysis. Thus, opal has a chance of surviving digestion by phosphoric acid, contrary to general expectation.

4.5.2. Hydrochloric acid

The most reactive horizon in the Pittsburg quarry (Pit-16, 1st lift) consisted essentially of argillaceous dolomitic limestone, contained 16.8 wt.% of insoluble residue by HCl, whereas 4.8 wt.% of quartz by H_3PO_4, the latter being mostly cryptocrystalline.

5. Discussion

5.1. General exceptions to ASR

Early researchers in Canada and USA in the 1960s, and more recently in China, believed that the following features distinguish ACR from ASR, that is, in ACR-affected concretes, 1) ASR gel is absent, 2) reaction takes place even with low alkali content, 3) coarse aggregate expands more than fine aggregate, and 4) lithium and other inhibitors are not effective. However, all these aspects also apply to typical ASR, as discussed below. In the previous discussions of ACR, however, these exceptions to ASR have been used as a proof of ACR without counterargument. Modern petrographic techniques applied here are useful in examining them.

5.1.1. Absence of apparent reaction rims

Concretes undergoing late-expansive ASR, some formerly called alkali-silicate reaction in the 1970s, lack conspicuous ASR gel which is invisible on a lapped surface. ASR gel may have been lost by inappropriate sample preparation, including excessive cooling water, or too rough cutting. In the present author's experience, internal reaction rims are less evident in some typical late-expansive aggregates on fracture surfaces free from sample preparation artifacts, e.g. quartzite (Old Smorral Lane Bridge, UK [25,26]), metaquartzite (Princess Highway Bridge, Victoria, Australia [27]), argillaceous limestone (R.H. Saunders Dam, Ontario [28]) and siliceous limestone (du Vallon Viaduct, Quebec, Canada [29]). Reactive constituents are cryptocrystalline quartz in the limestone and microcrystalline quartz in the quartzite, they are too scant and unevenly distributed (e.g. as veins and layers) to form evident internal reaction rims of ASR gel. In these cases, alkali-rich ASR gel originating from the reactive constituents fills cracks, forming veins within the aggregate. It is considered that the ASR gel formed with a volume increase within the aggregate particles expands, aided by the counter force from the rigid framework of surrounding minerals (coarsely grained non-reactive quartz or microcrystalline calcite) in the aggregate and from hardened cement paste and further expands upon absorption of water.

In the typical ACR reactive Pittsburg aggregate, no distinct rim was visible in the RILEM concrete microbar [3], but it was visible on some coarse aggregate particles in the CSA concrete prism and in

the field concrete. Thus, it is not a unique feature of ACR that the reaction products are macroscopically less apparent, but is common to ASR.

5.1.2. Low alkali to develop deleterious expansion

ASR has a well-known "pessimum proportion" effect of aggregate mix. It has been noted that the higher the reactivity of silica minerals, the smaller the pessimum proportion, and the lower the alkali content necessary to produce deleterious expansion in mortar and concrete, i.e. Na_2Oeq <3.0 kg/m^3. The pessimum proportion of the silica minerals from highly reactive to slowly reactive increases as follows: opal (<5 wt.%), cristobalite, tridymite (<10 wt.%), chalcedony (20 wt.%), cryptocrystalline quartz (50 wt.%), microcrystalline quartz (>80 wt.%) [30,31]. Aggregates containing these correspondingly range from early-expansive to late-expansive. With volcanic glasses, alkali reactivity increases with SiO_2 content: basaltic glass (non-reactive)<andesitic glass (marginally reactive)<dacitic glass<rhyolitic glass (reactive, pessimum proportion 100 wt.%)< hydrated rhyolitic glass (highly reactive) [30,31].

Let us review the currently accepted threshold value of cement alkali that produces deleterious ASR, i.e. Na_2Oeq 0.6 wt.%. This was first proposed by Stanton in the early 1940s based on the mortar bar test with early-expansive sand aggregate containing Neogene opaline shale and chert (Modelo formation) in California, USA [32]. However, this threshold should be greatly lowered when reactive aggregate is present at pessimum proportion. Woolf [33] indicated that opal at a pessimum proportion (1 wt.%) produces deleterious expansion even with low-alkali cements: e.g. cement alkali Na_2Oeq 0.22–0.24 wt.% and mortar alkali 1.4–1.5 kg/m^3 produced expansion >0.1 l/l% at 1 year; while Na_2Oeq 0.27–0.29 wt.%, 1.8 kg/m^3, produced expansion >0.1 l/l% at 6 months, when the cement content of 640 kg/m^3 is assumed here. In field concrete, Spratt limestone (Ordovician Bobcaygeon Formation) in Ontario, Canada, according to Hooton et al. [34], produced late-expansive ASR (cracking after 12 years) in the experimental pavement made with low-alkali cement (Na_2Oeq 0.43 wt.%), i.e. concrete alkali 1.9 kg/m^3. The reactive constituents of this limestone have been known to be chalcedony and cryptocrystalline quartz. Likewise, the combined presence of cristobalite in andesite that was accidentally included (2 vol.%) in coarse aggregate and crypto- to microcrystalline quartz in the sand aggregate (siliceous shale, chert, quartzite) in concrete, produced ASR in the retaining wall, with estimated concrete alkali of Na_2Oeq 2.2 kg/m^3 [9]. Thus, the well-accepted threshold for ASR of concrete alkali Na_2Oeq 3.0 kg/m^3 must be lowered for highly reactive opal and cristobalite, and moderately reactive chalcedony when pessimum condition is considered.

As for ACR, no pessimum proportion has been reported [35]. Newlon et al. [36] studied dolomitic limestone aggregate (Ordovician Beekmantown formation) in Virginia, USA, and revealed that harmless rim-formation due to dedolomitization develops in concrete prism made with low-alkali cement Na_2Oeq 0.43 wt.%, 1.2 kg/m^3, whereas deleteriously expansive ACR (expansion >0.03 l/l% at 1 year, >0.05 l/l% at 5 years) occurs with high-alkali cement Na_2Oeq 0.67 wt.%, 1.8 kg/m^3 (cement mix 270 kg/m^3). Based on concrete prisms with Pittsburg aggregate (bulk, 1st lift), Swenson and Gillott interpolated that a threshold of producing unacceptable expansion by ACR (e.g. cracking: expansion >0.06 l/l%) with cement alkali is around Na_2Oeq 0.4–0.45 wt.% [35]. This possibly corresponds to Na_2Oeq 1.2–1.4 kg/m^3 when the cement mix of 310 kg/m^3 is assumed. The above threshold is again lower than the conventionally accepted 3.0 kg/m^3 for ASR, and even lower than that of the above discussed ASR. However, considering that the storage period in the concrete prism test is longer than the mortar bar test, there seems to be no essential difference in the thresholds between ACR and above discussed ASR. Rapid reaction of the cryptocrystalline quartz in the dolomitic aggregates in comparison with the chert and flint aggregates with a dense texture, is probably due to the fact that rapid dedolomitization exposes the cryptocrystalline quartz to alkaline solution, enhancing the occurrence of chemical reactions.

5.1.3. Larger expansion in coarse aggregate

ASR also presents a "pessimum size" effect of aggregate. Contrary to general expectation, some aggregates produce less expansion in the mortar bar than in the concrete prism made with coarse aggregate, even tested at a pessimum proportion. Cretaceous British flint represents such a typical example [37]. It has a heterogeneous texture with a porous cortex around a dense core, with varying content of chalcedony and cryptocrystalline quartz, and possible presence of opal. Of Eocene flint in northern Germany, dense particles in the concrete bar expand the most in a coarse fraction (size 3–7 mm) with increased pessimum proportion [38]. These particular behaviors may be a result of separation of reactive silica during crushing of the aggregate due to inhomogeneity of the texture. This means that coarse and fine fractions obtained from the same material have different mineral compositions with different reactivity. However, it is also likely from a general account of *pozzolanic reaction* versus ASR for the same material, that fast-reacting material in a fine fraction is either absorbing calcium from cement paste and converting ASR gel into CSH gel by a pozzolanic reaction, or immediately consumed by dissolution into pore solution, and hence unable to cause expansion. In contrast, the same material in the coarse aggregate is protected by the larger particles, less exposed to immediate dissolution, and ASR gel is unaltered within the aggregate thus causing expansion. A similar situation probably applies to ACR, although the reaction product is not CSH gel, but Mg-silicate gel, as discussed later.

Another important feature of ASR testing is that late-expansive aggregates shall also be examined by means of concrete prism, like ACR aggregates. Concrete prism test (CSA 23.2–14A, ASTM C1293) reproduces deleterious expansion of aggregates with poor field records due to microcrystalline quartz which lacks pronounced pessimum phenomenon, whereas mortar bar test (ASTM C227) misses most of them, e.g. Canadian *alkali-silicate* reactive Paleozoic argillite and greywacke in Nova Scotia (Cambro-Ordovician Meguma Group) although with a tendency to develop larger expansion with larger particle size in the mortar bar [39], Australian granite and metaquartzite gravel in Victoria [40,41]. Similarly, the accelerated mortar bar tests (CSA 23.2–25A, ASTM C1260) using NaOH solution misses deleterious reactivity of several aggregates, including Canadian Potsdam sandstone [42], Precambrian granites and gneisses of Grenville age in Ontario [43], Brazilian quartzite [44], British flint and Japanese chert. The reason why coarse aggregate is used is because it can minimize the loss of reactive silica (microcrystalline quartz and quartz overgrowths) intercalated within hard matrix of the aggregate during crushing and sieving, and it has a long reaction path (radius of aggregate) so that alkali-rich ASR gel remains unaltered by the cement paste for a longer time to develop continuous expansion. Conversely, alkaline solution used in the accelerated test dissolves flint and chert thus producing less expansion.

ACR reactive aggregates (Pittsburg aggregate) present no pessimum size effect: the larger the aggregate, the more the expansion [35]. This aggregate produces small expansion in the mortar bar and in the accelerated mortar bar, which tests as innocuous, but generates deleterious expansion in the concrete prism. These expansion characteristics are not unique to ACR only, but common to ASR-reactive British flint.

5.1.4. Ineffective inhibitors to ASR expansion

Lithium compounds do not suppress deleterious expansion of some late-expansive aggregates [45]. Similar inefficiency is also known with slag and fly ash applied to ASR-reactive coarse aggregates, depending on their mix proportion and the pessimum proportion of reactive minerals. For example, crushed andesite aggregate with highly reactive cristobalite produced severe ASR damage to a viaduct in Japan which contained 18 wt.% of fly ash [46]. However, fly ash in a similar amount was generally effective in suppressing late-expansive ASR due

to quartzite, sandstone and devitrified rhyolitic welded tuff in the gravel aggregate in other viaduct, according to the author's experience. Japanese fly ash belongs to *low-Ca fly ash* and is capable of preventing ASR, when it is used in appropriate sufficient quantity and its reactivity is higher than that of reactive constituents in the aggregate. The same things apply to the slag in concrete.

5.2. Intra-deposit variation of geological origin

Austrian Jurassic carbonate aggregates, both crushed stone (no.9) and gravels (nos.10,12), vary considerably in rock lithology (Table 1). This inhomogeneity caused some inconsistency between the published amounts of total SiO_2 [5,7] and the amounts of extracted quartz in this study.

Canadian dolomitic rocks in the Pittsburg quarry (Ordovician Gull River Formation) are thinly bedded, and those from the first lift are the source of standard reactive aggregate (no.15, Pittsburg aggregate: bulk, 1st lift, MTO stockpile) capable of producing alkali-carbonate reaction. They contain argillaceous dolomitic limestone, argillaceous limestone, argillaceous dolostone and dolomitic limestone and calcisiltite [6,47], and the rock types shown in Table 1. Of these, the most reactive horizon, #16 (=Pit16) after Grattan-Bellew, was thinly bedded dark grey limestone [48], from which he collected a thickness of 1 m (Pt-16, 1st lift, CANMET stockpile) [8], which approximately corresponded to layers nos.35–37 after Rogers, who had performed the rock cylinder test earlier [6]. However, even within this horizon, the lithology of the carbonate rocks varies from argillaceous dolomitic limestone and micritic limestone (Table 1).

For instance, according to Grattan-Bellew et al. [49], the above mentioned most expansive layer of the quarry (Pit-16) contained 11 wt.% of acid insoluble residue (HCl) of which 96 wt.% was composed of cryptocrystalline quartz, whereas the present author's sample from the same stockpile was more argillaceous; containing only 5 wt.% of cryptocrystalline quartz, based on phosphoric acid treatment (Table 1), and a high amount of acid insoluble residue (17 wt.%) rich in illite and quartz as ascertained by XRD analysis. Such striking inhomogeneity of the aggregate explains the wide difference among interpretations of petrographic examinations by different authors in the past, and the difficulty in attributing the true cause of the expansion of this aggregate. The difference between the residues (11 wt.%) in the two treatment methods (H_3PO_4, HCl) may roughly represent the content of clay minerals and feldspar, if the solubility of cryptocrystalline quartz into phosphoric acid is not particularly high (cf. Fig. 6D,E,H). Previous work by the present author [1,3–5] reassigned the cause of deleterious ACR to be genuine ASR of cryptocrystalline quartz, which was recently confirmed by Grattan-Bellew et al. [49].

5.3. Geological background of silica minerals

It has been a long-standing enigma whether the Pittsburg aggregate contains opal or not, since this aggregate produces rapid and large expansion in concrete prism without showing any pessimum phenomenon that is characteristic of opal. In the early 1960s, Gillott [50] reported the absence of opal in the insoluble residue of acetic acid treatment of this aggregate. At that time, no account was made of this, because concepts of *diagenetic zonation* of strata had not yet been established in sedimentary geology. *Burial diagenesis* can explain the reason for this. During burial of sediments, authigenic minerals appear and tend to form an equilibrated assemblage, constituting the vertically arranged mineralogical zones in the thick profiles of strata, in accordance with progressive increase in temperature that promotes interactions between minerals with interstitial water.

5.3.1. Opal diagenesis

Silica minerals have been known to constitute a vertical distribution in thick piles of sedimentary formations. For example, Neogene profiles in Japan comprise 1) the biogenic opal zone, 2) the opal-CT zone, and 3) the quartz zone in descending order [24], with transformation of opal-CT through chalcedonic quartz to microcrystalline quartz [51]. In general, the grain size of quartz tends to be coarser in Paleozoic cherts than in Cenozoic cherts [52]. Kinetic study of opal by Mizutani [53] indicates that conversion of this mineral through cristobalite into quartz is promoted by the temperature and lapse of time, and that both opal and cristobalite should be transformed into stable quartz in pre-Tertiary rocks during progressive burial diagenesis. If opal is found in pre-Tertiary rocks, then it should be later material precipitated in a younger age [53]: flint nodules containing opal-CT in Cretaceous pelagic chalks in Western Europe are probably of this sort.

When the above principle could be applied to the Jurassic carbonate rocks from Austria (nos.9,12,13) and the Ordovician dolomitic rock from Kingston, Canada (no.15), it seems unlikely that these rocks preserve a primary biogenic opal, if there was any. All these could belong to the quartz zone. No development of caliche that forms opal was observed on the weathered surface of the carbonate rocks around the Pittsburg quarry in Kingston.

5.3.2. Assemblage of authigenic minerals

Another look at diagenesis is in terms of mineral assemblages of zeolite–clay mineral–silica mineral, which are useful in speculating the origin of secondary opal in the argillaceous carbonate rocks. Utada [54] subdivided Japanese Neogene profiles into five alteration zones from top to bottom based on zeolitic assemblage with accompanying authigenic minerals shown here in parentheses: I) altered glass zone, II) clinoptilolite–mordenite zone (secondary opal, smectite), III) analcime–heulandite zone (quartz, mixed-layer clay), IV) laumontite zone (quartz, mixed-layer clay, chlorite), and V) albite zone (quartz, sericite, chlorite, K-feldspar). The temperature of the top and the bottom of the zeolite zones was reported to be 40–50 °C and 80–100 °C, respectively, from borehole data in the areas where diagenesis is progressive [55]. These alteration zones reach the Mesozoic strata where geothermal gradient is low, or they grade into lower-grade metamorphism around the intrusive body, starting from the zone VI) characterized by the assemblage of prehnite–epidote–chlorite. In sedimentary rocks, illite corresponds to sericite in volcaniclastic rocks. Considering that the cryptocrystalline quartz in Kingston dolomitic limestone is in the process of coalescent grain growth into prismatic quartz (Fig. 6C,D) [3], and that neither zeolites nor metamorphic minerals are present, the assemblage of authigenic mineral is represented by illite–chlorite–quartz, corresponding to the zone V. There is again little possibility that opal exists in this rock.

5.4. Mechanisms of ACR

5.4.1. Dedolomitization

The process of dedolomitization, typically the formation of brucite, is thought to be a harmless reaction, because no expansion cracks formed in the cement paste with the Austrian dolostone aggregate (Fig. 2A,C). This can be understood by a simple calculation that the total molar volume of the solid materials within dolomite rhombs (cm^3/mol), i.e. molar weight (g/mol) divided by its density (g/cm^3), decreases after dedolomitization, as shown by Eq. (1). In the reaction rim, brucite and calcite form a pseudomorph after the dolomite rhombs. This type of calculation only holds when the solid phases form in the place same as the solid precursor. Actually, however, according to the observation, part of the liberated CO_3 ions migrates from the reacting dolomite crystal into the surface of aggregate, precipitating calcite along cracks within the aggregate [4]. As a result, the total solid volume of the phases that form within the dolomite crystal (brucite + portlandite) becomes smaller than the figure shown here.

The reason why a dense carbonate halo developed within interstices between two adjacent aggregate particles is that carbonate ions released from the reacting dolomitic aggregate were concentrated within a closed space.

	Aggregate			Reaction rim (dedolomitization)		
	$CaMg(CO_3)_2$ +	2NaOH	→	$Mg(OH)_2$ + $CaCO_3$ +		Na_2CO_3
	Dolomite	Water-soluble		Brucite	Calcite	Water-soluble
Molar volume:	184.41/2.85	(80.00/2.13)		58.34/2.38	100.09/2.71	(105.99/2.53)
	64.71	(37.56)		24.51	36.93	(41.89)

Volume change: [(24.51 + 36.93) – 64.71] × 100/64.71 = – 5.1 vol.% (1)

5.4.2. Formation of carbonate halo

The formation of the carbonate halo in cement paste can be simplified as Eq. (2). This is a dissolution–precipitation process involving mobile Ca, alkali and CO_3 ions in an open system, i.e. a kind of *metasomatism*. The liberated CO_3 ion from dolomite, while diffusing into the cement paste, dissolves portlandite to produce Ca ions. Unlike a closed system, reaction product calcite precipitates, not within the same position as the original reactant (portlandite), but within available interstitial voids in the cement paste that are in a small distance from the original portlandite. Consequently, the cement paste does not produce a volumetric expansion. From Eqs. (1) and (2), it is clear that alkalies (Na, K) are regenerated during dedolomitization. Though such dedolomitization reaction does not cause expansion, it maintains a high level of alkalinity or pH, which favors the speed of ASR and diminishes the efficiency of fly ash and other mineral additives to counteract ASR.

gel) that is characteristic of atmospheric decomposition [19] and intense aqueous leaching [56] occurs. In the carbonation process, calcite replaces CSH gel forming a calcite crust (Fig. 4F), while liberated water-soluble alkali-silicate diffuses into porous cement paste surrounding the calcite crust. Instead, liberated water-soluble silicate is further combined with Ca ion to regenerate CSH gel through a *pozzolanic reaction*, which presents a diffuse rim surrounding the coarse aggregate, as in Eq. (4) although this may not be a stable reaction depending on the Ca/Si ratio of the CSH gel formed. The newly formed pozzolanic CSH gel is absorbed within interstitial porosity of the cement paste, while regenerated alkalies are distributed as a narrow zone (Fig. 3A,B) that out-skirts the carbonate halo [3]. The pozzolanic CSH gel was not evident in old concrete hindered by the carbonation of cement paste, but could be seen in fresh laboratory specimens. Although these two processes accompany local volume changes, the overall reactions (sum of Eqs. (3), (4)) are equivalent to the simple Eq. (2), which is independent of the local dissolution and precipitation of CSH gel and alkali-silicate.

	Cement paste (hydroxide)			Carbonate halo (carbonation)	
	$Ca(OH)_2$ +	Na_2CO_3	→	$CaCO_3$ +	2NaOH
	Portlandite	Water-soluble		Calcite	Water-soluble
Molar volume:	74.09/2.21	(105.99/2.53)		100.09/2.71	(40.00 × 2/2.13)
	33.52	(41.89)		36.93	(37.56)

Volume change: (36.93 – 33.52) × 100/33.52 = + 10.2 vol.% (2)

5.4.3. Decomposition and regeneration of CSH gel

Upon carbonation of cement paste in pore solutions, CHS gel is decomposed into calcite and possibly water-soluble silicate with wet appearance, as in Eq. (3). Because CSH gel has a low Si content, it does not form expansive alkali-silica gel with higher polymerization of silicate. The composition of CSH gel was conveniently taken as $3CaO{\cdot}2SiO_2{\cdot}3H_2O$ [23] (afwillite or foshallasite, density of the latter to be used), not that of tobermorite (e.g. $5CaO{\cdot}6SiO_2{\cdot}5H_2O$) or more siliceous materials, because pore solution is saturated with Ca, it is unlikely that low-Ca CSH gel (e.g. $0.2CaO{\cdot}SiO_2{\cdot}nH_2O$, eventually silica

5.4.4. Formation of hydrotalcite

At the aggregate–paste interface dolomite *incongruently* dissolves, liberating Ca and CO_3 ions into cement paste, and absorbs aluminate ion $Al(OH)_4^-$ from the cement paste, as in Eq. (5). The origin of migrated aluminium was conveniently taken as gibbsite, $Al(OH)_3$ or $1/2(Al_2O_3{\cdot}3H_2O)$, because of its soluble nature under high-alkaline condition [$Al(OH)_3 + H_2O = Al(OH)_4^- + H^+$], and molar volume twice

	Cement paste (silicate)				Carbonate halo	Alkahi silicate sol (wet appearance)	
	$3CaO{\cdot}2SiO_2{\cdot}3H_2O$ +	$3Na_2CO_3$ +	$8H_2O$	→	$3CaCO_3$ +	$2(Na_2O{\cdot}SiO_2{\cdot}5H_2O)$ +	2NaOH
	CSH gel	Water-soluble	Water		Calcite	Water-soluble	Water-soluble
Molar volume:	342.48/2.5	(317.97/2.53)	(144.12/1.00)		300.27/2.71	(424.30/1.75)	(80.00/2.13)
	136.99	(125.68)	(144.12)		110.80	(242.46)	(37.56)

Volume change: (110.80 – 136.99) × 100/136.99 = – 19.1 vol.% (3)

	Alkali silicate sol (wet appearance)		Pozzolanic reaction (CSH gel)		
	$2(Na_2O{\cdot}SiO_2{\cdot}5H_2O)$ +	$3Ca(OH)_2$	→	$3CaO{\cdot}2SiO_2{\cdot}3H_2O$ + 4NaOH +	$8H_2O$
	Water-soluble	Portlandite		CSH gel	Water-soluble	Water
Molar volume:	(424.30/1.75)	222.27/2.21		342.48/2.5	(160.00/2.13)	(144.12/1.00)
	(242.46)	100.57		136.99	(75.12)	(144.12)

Volume change: (136.99 – 100.57) × 100/100.57 = + 36.2 vol.% (4)

	Aggregate–paste interface					
	$6[Ca{\cdot}Mg(CO_3)_2]$ +	$(Al_2O_3{\cdot}3H_2O$ +	$2H_2O)$ +	10NaOH +	$2H_2O$	
	Dolomite	Water-soluble (gibbsite)		Water-soluble		
Molar volume:	1106.46/2.85	(156.02/2.40)	(36.03/1.0)	(399.97/2.13)	(36.03/1.0)	
	388.23	(65.01)	(36.03)	(187.78)	(36.03)	
→	$6MgO{\cdot}Al_2O_3{\cdot}CO_2{\cdot}12H_2O$	+ $6(CaCO_3)$	+	$5(Na_2CO_3)$		
	Hydrotalcite	Calcite		Water-soluble		
Molar volume:	603.98/2.06	(600.64/2.71)		(529.95/2.53)		
	293.19	(221.64)		(209.47)		

Volume change: (293.19 – 388.23) ◊ 100/388.23 = – 24.5 vol.% (5)

that of the unit cell was used. A narrow rim composed of hydrotalcite forms on the dolomite rhombs that closely contact the cement paste (Figs. 1B, 3C), with a substantial volume loss leaving porosity within the rhombs. The liberated Ca and CO_3 diffuse into the porous cement paste contributing to produce a carbonate halo (calcite). This reaction is typical of metasomatism caused by the replacement of mobile components between dolomite and cement paste, keeping the texture of the original outlines of dolomite rhomb.

Incongruent dissolution can best be understood by the case with hydration of calcium silicates in Portland cement. Alite hydrates to produce CSH gel, leaving a porous pseudomorph and liberating Ca ions into pore solution. This Ca is precipitated as portlandite within interstitial spaces in the cement paste surrounding the alite. With alite hydration, no volume increase occurs in the alite, as in Eq. (6). For belite, some increase could occur depending on the compositions of CSH gel to be formed, but volume changes in the hydration process causes no problem during hardening.

$$\begin{array}{lcccc} & \text{Cement} & & \text{Hydration rim} & \text{External precipitate} \\ & 2(3CaO{\cdot}SiO_2) + 6H_2O & \rightarrow & 3CaO{\cdot}2SiO_2{\cdot}3H_2O + & 3Ca(OH)_2 \\ & \text{Alite} & & \text{CSH gel} & \text{Portlandite} \\ & \text{Precursor} & & \text{Alite pseudomorph} & \text{Pore filling in cement paste} \\ \text{Molar volume:} & 2\times 228.33/3.15 \quad (108.09/1.00) & & 342.48/2.5 & (222.27/2.21) \\ & 144.97 \quad (108.09) & & 142.7 & (100.57) \\ \text{Volume change:} & (136.99-144.97)\times 100/144.97 = -5.5\ \text{vol.\%} & & & \end{array} \tag{6}$$

5.4.5. Formation of Mg-silicate gel and chlorite-like phase

With the most reactive Pittsburg aggregate rich in cryptocrystalline quartz (Pit-16, 1st lift), both dedolomitization and expansion of concrete microbars continued steadily with time (0.21% l/l at 28 days [7]), but all brucite altered to Mg-silicate gel due to interaction with ASR gel (Fig. 8A,B), whereas ASR gel formed abundantly filling expansion cracks (Fig. 3A,B). Mg-silicate gel is deemed non-expansive or less expansive than the real ASR gel, because it accompanied no cracks [3–5]. Mg-silicate gel has also been identified from a marine concrete as a less-expansive material replacing ASR gel [57].

Sepiolite identified by XRD is thought to be a crystalline phase of Mg-silicate gel. Mitchell and Margeson [58] noted a basal peak at 7.3°2θ to occur in Pittsburg aggregate subjected to accelerated treatment and attributed it to a sheet silicate resembling 11 Å tobermorite. It is reasonable to assume that the new phase was sepiolite formed through crystallization of Mg-silicate gel. The reaction to form Mg-silicate gel may be expressed as Eq. (7), approximating composition and density by those of sepiolite. For simplification, as discussed later, ASR gel was represented here by kanemite, $NaHSi_2O_5{\cdot}3(H_2O)$ or $1/2(Na_2O{\cdot}4SiO_2{\cdot}7H_2O)$. Since the total of solid volumes decreases after the formation of Mg-silicate gel, expansion of concrete is attributable to real ASR that precedes Mg-silicate gel. In the dolomitic aggregate undergoing ACR, brucite decreases with increasing Mg-silicate gel.

Although a small amount of chlorite pre-exists in the virgin aggregate from Pittsburg quarry, it can also form in the mortar bar and field concrete with Pittsburg aggregate (Figs. 7E, 8C). This can be described as Eq. (8), a reaction between Mg-silicate gel, brucite, and aluminium hydroxide (gibbsite) originating from the argillaceous matrix, including feldspar, illite and chlorite. It is not certain whether the original chlorite contained in the aggregate behaves as a precursor to newly produced chlorite.

5.5. ASR in dolomitic aggregates

5.5.1. Alkali-silica reaction

In the province of Quebec, Canada, many concrete structures (Quebec City, Ste. Foy, Beauport, Bécancour, etc.) have been deteriorated by ASR of carbonate aggregates, not by ACR [59]. Katayama [4] revealed that ASR gel had formed from cryptocrystalline quartz in the dolostone, dolomitic limestone and limestone aggregates in concretes, and that, while dedolomitization was involved and Mg-silicate gel had formed, ASR gel was responsible for cracking.

Relevant to typical ACR in Ontario (Gananoque and Cornwall) which is the subject of this paper, ASR of cryptocrystalline quartz in the dolomitic aggregates is also thought to be responsible for the expansion cracks in concretes, because this quartz was identified as the actual reactive constituent in both the laboratory and in field-

$$\begin{array}{lcccc} & 4Mg(OH)_2 + 1.5(Na_2O{\cdot}4SiO_2{\cdot}7H_2O) & & & \\ & \text{Brucite} \quad \text{ASR gel (kanemite)} & & & \\ \text{Molar volume:} & 233.28/2.36 \quad 642.68/1.93 & & & \\ & 98.85 \quad 332.99 & & & \\ & \rightarrow 4MgO{\cdot}6SiO_2{\cdot}7H_2O + 3NaOH + 6H_2O & & & \\ & \text{Mg-silicate gel (sepiolite)} \quad \text{Water-soluble} & & & \\ \text{Molar volume:} & 647.89/2.14 \quad (119.99/2.13) \quad (108.091.00) & & & \\ & 302.75 \quad (56.33) \quad (108.09) & & & \\ \text{Volume change:} & [302.75-(98.85+332.99)]\times 100/(98.85+332.99) = -29.9\ \text{vol.\%} & & & \end{array} \tag{7}$$

$$\begin{array}{lcccc} & 4MgO{\cdot}6SiO_2{\cdot}7H_2O + 6Mg(OH)_2 + 2(Al_2O_3{\cdot}3H_2O + 2H_2O) & & & \\ & \text{Mg-silicate gel (sepiolite)} \quad \text{Brucite} \quad \text{Water-soluble (gibbsite)} & & & \\ \text{Molar volume:} & 647.89/2.14 \quad 349.92/2.36 \quad (312.01/2.40) \quad (72.06/1.00) & & & \\ & 302.75 \quad 148.27 \quad (130.00) \quad (72.06) & & & \\ & \rightarrow 2(5MgO{\cdot}Al_2O_3{\cdot}3SiO_2{\cdot}4H_2O) + 15H_2O & & & \\ & \text{Clinochlore} & & & \\ \text{Molar volume:} & 2\lozenge 555.84/2.55 \quad (270.23/1.00) & & & \\ & 435.95 \quad (270.23) & & & \\ \text{Volume change:} & [435.95-(302.75+148.27)]\lozenge 100/(302.75+148.27) = -3.3\ \text{vol.\%} & & & \end{array} \tag{8}$$

deteriorated concretes. In both concrete prism and field concretes, evidence of ASR is often obliterated, as indicated by later carbonation of crack-filling ASR gel. Nevertheless, ASR gel can be identified in polished thin sections by the combination of SEM and SEM-EDS analysis. As shown earlier, the compositions of ASR gel in both field (Fig. 9G,H) and laboratory specimens (Fig. 9A–F) were similar to typical ASR in different aggregates from across the world, including Japan with [22] and without freeze–thaw [20] and Newfoundland, Canada [21], as well as to the concrete prism stored in alkaline solution with and without freeze–thaw cycles [9]. This means that ASR gel in the dolomitic aggregates, during migration from the reacted aggregate, exchanges initial alkalies for calcium, approaching the "convergent point" where ASR gel and CSH gel seem to coexist in chemical equilibrium. The wide scatter of ASR gel in compositions results in a short parallel compositional line with Canadian field concretes (*type II evolution*), and can be attributed to leaching of alkalies during freeze–thaw weathering combined with carbonation along cracks.

5.5.2. Reviewing typical ASR for comparison

A comparison was made here between ASR gel in typical ASR-affected concretes with ASR gel in ACR-affected concretes. What characteristics do typical ASR products (gel, foils, rosettes, etc.) have? In the 1980s, comparative studies were done of ASR gel based on XRD analysis and spot chemical analysis by EDS or WDS, but none of the published XRD peak patterns of crystallized ASR gel (rosette-type) exactly fitted with known calcium-alkali-bearing sheet silicates.

A moisture-sensitive 12 Å phase (rosette-type) in ASR gel has been identified by Cole and Lancucki [60,61] from an old dam concrete in Australia, whose XRD peak patterns did not match any known substance. They interpreted that rhodesite with 12 Å reflection [$KHCa_2Si_8O_{19}\cdot 5H_2O$ or $1/2(K_2O\cdot 4CaO\cdot 16SiO_2\cdot 11H_2O)$] was converting to okenite. The reaction might be described as: $4\times$okenite $=2\times$rhodesite (with substitution $K_2O=CaO$) $+$ $3\times$portlandite $+2H_2O$. Another 12 Å phase was reported by Shayan and Lancucki [62] in freshly exuded ASR gel from a bridge concrete in Australia, which readily crystallized into a rosette. The analytical data they gave indicates an average composition to be $(Na_{0.53}, K_{0.49})_2O\cdot 0.98CaO\cdot 4.98SiO_2\cdot 4.03H_2O$ with ratios [Ca/Si] = 1/5.08, [Ca]/[Na + K] = 1/2.08, based on EDS analysis (pressed powder, 15 kV, 5 nA, counting time 100 s) along with wet chemical analysis of water after correcting the contamination during the sampling. This phase has no corresponding mineral but its [2Na + 2K + Ca]/[Si] ratio is 1/2.49, intermediate between that of rhodesite (1/3.2), okenite (1/2) and mountainite (1/2).

Durand and Berard [63] conducted SEM-EDS analysis (polished, 15 kV, 15 nA, counting time 300 s) of ASR gel in siliceous limestone aggregates in deteriorated concretes from Quebec province, Canada (Montreal, Trois-Rivieres, Quebec City and Temiscaming). Chemical composition of ASR gel veins within reacted limestone aggregates had a constant composition: 51.3 wt.% SiO_2, 12.4 wt.% CaO, 7.8 wt.% K_2O, 6.3 wt.% Na_2O, 2.3 wt.% FeO, with remaining 19.9 wt.% attributed to H_2O. Compositional formula calculated here from the above analysis is $[Ca_{0.52}, (Na_2)_{0.24}, (K_2)_{0.19}, Fe_{0.07}]_{1.02}O\cdot 2SiO_2\cdot 2.59H_2O$, with [Ca/Si] = 1/3.86, [Ca]/[Na + K] = 1/1.67, [2Na + 2 K + Ca + Fe]/[Si] = 1/1.96. If a substitution of CaO = (2Na,2K,Fe)O is possible, then this material corresponds to okenite, $CaO\cdot 2SiO_2\cdot 2H_2O$. Bérubé and Fournier reported from several structures a set of XRD peaks (10.4–10.6 Å, 8.4–8.5 Å) resembling okenite (10.3 Å, 8.8 Å, 21.0 Å), except for the lack of 21 Å peak and that one specimen presented a 12 Å peak [59].

In order to avoid contamination of quartz and calcite during sample collection, the use of micro-XRD analysis of ASR gel was very helpful. Such a measurement of ASR gel from old bridges in New Brunswick, Canada [64] presented diffraction peaks, ranging from poorly crystalline to well crystalline with up to 40 peaks between 5 and 60°2θ, (Rigaku PSPC-MDG, CuKα, 60 kV, 200 mA, beam diameter 100 μm, step size 0.08°2θ). One of old void-filling gel with a rosette-type texture had both 12 Å and slightly dehydrated 10 Å reflections. The average composition calculated here from published data by WDS analysis (polished, 15 kV, 10 nA, counting time for alkalies first 5 s, average of 4 points in void B [64]) is: $(Na_{0.44},K_{0.56})_2O\cdot 1.94CaO\cdot 5.77SiO_2\cdot nH_2O$, [Ca/Si] = 1/2.98, [Ca]/[Na + K] = 0.97, [2Na + 2K + Ca]/[Si] = 1/1.96 (n = 8.7, if the difference 22.6 wt.% from 100 wt% is simply attributed to water, ignoring porosity). This was different from the 12 Å phase in Australia but was close to a modified composition of mountainite $[(Na,K)_2O\cdot 2CaO\cdot 6SiO_2\cdot 4.5H_2O]$, except for water content and XRD peak patterns. Larger amount of Ca in the Canadian material than in the Australian material is due to the old gel, in which diffusion of Ca ion from cement paste into ASR sol/gel had proceeded, followed by later crystallization into rosette.

Mountainite has been identified in ASR products in a deteriorated gravity dam in India [65]. It is interesting to note that both rhodesite and mountainite have a habit of presenting flattened rosettes, similar to the rosettes crystallized from ASR gel, but rhodesite has [Ca/Si] = 1/4, [Ca]/[Na + K] = 2.0 and hence does not fit with any reported compositions of ASR gel on the compositional lines presented in this study (Fig. 9). Contrary to this, typical ACR reactive dolomitic limestone aggregate (Pittsburg aggregate) in this study produced ASR gel in the concrete microbar, corresponding to the composition of mountainite with [Ca/Si] = 1/3, [Ca]/[Na + K] = 1.0. It is therefore evident that a series of ASR gel found in ACR-affected concretes are quite similar in compositions to those of typical ASR, albeit their XRD data is not available due to scarcity in these specimens. Natural analogues most akin to ASR gel in composition, with the author's concrete samples examined, appear to be mountainite and, to a lesser extent, kanemite, makatite, gyrolite, okenite, etc. However, as discussed earlier, there is an as-yet undiscovered natural mineral, and there will be a fertile field of research on Na–K–Ca silicate hydrate minerals lying on the compositional trend lines presented in this paper.

5.5.3. Formation of ASR gel

Molar volume changes on ASR were calculated. For simplification, ASR gel was first represented by kanemite with its density, as in Eq. (9). The volume increase from quartz to ASR gel is very large, exceeding 100 vol.%. Wieker et al. [66] observed that the formation of kanemite from an intermediate product $\delta Na_2Si_2O_5$, one of natrosilite polytypes, by the reaction with SiO_2 and water accompanied substantial expansion, and that addition of $Ca(OH)_2$ did not hinder the expansion.

	Aggregate		Diffusion from cement paste				Aggregate
	$4SiO_2$	+	$2NaOH$	+	$6H_2O$	→	$Na_2O\cdot 4SiO_2\cdot 7H_2O$
	Quartz		Water-soluble				ASR gel (kanemite)
Molar volume:	240.36/2.65		(80.02/2.13)		(108.12/1.00)		428.45/1.93
	90.70		(37.57)		(108.12)		221.99

Volume change: (221.99 − 90.70) × 100/90.70 = + 144.8 vol.% (9)

The formation of ASR gel typically represented by mountainite is more realistic, incorporating Ca by substitution with Na and K, as Eq. (10), which produces about 100 vol.% of volume expansion. In this case, the Ca ion is the mobile component diffusing into the aggregate, hence the volume of portlandite should be neglected at the interior of the aggregate where reactive cryptocrystalline quartz is present. However, even when the solid volume of portlandite is taken into consideration, more than 30% volume increase is expected [535.48-(272.11 + 134.10)] × 100/(272.11 + 134.10) = + 31.8 vol.%. For convenience, multipled molar volumes of the original unit cell of kanemite and mountainite were used to look at oxide combinations. It is necessary to discount the calculated volume increases to some degree, because ASR gel is originally a mobile water-glass or *sol* with lower polymerization of silicate and hence does not stay in the original position of quartz, tending to migrate into porous texture within the aggregate before hardening into a solid gel by maturation and drying. ASR gel may further swell its volume by adsorbing water, whereas the crystalline form (rosette) in aged concretes loses its swelling nature.

section or even smaller, individual grains are overlain by others, particularly interfered by high-birefringent carbonates, obstructing free view in transmitted light. Thus, their appearance in the microscope will be some sum of optical properties, unsuitable for identification. Meanwhile, this inhibits point-counting as it is unclear which phase should be counted. To avoid overlapping images, thin section should be observed under reflected light, like cement clinker, or by SEM.

5.6.2. Why does fine aggregate expand less than coarse?

Conversion of ASR gel into non-expansive Mg-silicate gel in fine dolomitic aggregate is probably the reason why mortar bar produces smaller expansion than concretes. Dolomitic aggregate produces spots of brucite and secondary calcite through dedolomitization (Eq. (1)). Hydrotalcite rims are formed on the surface of dolomite by the reaction between brucite and aluminate ion in the pore water within cement paste without causing cracking (Eq. (5)). When this aggregate contains cryptocrystalline quartz as an impurity, Mg-silicate gel precipitates from

	Aggregate		Diffusion from cement paste				
	$12SiO_2$	+	2NaOH	+ 2KOH	+ $4Ca(OH)_2$	+	$3H_2O$
	Quartz		Water-soluble	Water-soluble	Portlandite		
Molar volume:	721.09/2.65		(80.02/2.13)	(112.21/2.04)	(296.36/2.21)		(54.05/1.00)
	272.11		(37.57)	(55.00)	(134.10)		(54.05)

$$\xrightarrow{\text{Aggregate}} Na_2O{\cdot}K_2O{\cdot}4CaO{\cdot}12SiO_2{\cdot}9H_2O = 3(1/3Na_2O{\cdot}1/3K_2O{\cdot}4/3CaO{\cdot}4SiO_2{\cdot}3H_2O) \quad (10)$$

ASR gel (mountainite)

Molar volume: 1263.73/2.36

535.48

Volume change: (535.48 – 272.11) ◊ 100/272.11 = + 96.8 vol.%

5.6. Correct identification of ACR

In general, typical ASR in concrete proceeds in the following sequence: 1) formation of reaction rims, 2) formation of gel-filled crack within aggregate, 3) extension of gel-filled crack into cement paste, 4) precipitation of ASR gel in air voids along cracks in cement paste [9,19–22,67]. This means that external concrete deterioration appears only when cracks from the aggregate extends into cement paste, and not by the formation of reaction rims. This principle holds well with ACR, but a slight difference in ACR is that the process of 1) involves dedolomitization and formation of carbonate halo, and the process of 4) is rarely noticeable due to consumption of ASR gel by the formation of Mg-silicate gel within reacted aggregate.

In classical petrographic investigations of ACR, the presence of reaction rims has been simply mistaken as evidence of concrete expansion, without observing the presence of cracks in the cement paste which should be the real evidence of deleterious expansion of concrete.

5.6.1. Are reaction products truly scarce?

Classical petrographic techniques are inadequate for identifying reaction products in ACR-affected concretes. This is because Mg-silicate gel that forms abundantly within dolomitic aggregate is too small to be identified by stereomicroscopy on lapped concrete (ASTM C457 [68]), and both cryptocrystalline quartz and cracks filled with ASR gel are smaller (often <5 μm) than what can be resolved using conventional cover-mounted 30 μm thin sections (ASTM C856 [69]). That is, the size of the dolomite crystals are chiefly 10–30 μm, comparable to the thickness of the thin section, but the size of the brucite and Mg-silicate gel that form within part of the dolomite crystals are smaller. In addition, the formation of Mg-silicate gel traps excess ASR gel before exuding into cement paste. If the grain size of the materials to be studied is on the same size order as the thickness of the reaction between brucite and ASR gel, forming spots and/or filling interstices (Eq. (7)). In dolomitic aggregate containing substantial argillaceous matter, a chlorite-like phase (clinochlore) or Mg–Ca–Al silicate gel with or without calcium is deposited without producing cracks, implying negligible expansion or none at all (Eq. (8)) [5].

In mortar bars made with fine dolomitic aggregate (<4 mm), both dedolomitization and ASR proceed faster and ASR gel is consumed by the above reactions, forming Mg-silicate gel throughout the entire cross-section of the fine aggregate, rarely forming expansion cracking. In contrast, when using coarser aggregate as in the concrete microbar (4–8 mm) and concrete prism (5–24 mm) tests, dedolomitization is limited to the surface of the coarse aggregate forming reaction rims, whereas ASR gel (sol) accumulates inside the aggregate as a pool or veins which remain unaltered, thus causing expansion pressure to produce expansion cracks that propagate from the aggregate into surrounding cement paste in concrete.

The above nature of ACR most probably stems from different surface/volume ratio of fine and coarse aggregate. That is, coarse aggregate has enough volume against the surface area that develops an outer zone, effectively armoring a secluded inner volume, thereby allowing reactions to evolve real ASR gel. In contrast, fine aggregate consists entirely of outer zone without such an inner volume, thus forming less expansive Mg-silicate gel by the interaction between ASR gel and brucite. This effect in ACR may be similar to the commonly observed dark internal rims represented by less expansive calcium silicate gel (pozzolanic CSH gel) in highly alkali-silica reactive particles.

5.6.3. Why are ASR inhibitors ineffective?

Durand [45] revealed that lithium compounds, including LiOH (actually $LiOH{\cdot}H_2O$), Li_2CO_3, LiF and $LiNO_3$, do not suppress deleterious expansion of some aggregates that cause ACR (Pittsburg aggregate) or late-expansive ASR (Canadian Sherbrooke schist and Potsdam sandstone, Canada) in the concrete prism. Tang et al. [70]

proposed using LiOH to distinguish ACR from ASR because this compound produces more expansion in the concrete bar made with ACR reactive aggregate. However, if this principle could be applied to the above Canadian cases, then, late-expansive ASR would have to be called ACR, not ASR. A common characteristic of these aggregates is a dense matrix around the reactive silica, obstructing Li in solution to proceed, or Li may be absorbed by interstitial clay minerals. Both prevent immobilization of ASR gel by conversion into non-expansive Li-silicate gel.

The ineffectiveness of slag and fly ash in suppressing the expansion of coarse aggregate may be due to two reasons: 1) a slower rate of pozzolanic reactions relative to ASR of fast reactive silica, and 2) the high alkalinity and pH maintained by the dedolomitization process. According to Japanese experience with the most reactive layer of the Pittsburg quarry (Pit-16, 1st lift), a 50 wt.% substitution of a fine-grained Japanese blast furnace slag (Blaine fineness 6050 cm^2/g) to cement, reduced expansion of AAR-5 concrete microbar (0.11%l/l vs. 0.16%l/l at 14 days) by almost a third, with reduced exudation of ASR gel. However, this may be a result of slower infiltration of the alkali buffer solution by the reduced permeability of cement-slag hydrates [47]. Sommer reported that the use of a super sulfated cement with 85 wt.% of Austrian slag with the Pittsburg aggregate prevented expansion in both the microbar test and the RILEM AAR-3 concrete bar test. Thus, finely ground slag may suppress expansion of so-called ACR if sufficient amounts are used [71].

In ACR with the Pittsburg aggregate, fly ash was not effective and only had a dilution effect of the cement used [72]. This is probably because the reaction of the fly ash used was slower than the cryptocrystalline quartz in the dolomitic aggregate.

5.6.4. Do weathering and leaching of concrete interfere with identification of ASR gel?

When field concretes available for study are limited, e.g. samples are only from the surficial portions (depth <5 cm) due to the difficulty in obtaining core specimens, special care is necessary in conducting petrographic examination and in interpreting results, because they are more or less affected by weathering and leaching. Specimens used in this study are of such kind. Secondary carbonation of cement paste due to the weathering and dedolomitization is very common in ACR-affected concrete, which often produces composite veins of ASR gel, carbonated ASR gel and calcium carbonate. Such an example in the concrete prism suggests that some changes had occurred during the long-term storage of test specimen, e.g. reactivity of the aggregate, formation of new cracks that introduce later ASR gel, and curing environment in the fog room. SEM observation coupled with EDS analysis of polished thin section clearly identifies the presence of ASR gel in these gel veins.

Leaching of alkali from ASR gel by water is important in field conditions because it develops in the concrete surface. This aspect has been examined by Davies and Oberholster by washing the accelerated mortar bar using water [73]. They indicated that calcium in the cement paste replaces alkalies by absorption or ion-exchange, converting the ASR gel and its crystalline form rosette into calcium silicate hydrates, some resembling a tobermorite gel. At that time, the compositional trend lines as shown in Fig. 9, or most typically those in [9], had not yet been known. However, it may be conceivable that if the leaching of alkali is so intense, the evolutionary trend of ASR gel will deviate from the main compositional line to a parallel line with lower [Ca/Si] and [Ca]/[Na + K] ratios, indicative of the *type II evolution* [9], as was notable in surface concrete from Cornwall (depth 2 cm). Quantitative SEM-EDS analysis is capable of distinguishing this type of alteration of ASR gel, contrary to the qualitative EDS analysis which is very likely to miss a small amount of alkali on the EDS spectra.

5.6.5. Does deicing salt affect identification of reaction products?

The recognition of external alkali added to concrete is important, because deicing salt (NaCl) applied in winter supplies sodium which may accelerate AAR. On the concrete wall of a lock in Quebec, exposed to the deicing salt, frost attack, and cracking due to ASR, concentration of Cl has been noticed within brucite that was formed on dolomite crystals in the dolomitic aggregate undergoing dedolomitization [4]. This suggests a possibility of further formation of water-soluble $MgCl_2$ which accelerates deterioration of concrete. In the field-deteriorated concretes of Gananoque and Cornwall in Ontario, the extent of chloride ingress into concrete was not as severe as the above case. However, local chloride content within CSH gel (Tables 5, 6), not including Friedel's salt, amounted to Cl 11 kg/m^3 in concretes [Table 5, thin section no.K0: Cl in CSH gel on alite pseudomorph (3.34 wt.% × 0.55/100), plus Cl in CSH gel on belite pseudomorph (2.81 wt.% × 0.25/100), multiplied by the unit weight of cement and water (300 kg/m^3 + 150 kg/m^3), gives 11.4 kg/m^3]. If the Cl is supplied entirely in halite (NaCl), this amount corresponds to about 7 kg/m^3 of Na. However, with the sample examined (depth 3 cm), such a high level of Na concentration was not detected by EDS analysis: alkali contents similarly calculated for the same CSH gel are Na_2O 0.2 kg/m^3 and K_2O 0.6 kg/m^3.

The observed imbalance between Cl and alkalies (Na + K) is attributable to the separate diffusion of cations and anions into deeper sections of concrete, followed by later leaching of water-soluble alkalies due possibly to the lack of Na-fixing materials, including ASR gel. Thus, effects of surface leaching of alkali appeared remarkable in the concrete with limited thickness (<5 cm) examined here. In a Japanese case with highway structures undergoing ASR under the influence of deicing salt, up to 0.9 kg/m^3 of Na_2Oeq, based on the 0–20 cm depth of concrete, has been known to be contributed by the deicing salt [67]. More precisely, chloride ion in these structures was always concentrated in the concrete surface (depth 0–2 cm), whereas, with many structures (about 40%), water-soluble alkalies were somewhat lower in the surface compared to the interior (depth 8–10 cm) because of leaching [74].

It follows from the above discussion that, if special care is taken in the petrographic examination and interpretation of results, concrete specimens from the structure surface are useable for the diagnosis of ACR and ASR, although there are associated limitations. The abundance of Cl and the lower [Ca]/[Si] ratios of CSH gel in these concretes are indicative of long-term weathering of concretes subjected to freezing and thawing, leaching, and ingress of deicing salt. Hence, to investigate ACR in detail and more completely free from the secondary alteration effects on concrete, it would be useful to examine freshly cored concrete samples made with the Pittsburg aggregate, e.g. the experimental concrete pavements in Kingston placed by MTO [47–49], based on the modern petrographic techniques adopted here (polarizing microscopy, SEM and quantitative SEM-EDS analysis).

5.7. Recommendations for correct analysis of ACR concrete

Straightforward application of common and conventional methods for concrete petrography is scarcely able to assess the specific properties and qualities required for correct analysis of ACR. Some methods are unsuitable and must be avoided, others may require adaptation of procedures, materials and/or instrumentation. A number of recommendations and precautions are given below.

5.7.1. Sample preparation artifacts

Artifacts that are encountered during the preparation of polished thin section are the main sources of misinterpretation (e.g. [75]), which include: removal of soft and/or fragile materials during cutting; mechanical cracking during grinding; strain-birefringence of resin caused by enforced grinding with a cup-wheel, appearing within empty cracks; dissolution and leaching of water-soluble materials during cutting, grinding polishing and cleaning; contamination by the lapping debris and abrasive powders; dehydration by heating and vacuum treatment; carbonation of cement paste on cut surfaces, etc.

Among these, cutting a concrete core to obtain a plane section is a harsh treatment with a large potential for introducing artifacts. Some of these problems may escape attention in optical microscopy, but are critical to quantitative SEM-EDS analysis or more sensitive analysis. Impregnation with a high-capillary epoxy before cutting to reinforce the cracked concrete, and cutting with a non-polar solvents as coolant helps preserve features essential for identification and reliable assessment [76]. When mounting a ground concrete chip to the slide glass, ultraviolet-hardening resin should be avoided, because it contains substantial amount of sulfur which causes serious contamination within cement paste and misleads SEM-EDS analysis. Old concrete specimens, that were sawed with water without impregnation and then exposed to the atmosphere for a long time, are prone to produce empty cracks due to the loss of soft reaction materials along cracks, even if careful treatment was later taken to produce polished thin sections. Hence, it is recommended to use methods in line with those described earlier.

5.7.2. Solvents for cleaning lubricant oil

How to clean the specimen without producing contamination and leaching is a more serious subject than previously considered. This aspect has been scarcely documented. From a practical view point, to what extent is allowable depends on the spec and the purpose of analysis, but non-polar solvents are generally recommended. Classical standard procedure by Insley and Fréchette [77] for preparing thin section of hydratable material, such as Portland cement clinker, consists of the use of kerosene for cutting and grinding, light spindle oil for later grinding, petroleum ether for rinsing oils, and alcohol for polishing. In preparing concrete thin section, removal of grinding oil is a critical process. Abbott and StJohn [78] used a combination of xylol for rinsing the ground slab, acetone for a short repeat, then ethanol for washing, and finally a cleaning compound (actually 1.1.2-trichloro-1.2.2 trifluoroethane) for soaking in ultrasonic bath. They noted that acetone may attack a thin surface layer of epoxy resin. These procedures were successful in obtaining unhydrated optical images of specimens both in transmitted and reflected lights.

Recent growing need of analyzing materials in thin section by EPMA tends to avoid polar solvents because they may produce leaching. For preparation of polished concrete slab for EPMA analysis, Japanese standard [79] recommends use of kerosene for grinding and 2-propanol (isopropanol) for rinsing, while polar solvents ethanol and acetone are less acceptable. However, 2-propanol is a polar solvent (alcohol) known to dissolve alkali hydroxides (NaOH, KOH), whereas acetone does not dissolve alkali-bearing compounds (NaOH, NaCl, KCl, Na_2CO_3). Acetone is marginally acceptable, according to the author's experience with SEM observation of polished thin section, because crack-filling halite within deteriorated field concrete survived ultrasonic cleaning soaked in acetone, while it did not in ethanol. Methanol was used by Durand and Berard [63] as a lubricant for polishing, but it does not seem to have caused a noticeable leaching of alkali from ASR gel, because their results of EDS analysis indicate a stoichiometry of okenite with substituting alkalies and Fe, as discussed earlier. Considering that polar solvents have a chance to contain water as an impurity to cause leaching, non-polar solvents with a good result (e.g. hexane) are recommended.

5.7.3. Storage in vacuum

In order to avoid artifacts due to secondary alteration, polished thin section of concrete without cover glass *must* be stored in a vacuum, as are those of Portland cement clinker. This is because unhydrated cement particles newly exposed to the atmosphere (e.g. alite, belite and CSH gel) *in situ* decompose into calcium carbonate and silica gel, or low-Ca CSH gel (<6 months), while alkali-rich ASR gel tends to be carbonated. Once such alterations occur, repolishing of thin section is no longer useful since original components were driven away as a new product, thereby giving a misleading result in EPMA analysis [19]. The oldest polished thin sections used in this study have been stored in vacuum desiccators since 1988, except in 1995 when the author moved, transporting each of them wrapped tightly within small polyethylene envelopes in a compact plastic pail, which gave a good result. However, those thin sections of NaOH-immersed bars frequently removed from the vacuum desiccator tend to produce deliquescence and carbonation around Na-rich phases, which causes a charge-up and needs re-polishing for additional SEM observation (6–10 years). In general, temporary vacuum processes (carbon coating, sample storage) have a limited influence on the hydrous phases (typically, partial dehydration of ettringite), whereas continuous evacuation and heat generated by the scanned electron beam during SEM-EDS analysis promote dehydration of CSH gel and ASR gel, thus producing drying shrinkage cracks on the coated carbon layer and a growing local charge-up phenomenon.

Storage of uncovered thin sections in a wood box in the atmosphere should be avoided, because white whiskers of calcium formate may form on them as a result of a reaction between calcium silicates and formalin-gas evaporated from the plywood. Such an alteration of Portland cement clinker in thin section, deposited intentionally in an old box, was noticed in the 1980s, which presented distinct XRD peaks (3.40 Å, 5.53 Å, 2.86 Å, 2.20 Å, 3.20 Å, 2.04 Å), whose natural form formicaite $Ca(HCO_2)_2$ was later described in Russia in 1999 [80]. To avoid weathering of the polished thin section, vacuum storage is recommended, but silicon grease should be avoided, as discussed later.

5.7.4. Binocular stereomicroscopy

Binocular microscopic observations of polished concrete core specimens have been used for preliminary examination of AAR under low magnification. Measurement of the *damage rating index of concrete* (DRI) developed by Grattan-Bellew and Danay [28], originally practiced by Sims et al. for quantitative polarizing microscopy [81], presents apparent difference between typical ASR and so-called ACR [49]. Although open cracks without gel have long been accepted as a characteristic of the ACR-affected concrete, this was also found to be the case with ASR of quartzite aggregate in a concrete dam in Canada [82], when the DRI data was reduced to original measurement data, reducing arbitrarily introduced multiplication factors. Gel-free cracks even dominate in dry sections of a concrete dam undergoing ASR due to limestone aggregate [28]. No relationship was seen between the measured amount of ASR gel and expansion in concrete prisms made with either the Spratt limestone or the Potsdam sandstone, whereas the expansion correlated well with crack density and crack length [83].

These observations suggest that ASR gel originally filling cracks in and around the aggregate was lost during the cutting and polishing of the concrete, leaving open cracks [82,83], particularly when the coarse aggregate was harder than the cement paste. It should be noted that water, when used as a lubricant during sample preparation (e.g. ASTM C457 [68]), may dissolve fragile materials formed through dedolomitization and carbonation. Because Mg-silicate gel formed abundantly within the dolomitic aggregate has so fine a texture, it is inevitably missed under the binocular microscope. Thus, binocular microscopy, although very useful, is not suitable for discussing the mechanisms of ACR in terms of reaction products.

5.7.5. Polarizing microscopy with polished thin section

Standard geological petrographic thin sections (thickness 20–30 μm, mostly 30 μm) are too thick for examining carbonate aggregates, chert aggregates, or even volcanic aggregates. According to the author's experience with RILEM committee activities on AAR and observation of thin sections of AAR-affected concretes exhibited at several ICAARs and related opportunities, large-area thin sections (>75 mm) have been used widely by concrete petrographers in Europe, North America and Oceania, where larger sizes tend to be appreciated (e.g. 150 mm by

200 mm) [78,84,85]. They are generally thick (30 μm, ASTM C856 [69]), with an unpolished surface, but finished with a rough ground surface mounted with a cover glass, presenting an ambiguous image under higher magnifications in transmitted light. Because of general technical difficulty, the larger the section, the harder the preparation of thinner thin section. Thus, large-area thin sections are not suitable for identifying such minute textures as crypto- to microcrystalline quartz in the aggregate, and fine cracks filled with ASR gel in concrete. This is probably one of the main reasons why definitive petrographic data have rarely been obtained for concrete specimens undergoing so-called ACR, as well as late-expansive ASR due to crypto- to microcrystalline quartz in argillaceous aggregates, formerly called *alkali-silicate reaction* in some continental regions of the world.

It has been common practice in Europe to impregnate large-area thin sections with resin containing a fluorescent dye for observation under ultraviolet illumination [86]. They are applied to visualize the cracking within reacted aggregate and cement paste for studying AAR [81], as well as the distribution of air voids and capillary pores in concrete for the estimation of air content and water/cement ratio [86]. However, these two purposes are generally incompatible, except for polished ultra-thin sections (thickness 10 μm) designed for the estimation of the water/cement ratio [87]. Because the color of the fluorescent dye in thin section (thickness 30 μm), as illustrated by all papers at the 13th ICAAR, is extremely deep, i.e. darker than the absorption by the pleochroism of rock-forming minerals, it generally obscures details in the transmitted light. There is no merit in using this technique in the study of the mineralogical aspects of ACR.

In contrast, ordinary-sized but thinner (20 mm by 30 mm, thickness 15 μm) polished thin sections not impregnated with fluorescent dye, used throughout this paper, gave a very sharp image under transmitted light (Figs. 1, 2, 4, 5). As stated earlier, ACR involves high-birefringent carbonate minerals intermixed with fine-grained reaction products. Hence, the thickness of thin section for petrographic examinations of ACR should be 10 μm or less. However, for electron-probe analysis, thin sections should have enough thickness to secure the quality, i.e. grade of polishing, retention of soft materials, production of uniform thickness, etc. Thus, having thin sections for both good observation and good analysis is often a trade-off, with optimum conditions being thickness 15 μm. Even though soft materials, cement hydrates and ASR gel, tend to be thinner compared with quartz, as indicated by their relief in reflected light.

Another merit of polished thin sections is that microcracks and porosities in both aggregate and cement paste can be ascertained under reflected light, without any duplication of the images within the thickness of thin sections. Because polished thin sections are useable for SEM observation with EPMA analysis to identify reaction products, they are most suitable for the study of ACR-affected concretes.

5.7.6. SEM on the fracture surface

Most previous studies in the world on ACR and ASR, using SEM, have conventionally been done on the fracture surfaces of concrete by concrete engineers. This was partly because, with easy sample preparation, it is a convenient method for viewing outer shapes of reaction products, particularly those facing the open spaces in concrete, crystal habits, surface textures including dissolution etch pits. However, concrete tends to fracture along weak points: at pre-existing cracks, and at the porous boundaries between the cement paste and aggregate, and hence *never* presents a random cross-section through the inhomogeneous textures of concrete. In the case of ACR in concrete, reaction products are generally fine-grained, so it is difficult to discriminate the textural relationships, including the boundaries between the aggregate and reaction products, and reaction products and host minerals.

In this study, however, SEM observation of the polished thin sections provided clear-cut images of fine-grained textures composed of reaction products (Figs. 1–5) [3–5]. It is therefore suggested that SEM observation of the fracture surface should be used as a supplemental method to polished thin sections.

5.7.7. Backscatter imaging in SEM

Backscatter mode SEM imaging (BSI) has been widely used by cement chemists, because images can show a wide variety of grey tones depending on the difference in the average atomic weight and packing density of materials [88], particularly the constituents in the cement clinker. Another merit of BSI is that this mode is free from the charge-up phenomenon that is encountered in the secondary electron imaging (SEI) used for common SEM observations, when dehydration and shrinkage cracking of cement paste proceed in a vacuum.

However, in carbonate rock reactions including ACR, some reaction products with different compositions (Mg-silicate gel, low-Ca ASR gel and reacting quartz) yield similar greyish images in BSI, almost indistinguishable from each other. For instance, average atomic weights (Z) of relevant materials calculated are: hydrotalcite (9.1), brucite (9.4), kanemite (9.9), Mg-silicate gel (as sepiolite:10.0), periclase (10.4), low-Ca ASR gel [as mountainite $(Na_{0.5},K_{0.5})_2O\cdot 2CaO\cdot 6SiO_2\cdot 4.5H_2O$: 10.8], quartz (10.8), dolomite (10.9), high-Ca ASR gel [as $0.25(Na_{0.5},K_{0.5})_2O\cdot 4.75CaO\cdot 6SiO_2\cdot 5H_2O$: 12.5], tobermorite ($5CaO\cdot 6SiO_2\cdot 5H_2O$: 12.6), calcite (12.6), CSH gel (as afwillite $3CaO\cdot 2SiO_2\cdot 3H_2O$: 13.1), alkali-aluminate [as $1/6(Na_{0.5},K_{0.5})_2O\cdot 17/6CaO\cdot Al_2O_3$: 14.3], aluminate (14.3), belite (14.6), alite (15.1), ferrite (as $4CaO\cdot Al_2O_3\cdot Fe_2O_3$: 16.7). Goldstein et al. [89] presented a regression curve in the cubic equation to estimate the backscatter electron coefficient (η). Within the above range of Z (9–17), η is almost linear and can be simply expressed as: $\eta = 0.0114 \times Z$. This means that the contrast in brightness between two phases depends primarily on the difference in Z. Since the composition of ASR gel and Mg-silicate gel varies considerably place to place, the brightness of the BSI images varies correspondingly, which obstructs correct identification of reaction products by this method.

Beside these, some of the fine textures of grain boundaries, including overgrowths, pseudomorphs, twinning boundaries, striations, zonal structures and reaction rims without any notable accompanying compositional or topographic changes, cannot be better discriminated by BSI than by SEI. This is because of lower spatial resolution of higher energy electrons (>50 eV) used in BSI. Thus, this technique should not be relied upon too heavily in the study of carbonate rock reactions. Instead, mapping of elements or quantitative spot analysis by the SEM-EDS, applied in this study, should rather be used to identify these materials on the polished thin section.

5.7.8. Quantitative EDS analysis

SEM-EDS has been used for quantitatively analyzing compositions of mineral phases and reaction products in concrete, although it is less sensitive and less quantitative than EMPA (WDS) [90]. Although EDS in early times could not detect sodium, it was used admirably by Bérubé and Fournier to characterize ASR gel products within reacted limestone aggregates in concrete, coupled with careful petrographic examination and XRD analysis [59]. Nowadays, SEM-EDS is a popular tool with improved detection capacity (range B-U), and non-geological users in concrete science perform analysis of minerals and rocks with this equipment.

However, apart from the inherent problems with SEM-EDS, there are several factors that make this method less reliable. In many cases, the setup of the equipment is not aimed for quantitative analysis: e.g. 1) an EDS detector is later attached to SEM, often without a device for stabilizing and reading electric current, occasionally without built-in software for *quantitative correction* (e.g. ZAF), thus limiting to qualitative usage; 2) standard materials for calibration are often ignored, because *standard-less analysis* without reading electron beam current tends to be welcomed by common users, resulting in semi-quantitative analysis

of elements (Ca, Si, Na, K, etc.) with fairly deviated atomic ratios from true values. In addition, 3) polished thin section essential for quantitative analysis is rarely used. Instead, polished slab or even fracture surface of concrete is used *without* performing petrographic examination under the polarizing microscope, because main users of SEM are not geologists. This makes it difficult to identify what part of the mineral or rock in the concrete sample was analyzed, as well as to check the quality of the analytical data obtained.

In an example of Japanese andesites, analyzed for bulk chemical composition by standard-less EDS analysis with BSI imaging of polished rock specimens [91], the obtained compositions were unrealistic for andesite, i.e. 11–12 wt.% of Na_2O, 18–24 wt.% of Al_2O_3, somewhat resembling a plagioclase (albite-oligoclase) but with SiO_2 10 wt.% lower. This inconsistency was due to less quantitative standard-less analysis, as well as small number of analyses (>5 points) applied to inhomogeneous textures of andesites. In order to obtain bulk chemical composition, it is generally desirable to homogenize the rock specimen by pulverizing or fusing it into glass beads, then subject to XRF, EPMA, or ICP analysis. Another example of interest is an andesite reported from Turkey, which was regarded as olivine basalt with reactive interstitial glass mentioned as basaltic glass [92], whereas SiO_2 content of this rock (59.6 wt.%) clearly indicates that this is andesite (i.e. SiO_2>52.5 wt.%). The *CIPW norm* calculated here from the bulk chemical composition indicates that this rock is oversaturated with silica, containing normative quartz (11.9 wt.%), augite (3.4 wt.%) and hypersthene (16.4 wt.%) and naturally lacks olivine, i.e. again suggestive of typical andesite. It is very likely that orthopyroxene (hypersthene) was mistaken for olivine in thin section that was too thick to characterize volcanic rocks, and that estimated [Mg]/[Mg + Fe] ratio of the phase identified as olivine was not of olivine but of orthopyroxene. With aggregates having a fine texture, such as volcanic rocks and carbonate rocks, misidentification of minerals and misinterpretation of analytical results may occur. But this could be avoided if fundamental knowledge of petrology is attended.

Despite the problems above mentioned, EDS is useable if it is at first set up as quantitative equipment towards use as EPMA (EDS), and a customized sample holder for the polished thin section set with standard materials is prepared. To secure a necessary precision, enough to discuss compositional trends of ASR gel in concretes on the [Ca/Si]–[Ca]/[Na + K] diagram, e.g. up to 10^3 of [Ca]/[Na + K] ratio with EDS (or, up to 10^4 with WDS), calibration of good standard is necessary. Optimal conditions for analysis (accelerating voltage, beam current, spot size, thickness of thin section, etc.) may differ by rock types and reaction products, but the condition used in this paper (around 0.1 nA, 15 kV) is generally recommended (0.8 nA in [9] should read 0.08 nA). Another important application of EDS is elemental mapping, which is useful in visualizing reaction rims, carbonate haloes, compositional zoning and gradient of elements within gel veins and minerals, and distribution of particular phases in concrete, such as Friedel's salt, and by far informative than the backscatter imaging in SEM. Because the mapping by EDS employs small electron beam currents (e.g. around 0.1 nA), it has an advantage in obtaining high spatial resolution with sharp image, suitable to avoid overlapping image with underlying minerals, and to distinguish very minute reaction products formed on fine-grained carbonate minerals (Mg-silicate gel, brucite, ASR gel, etc.) [3,4].

5.7.9. EPMA analysis

EPMA (WDS) is very sensitive and accurate – more than 10 times – compared with EDS, and capable of providing stable results. In the early 1980s Poole and Sotiropoulos [93] superbly used WDS coupled with thin section petrography in the study of ACR, to characterize the process of dedolomitization (reaction rim and carbonate halo) in dolostone aggregate from Bahrain in the laboratory concrete prism. Since then, application of WDS to ACR study has scarcely been documented, but accumulated experience and learning with this technique in ASR are applicable to ACR, if sufficient care is attended as discussed below.

WDS for spot analysis employs a strong electron beam current, commonly with 10 nA at 15 kV being about 100 times that of EDS, which causes local damage in volatile-bearing materials (ASR gel, cement hydrates, zeolites, carbonate minerals, etc.). Japanese standard of EPMA (WDS) analysis of concrete specimen [79] recommends 15 kV with a combination of 5–50 nA for quantitative spot analysis. The above upper limit is too strong for spot analysis, because sodium has a tendency to evaporate at high electron beam current (in particular, high current density [94]), and the aspect of whether the observed alkali content of ASR gel represents the true nature has been discussed [62]. Oberholster reported products of ASR (rosette) depleted in sodium in South African concretes [95], which was likely a result of leaching of sodium and replacement by calcium in cement paste in outdoor conditions, as demonstrated later by the leaching test [73]. It was natural however that Shayan and Lancucki [62] attributed the above low sodium content to a high electron beam current (25 nA) employed in WDS analysis, i.e. an analytical artifact, because count rate of X-ray from evaporable elements (Na,K,S,Cl) generally tends to decrease with time during measurement, particularly when current density increases [94]. Actually, in the present author's experience, a substantial loss of alkali in ASR gel was observed when the bombarding electron beam was aimed intentionally too long at a particular spot or zone, e.g. for several hours for multiple mappings or by multiple spot analyses for comparison: in these cases, the surface of epoxy resin covered with a carbon coating was baked into a pale tan color. However, such extreme situations are rarely met in routine analysis otherwise intended, so that commonly accepted measuring condition (e.g. 15 kV, 10 nA, probe size 2 μm, alkalies measured at first run for 5 s) can safely be used.

5.7.10. Quantitative elemental mapping by EPMA

Modern EPMA (WDS) provides digitalized mapping data of elements, which has been utilized since the 1990s in the study of cement hydration, pozzolanic reaction, sulfate attack, electrophoresic leaching of ions, and chloride penetration into concrete. Owing to recent development of high-speed computers with large memory for data-processing, digital mapping can 1) depict scatter diagrams of selected elements, 2) produce quantitative elemental maps with specified atomic ratios, applicable to automatic identification of mineral phases in some simplest cases, and 3) count pixel numbers with selected compositions very quickly, to represent volume ratios of individual phase in a similar way to point-counting. These greatly help non-geological users to identify and quantify mineral phases in the aggregate and in concrete. Japanese standard [79] recommends electron beam current 10–50 nA for mapping small specimen (<4 mm by 4 mm), and 50–300 nA for large polished concrete specimen (<80 mm by 80 mm). Since 2000, digital mapping by EPMA (WDS) has increasingly been utilized by users without extensive petrographic training to identify or quantify interstitial glass in volcanic aggregates, as well as to discriminate cement paste from aggregate.

In view of the present state-of-the-art phase analysis by quantitative elemental mapping, it is essential to check the accuracy of the output data. The presence on the scatter diagrams of compositions apparently intermediate with basalt [96,97] and andesites [98,99], e.g. among volcanic glass, plagioclase, pyroxene, and olivine or cristobalite, is an analytical artifact of both “thin-film effect” and “edge effect” enhanced by the strong *beam current* employed (15 kV, 50–100 nA, probe diameter 2 μm to minimum), which penetrates the target mineral with thickness of a few μm and diffuses into underlying or surrounding phases with edge contacts, thus acquiring mixed information from wide areas around the locus of analysis and eventually resulting in poor spatial resolution, even if the probe

diameter is set up to a small size. In order to reduce overlapping spectra from other phases, beam current and/or accelerating voltage should be lowered from the value specified in the standard [79]. The low resolution observed between cement paste and ISO standard quartz sand (size <2 mm) with mortar specimen presenting an entire mixture with continuous distribution [100,101] was another analytical artifact chiefly due to the selection of larger *probe diameter* and larger pixels that contain both paste and aggregate, in addition to the strong beam current that diffuses widely (15 kV, 100 nA, probe diameter 50 μm, pixel size 100 μm). On the other hand, the huge gaps noticeable in the composition in the quantitative elemental mapping, e.g. about 15 wt.% short of SiO_2 with plagioclase (oligoclase-labradorite) and glass in the volcanic aggregates on the SiO_2-Al_2O_3 diagram [96–99], and about 5 wt.% excess of CaO with quartz in the mortar specimen on the SiO_2-CaO diagram [100,101], are attributable to the software used, which cannot perform *quantitative corrections* (e.g. ZAF, Bence-Albee, Φρz) in converting count data of each pixel into concentrations, but simply presents K-values proportional to the counts obtained. This gap becomes large when the average atomic weight and absorption of the target mineral differ to some extent from those of the standard minerals. These are in contrast to the well-established quantitative spot analysis by WDS with probe diameters (e.g. 2 μm) similar to the above quantitative mapping, operated in association with polarizing/reflecting thin section microscopy to select the target interstitial glass before analysis, followed by the measurement of elements and ZAF correction for them [15,16]. Similar situation holds well with quantitative spot analyses of CSH gel by WDS [21] and EDS [9,20,22], which distinguish precursor alite and belite using small probe diameters and never confuse with aggregate particles.

It can be said that digital mapping by EPMA is a versatile technique for processing all pixel data into visually attractive outputs (color map, extracted phase map, scatter diagram, histogram, etc.). However, such convenience does *not* excuse the user to skip or substitute the petrographic examination, because there are plenty of sources for analytical artifacts related to the user's choice or omission which cannot be checked without petrography. Digital elemental mapping by EPMA will be useful in the study of ACR of carbonate aggregates, if operating conditions be adequately adjusted to very fine-grained reaction products in the dolomitic aggregates. Detailed petrographic examination, coupled with careful SEM observation of polished thin section under high magnification, is necessary to check the size of individual phase, textural relationships and extent of duplication of each phase before analysis, as well as to evaluate the quality of the output data and interpret the meaning, not to be misled by the analytical artifacts.

5.7.11. TOF-SIMS for mapping lithium

Ion-mapping with TOF-SIMS is useful in characterizing the presence of Li-compounds in concrete, because Li cannot be detected by EDS or WDS. Era et al. [102] visualized the distribution of Li ions injected into concrete as an ASR-inhibitor, and quantified the content in ASR gel within reacted andesite aggregate, coupled with quantitative measurement of other elements by SEM-EDS analysis. TOF-SIMS only detects surface information of the specimen (depth <1 nm) and is highly sensitive for alkali ions (ppm order), which is far below the detection limits of electron-probe analyses (EDS and WDS) that acquire much deeper information (depth 1–5 μm) through the carbon coating (depth 15 nm). Although this technique has been chiefly applied to anhydrous conductive materials such as metal under high-vacuum condition, it was revealed that even typical non-conductive material like a concrete with substantial gel-water can be analyzed, by using a polished thin section without coating a conductive carbon layer aided by the electron gun for charge neutralization.

TOF-SIMS even detects a traceable amount of contaminations on samples. In one case with a thin section of concrete containing NaCl, cleansed with acetone, a faint halo of Na ions was detected on the epoxy resin embedded within ASR gel vein (TOF-SIMS IV: Ga^+ 25 keV, 0.12 pA, vacuum 10^{-7}–10^{-6} Pa). This is suggestive of the leaching and/or adsorption of Na from the gel and/or surrounding cement paste. In other case, dimethyl siloxane from evaporated vacuum grease was detected over the surface of thin section that was temporary stored in one desiccator before analyses. However, these contaminations were only superficial (depth: Si <1 nm, Na >1 nm), as confirmed by the ion-spattering (Ar^+), and were not detected by elemental mapping and spot analysis by EDS, thus being practically negligible in quantitative EDS analysis.

It would be worthwhile to apply TOF-SIMS to measure stable isotope ratios of carbonate CO_3^{2-} in ACR-affected concrete. This might distinguish the difference in the origin of reservoirs of carbon (^{12}C,^{13}C) and oxygen (^{16}O,^{18}O) between 1) carbonate aggregate, 2) carbonate halo formed by dedolomitization, and 3) carbonate veins formed within cracks of aggregate and concrete by later carbonation. In the past, measurement of stable isotopes was performed with bulk rock samples in the study of dolomitization of limestone formation, digesting carbonate minerals by phosphoric acid with different reaction time, to estimate temperature of formation of calcite and dolomite [103]. It would be informative if such isotropic ratios can be determined separately for individual texture on the ion-map image. In order to do so, anion contamination that interferes the target ions (e.g. CH for ^{13}C) must be overcome to separate, which has every chance to adsorb on the specimen (e.g. oil, grease, resin, organic solvents, vapor, etc.) during sample preparation and analysis.

5.7.12. Etching and staining

Etching of reactions rims by concentrated HCl solution (6N–3N), on the carbonate aggregate in concrete has been applied to characterize the nature of carbonate rock reactions since the 1960s in the USA [104], as presently adopted by ASTM C856 [69]. This technique destroys reaction products for detailed SEM observation and SEM-EDS analysis, hence should not be used. Staining to assist in identification of particularly carbonates (e.g. Friedman [105], Warne [106]) is difficult as the required acid-etching may actually destruct the material beyond identification. For instance, alizarin Red S solution, which stains calcite red by dissolving its calcium by dilute HCl, has occasionally been used by the petrographer to distinguish calcite spars from dolomite in thin section. However, this method is not suitable for fine-grained dolomitic limestone with a micritic texture like the Pittsburg aggregate, which gives a dark image in the transmitted light, and harms reaction products brucite and secondary calcite. Thus neither etching nor staining should be used, particularly if chemical analyses of reaction products are intended. There is no merit to using destructive HCl etching to check reaction rims on the carbonate aggregate (ASTM C856) because they obscure the details of textures.

5.7.13. Summary

The above deliberation demonstrates that the specific properties and quantities of ACR reaction products and phenomena require sample and specimen preparation techniques, instrumentation and settings, as well as operator skills well beyond those adequate for “routine concrete petrography” or “classical” concrete petrography. The great diversity in published observations and data on ACR, and their broadly variable interpretation may very well be attributable to these special requirements left unattended. In turn, these may explain the long-standing dispute in interpretation of nature and mechanisms of ACR, the identification of potentially reactive aggregate and ACR reaction products in concrete. Modern analytical techniques being used for ASR are also useful for ACR but need special care to avoid analytical artifacts.

6. Conclusions

1. Detailed petrographic examinations with SEM-EDS analysis reconfirmed that so-called alkali-carbonate reaction (ACR) is a

combination of deleteriously expansive alkali-silica reaction of cryptocrystalline quartz, and harmless dedolomitization which produces brucite and carbonate haloes without any accompanying expansion cracks. Dolomitic aggregates did not develop expansion cracks in the embedding cement paste, unless ASR was involved.

2. ASR gel formed in the dolomitic aggregate is responsible for crack formation in concrete. This gel has a common nature to that in the typical ASR, which migrates within concrete, taking up calcium from the cement paste and leaching alkalies, approaching the compositions of CSH gel at a "convergent point" around [Ca/Si] = 1.3–1.8, [Ca]/[Na + K] = 100, where a chemical equilibrium is attained between ASR gel and CSH gel that had formed by the hydration of cement silicates alite and belite.

3. Well-known features of ACR, e.g. absence of reaction products, occurrence of reaction in low-alkali condition, large expansion with coarse aggregates, and ineffective behavior of ASR inhibitors, also apply to several types of alkali-silica reactive aggregates. All these behaviors can be explained in terms of ASR, and hence cannot be the criteria used to distinguish so-called ACR from ASR.

4. Phosphoric acid treatment extracted cryptocrystalline quartz from all the carbonate aggregates examined, including the Canadian Pittsburg aggregate and the Austrian carbonate aggregates. Although some type specimens of opal (Bohemia) survive this treatment, leaving 40 wt.% of residue, it was difficult in practice to identify opal in the silica residue from these carbonate aggregates, based solely on the SEM-EDS analysis for the morphology and chemical composition. However, consideration on diagenesis suggests that the presence of opal is very unlikely in these pre-Tertiary rocks all belonging to the quartz zone.

5. XRD analysis of field concretes revealed the presence of cement hydrates: ettringite, Friedel's salt and monocarboaluminate. Dedolomitization product brucite was not detected from the mortar bar, concrete microbar and field concrete using the Pittsburg aggregate, which is a result of reaction between brucite and ASR gel converting to Mg-silicate gel. Instead, a small XRD peak (7.2–7.3°2θ) suggestive of sepiolite was detected in both laboratory concrete microbar and field concrete containing the Pittsburg aggregate. Acid insoluble residue of this aggregate contained illite, chlorite, quartz, K-feldspar and albite.

6. SEM observation of polished thin section revealed that fine dolomitic aggregate tends to dedolomitize, and ASR gel that formed earlier converts to non-expansive Mg-silicate gel, consuming brucite, which explains why mortar bar produces smaller expansion than concrete microbar with larger aggregate. The size of Mg-silicate gel is very small, only visible in SEM, and the formation of Mg-silicate gel traps ASR gel before exuding into cement paste; that is why products of ACR are often said to be scarce in the conventional stereomicroscopy and polarizing microscopy.

7. Analysis by SEM-ESD indicated that Mg-silicate gel has a composition with [Mg/Si] about 4:6, suggestive of sepiolite $4MgO\cdot 6SiO_2\cdot 7H_2O$. This is supported by XRD analysis of concrete microbar and field concrete specimens. The formation of Mg-silicate gel through the reaction between ASR gel and brucite indicates a small decrease in molar volume, so that the presence of this material does not represent a proof of expansion in concrete.

8. SEM-ESD analysis revealed that the atomic ratio [Ca/Si] of ASR gel formed in the ACR-affected specimens, at which compositional lines intersect [Ca]/[Na + K] = 1.0 on the [Ca/Si]–[Ca]/[Na + K] diagram, ranged 1/2–1/6 wide across the mortar bar, RILEM concrete microbar and field-deteriorated concrete in Ontario. One of typical compositions obtained was $(Na,K)_2O\cdot 2CaO\cdot 6SiO_2\cdot nH_2O$, corresponding to those of mountainite $1.5\times[2(Ca,Na_2,K_2)O\cdot 4SiO_2\cdot 3H_2O]$ with substituting alkali ratio of CaO: $(Na,K)_2O = 2{:}1$. There is nothing different in this trend from typical ASR gel reported elsewhere.

9. Typical field concretes affected by so-called ACR in Gananoque and Cornwall, Ontario exhibited evidence of chloride ingress from deicing salt and weathering. The surface area of these concretes available for examination (<5 cm) were depleted in alkali relative to applied NaCl, but contained Cl-bearing CSH gel, Friedel's salt with compositions ranging from $3CaO(Al_{0.83}, Fe_{0.02}, Si_{0.16})_2O_3\cdot Ca[(Cl_2)_{0.69}, (SO_4)_{0.06}, (2OH)_{0.25}]\cdot nH_2O$ to $3CaO(Al_{0.82}, Fe_{0.05}, Si_{0.09})_2O_3\cdot Ca[(Cl_2)_{0.95}, (SO_4)_{0.05}]\cdot nH_2O$, monocarboaluminate, and, occasionally, NaCl-doped CSH gel. Careful petrographic examinations successfully distinguished hidden ASR from ACR, although these reactions were to some extent masked by superimposed chloride attack, leaching and carbonation of concrete.

10. ASR was most evident with the most expansive argillaceous dolomitic limestone aggregate in the Pittsburg quarry, Ontario. In contrast to late-expansive nature of ASR with chert and flint aggregates having a dense texture of cryptocrystalline quartz, rapid reaction of the cryptocrystalline quartz in the dolomitic aggregates is probably brought about by rapid progress of dedolomitization that exposes this fine-grained quartz to alkaline solution, thus enhancing ASR and subsequent chemical reactions to occur. The term alkali-carbonate reaction is misleading and should be placed in the museum of concrete history, like the former alkali-silicate reaction; both are forms of ASR.

11. Methods of conventional petrography, including HCl etching, binocular microscopy, large-area and fluorescent thin section microscopy, SEM observation of the fracture surface, less quantitative EDS analysis of reaction products on the fracture surface, and backscatter imaging in SEM, are unsuitable for the study of so-called alkali-carbonate reaction, and are responsible for the long-term missing of reaction products in concrete. Modern quantitative digital mapping of elements by EPMA (WDS) needs special care to avoid analytical artifacts (overlapping data, low spatial resolution compositional shifts) caused by strong beam current and software, and hence to check the data quality based on knowledge of petrology.

12. The combination of thin sectioning with epoxy impregnation, polarizing microscopy, SEM observation and SEM-EDS analysis using the same polished thin section in normal size without a cover glass (20 mm by 30 mm, thickness 15 μm) stored in the vacuum, is most suitable in approaching this problem.

Acknowledgements

The author is indebted to Prof. Hermann Sommer, formerly at the Research Institute of Austrian Cement Industry (VÖZFI), for providing the RILEM AAR-2 and AAR-5 test specimens with Austrian aggregates, as well as the fruitful discussion in developing the theory and interpretations of the mechanisms of ACR. He is grateful to Dr. Chris Rogers, formerly of Ontario Ministry of Transportation, Canada, for the ACR-affected concrete from Gananoque and the CSA concrete prism specimen. The most reactive Pittsburg aggregate was collected by Dr. Paddy Grattan-Bellew, formerly of National Research Council, Canada, and provided by Dr. Benoit Fournier, formerly of CANMET. Mr. Yoshinori Sarai of Kawasaki Geological Engineering Co.Ltd. (KGE) prepared the RILEM AAR-5 concrete microbar specimens for examination. This paper is an extended version of contribution to the proceedings of the 13th ICAAR in Trondheim, Norway. The author would like to greatly thank Dr. Maarten A.T.M. Broekmans at Norwegian Geological Survey for the insightful discussion. Polished thin sections from before 1994 were prepared while the author was working at Sumitomo Cement Co.Ltd.

References

[1] T. Katayama, A critical review of carbonate rock reactions — is their reactivity useful or harmful? in: A.B. Poole (Ed.), Proceedings of t + he 9th International Conference on Alkali-Aggregate Reaction in Concrete (ICAAR), London, UK, 1992, pp. 508–517.
[2] T. Katayama, M. Ochiai, H. Kondo, Alkali-reactivity of some Japanese carbonate rocks based on standard tests, in: A. Shayan (Ed.), Proceedings of the 10th International Conference on Alkali-Aggregate Reaction in Concrete (ICAAR), Melbourne, Australia, 1996, pp. 294–301.
[3] T. Katayama, How to identify carbonate rock reactions in concrete, Materials Characterization, vol. 53, nos.2–4 (2004), 85–104, Special Issue 29. Printed version of the Proceedings of the 9th Euroseminar on Microscopy Applied to Building Materials (EMABM), Trondheim, Norway (2003).
[4] T. Katayama, Modern petrography of carbonate aggregates in concrete — diagnosis of so-called alkali-carbonate reaction and alkali-silica reaction, in: B. Fournier (Ed.), Marc-André Bérubé Symposium on Alkali-Aggregate Reactivity in

Concrete, 8th CANMET/ACI International Conference on Recent Advances in Concrete Technology, Montreal, Canada, 2006, pp. 423–444, (supplementary paper, available as a separate copy).
[5] H. Sommer, T. Katayama, Screening carbonate aggregates for alkali-reactivity, Proceedings of the 16th International Conference on Building Materials (IBAUSIL), Weimar, Germany, 2006, 2-0461-0468.
[6] C.A. Rogers, General information on standard alkali-reactive aggregates from Ontario, Canada, Ministry of Transportation, Ontario, 1988 59 pp.
[7] H. Sommer, P. Grattan-Bellew, T. Katayama, M. Tang, Development and inter-laboratory trial of the RILEM AAR-5 rapid preliminary screening test for carbonate aggregates, in: M. Tang, M. Deng (Eds.), Proceedings of the 12th International Conference on Alkali-Aggregate Reaction in Concrete (ICAAR), Beijing, China, 2004, pp. 407–412.
[8] D. Lu, B. Fournier, P.E. Grattan-Bellew, Evaluation of the Chinese accelerated test for alkali-carbonate reaction, in: M. Tang, M. Deng (Eds.), Proceedings of the 12th International Conference on Alkali-Aggregate Reaction in Concrete (ICAAR), Beijing, China, 2004, pp. 386–392.
[9] T. Katayama, ASR gel in concrete subject to freeze–thaw cycles — comparison between laboratory and field concretes from Newfoundland, Canada, in: M.A.T.M. Broekmans, B.J. Wigum (Eds.), Proceedings of the 13th International Conference on Alkali-Aggregate Reaction in Concrete (ICAAR), Trondheim, Norway, 2008, pp. 174–183.
[10] H.F.W. Taylor, Cement chemistry2nd edition, Thomas Telford, London, UK, 1997 459 pp.
[11] Powder Diffraction File, Inorganic Phases, International Center for Diffraction Data (ICDD), Park Lane, Swarthmore, Pennsylvania, USA, 1991.
[12] JCAS I-31-1996, Quantitative measurement of quartz (phosphoric acid method), Japan Cement Association, Tokyo, 1996 11 pp. (in Japanese).
[13] N.A. Talvitie, Determination of quartz in the presence of silicates using phosphoric acid, Analytical Chemistry 23 (1951) 623–626.
[14] The Cement Association of Japan, Quantitative analysis of quartz by phosphoric acid method, report of Committee on Chemical Analysis, I-5 (1959), 1–16. (in Japanese).
[15] T. Katayama, D.A. StJohn, T. Futagawa, The petrographic comparison of some volcanic rocks from Japan and New Zealand-potential reactivity related to interstitial glass and silica minerals, in: K. Okada, S. Nishibayashi, M. Kawamura (Eds.), Proceedings of the 8th International Conference on Alkali-Aggregate Reaction in Concrete (ICAAR), Kyoto, Japan, 1989, pp. 537–542.
[16] T. Katayama, T.S. Helgason, H. Ólafsson, in: A. Shayan (Ed.), Proceedings of the 10th International Conference on Alkali-Aggregate Reaction in Concrete (ICAAR), Melbourne, Australia, 1996, pp. 377–384.
[17] JIS R 5202-1999, Methods for chemical analysis of Portland cements; Chapter 9, Analysis of acid insoluble residue by HCl, JIS Handbook of ready mixed concrete, Japanese Standards Association, Tokyo, 2002, p. 482, (in Japanese).
[18] Personal communication, C.A.Rogers (1992).
[19] T. Katayama, Petrographic diagnosis of alkali-aggregate reaction in concrete based on quantitative EPMA analysis, in: V.M. Malhotra (Ed.), Proceedings of the 4th CANMET/ACI/JCI International Conference on Recent Advances in Concrete Technology, Tokushima, Japan, 1998, pp. 539–560, SP-179.
[20] T. Katayama, T. Oshiro, Y. Sarai, K. Zaha, T. Yamato, Late-expansive ASR due to imported sand and local aggregates in Okinawa Island, southwestern Japan, in: M.A.T.M. Broekmans, B.J. Wigum (Eds.), Proceedings of the 13th International Conference on Alkali-Aggregate Reaction in Concrete (ICAAR), Trondheim, Norway, 2008, pp. 862–873.
[21] T. Katayama, D.J. Bragg, Alkali-aggregate reaction combined with freeze/thaw in Newfoundland, Canada — Petrography using EPMA, in: A. Shayan (Ed.), Proceedings of the 10th International Conference on Alkali-Aggregate Reaction in Concrete (ICAAR), Melbourne, Australia, 1996, pp. 243–250.
[22] T. Katayama, Y. Sarai, Y. Higashi, A. Honma, Late-expansive alkali-silica reaction in the Ohnyu and Furikusa headwork structures, central Japan, in: M. Tang, M. Deng (Eds.), Proceedings of the 12th International Conference on Alkali-Aggregate Reaction in Concrete (ICAAR), Beijing, China, 2004, pp. 1086–1094.
[23] S. Brunauer, D.L. Kantro, The hydration of tricalcium silicate and β-dicalcium silicate from 5°C to 50°C, in: H.F.W. Taylor (Ed.), The chemistry of cements, vol. 1, Academic Press, 1964, pp. 288–309.
[24] A. Iijima, R. Tada, Silica diagenesis of Neogene diatomameous and volcaniclastic sediments in northern Japan, Sedimentology 28 (1981) 185–200.
[25] W.J. French, An illustration of the main alkali reactive rock type in the United Kingdom: distributed at the post-conference field trip, 9th International Conference on Alkali-Aggregate Reaction in Concrete (ICAAR), London, UK, 27–31 July, 1992, 32 pp.
[26] J.G.M. Wood, Brief notes on structures and sites: distributed at the post-conference field trip, 9th International Conference on Alkali-Aggregate Reaction in Concrete (ICAAR), London, UK, 27–31 July, 1992, pp. 3–12, plus 3 maps.
[27] Victorian Field Trip Notes: distributed at the post conference field trip, 9th International Conference on Alkali-Aggregate Reaction in Concrete (ICAAR), Melbourne, Australia, 23–25 August (1996), Geological notes 3p., Inspection notes, 16 pp.
[28] P.E. Grattan-Bellew, A. Danay, Comparison of laboratory and field evaluation of alkali-silica reaction in large dams, Proceedings of the International Conference on Concrete Alkali-Aggregate Reactions in Hydroelectric Plants and Dams, Fredericton, Canada, 1992, 23 pp.
[29] Visit of structures affected by AAR in the Quebec City Area, 14 June (2000), 11th International Conference on Alkali-Aggregate Reaction in Concrete (ICAAR), Quebec, Canada, 20 pp.
[30] T. Katayama, Durability of aggregate, Report of materials committee, subcommittee on the revision of standard specifications for concrete structures, Japan Society of Civil Engineers, 1993, Chapter 3, 1–35. (in Japanese).
[31] T. Katayama, Petrography of alkali-aggregate reactions in concrete — reactive minerals and reaction products, in: S. Nishibayashi, M. Kawamura (Eds.), East Asia Alkali-Aggregate reaction Seminar, Supplementary papers, Tottori, Japan, 1997, pp. A45–A59.
[32] T.E. Stanton, Expansion of concrete through reaction between cement and aggregate, Proceedings. American Society of Civil Engineers 66 (1940) 1781–1811.
[33] D.O. Woolf, Reaction of aggregate with low-alkali cement, Public Roads 27 (3) (1952) 49–56.
[34] D. Hooton, C.A. Rogers, T. Ramlochan, The Kingston outdoor exposure site for ASR — after 14 years what have we learned? in: B. Fournier (Ed.), Marc-André Bérubé Symposium on Alkali-Aggregate Reactivity in Concrete, 8th CANMET/ACI International Conference on Recent Advances in Concrete Technology, Montreal, Canada, 2006, pp. 171–193.
[35] E.G. Swenson, J.E. Gilott, Characteristics of Kingston carbonate rock reaction, Highway Research Board Bulletin 275 (1960) 18–31.
[36] H.H. Newlon Jr., M. Ozol, W.C. Sherwood, Potentially reactive carbonate rocks progress report No.5—an evaluation of several methods for detecting alkali-carbonate reaction, 71-R33, Virginia Highway Research Council, 1972, 78 pp.
[37] I. Sims, The importance of petrography in the ASR assessment of aggregate and existing concretes, in: P.E. Grattan-Bellew (Ed.), Proceedings of the 7th International Conference on Alkali-Aggregate Reaction in Concrete (ICAAR), Ottawa, Canada (1986), Concrete Alkali-Aggregate Reactions, Noyes Publications, Park Ridge, New Jersey, USA, 1987, pp. 358–367.
[38] S. Sprung, Influence on the alkali-aggregate reaction in concrete, in: Ó.P. Halldórsson (Ed.), Proceedings of the 2nd International Conference on Alkali-Aggregate Reaction in Concrete (ICAAR), London, Reykjavik, Iceland, 1975, pp. 231–244.
[39] M.A.G. Duncan, E.G. Swenson, J.E. Gillott, M.R. Foran, Alkali-aggregate reaction in Nova Scotia, 1. Summary of a five-year study, Cement and Concrete Research 3 (1973) 55–69.
[40] A. Shayan, W.K. Green, F.G. Collins, Alkali-aggregate reaction in Australia, in: A. Shayan (Ed.), Proceedings of the 10th International Conference on Alkali-Aggregate Reaction in Concrete (ICAAR), Melbourne, Australia, 1996, pp. 85–92.
[41] A. Shayan, J.A. Ferguson, Reactive quartz gravel from eastern Victoria, in: A. Shayan (Ed.), Proceedings of the 10th International Conference on Alkali-Aggregate Reaction in Concrete (ICAAR), Melbourne, Australia, 1996, pp. 703–710.
[42] A. Blanchette, Evaluation of potential alkali reactivity of aggregates by means of accelerated test, Presented at Progress in Concrete, American Concrete Institute, Eastern Ontario-and Quebec Section, Meeting, Montreal, Canada, 1989, 18 pp. (in French).
[43] CSA A23.1-94-Appendix B: Alkali-aggregate reaction, concrete materials and methods of concrete construction, In: Methods of Test for Concrete, Canadian Standards Association (1994), Rexdale, Ontario, Canada, 112–135.
[44] L. Sanchez, S.C. Kuperman, P. Helene, Y. Kihara, Trials to correlate the accelerated mortar bar test, the standard and the accelerated concrete prism tests, in: M.A.T.M. Broekmans, B.J. Wigum (Eds.), Proceedings of the 13th International Conference on Alkali-Aggregate Reaction in Concrete (ICAAR), Trondheim, Norway, 2008, pp. 1154–1164.
[45] B. Durand, More results about the use of lithium salts and mineral admixtures to inhibit ASR in concrete, in: M.A. Bérubé, B. Fournier, B. Durand (Eds.), Proceedings of the 11th International Conference on Alkali-Aggregate Reaction in Concrete (ICAAR), Quebec, Canada, 2000, pp. 623–632.
[46] H. Imai, T. Yamasaki, H. Maekawa, T. Miyagawa, The deterioration by alkali-silica reaction of Hanshin Expressway concrete structures — investigation and repair, in: P.E. Grattan-Bellew (Ed.), Proceedings of the 7th International Conference on Alkali-Aggregate Reaction in Concrete (ICAAR), Ottawa, Canada (1986): Concrete Alkali-Aggregate Reactions, Noyes Publications, Park Ridge, New Jersey, USA, 1987, pp. 131–135.
[47] D.A. Williams, C. Rogers, Field trip guide to alkali-carbonate reactions in Kingston, Ontario, Ontario Ministry of Transportation, Report MI-145, 1991 26 pp.
[48] P. Gtattan-Bellew, J. Gillott, Three decades of studying the alkali reactivity of Canadian aggregates, in: J.M. Scanlon (Ed.), Katharine and Bryant Mather International Conference on Concrete Durability. Atlanta, Georgia, USA. ACI SP-100, 1987, pp. 1365–1384.
[49] P.E. Grattan-Bellew, J. Margeson, L.D. Mitchell, M. Den, Is ACR another variant of ASR? comparison of acid insoluble residues of alkali-silica and alkali-carbonate reactive limestones and its significance for the ASR/ACR debate, in: M.A.T.M. Broekmans, B.J. Wigum (Eds.), Proceedings of the 13th International Conference on Alkali-Aggregate Reaction in Concrete (ICAAR), Trondheim, Norway, 2008, pp. 706–716.
[50] J.E. Gillott, Petrology of dolomitic limestones, Kingston, Ontario, Canada, Geological Society of America Bulletin 74 (1963) 759–778.
[51] R. Tada, A. Iijima, in: A. Iijima, J.R. Hein, R. Siever (Eds.), Siliceous Deposits in the Pacific Region, Elsevier, 1983, pp. 229–245.
[52] T. Katayama, T. Futagawa, Diagenetic changes in potential alkali-aggregate reactivity of siliceous sedimentary rocks in Japan — a geological interpretation, in: K. Okada, S. Nishibayashi, M. Kawamura (Eds.), Proceedings of the 8th International Conference on Alkali-Aggregate Reaction in Concrete (ICAAR), Kyoto, Japan, 1989, pp. 525–530.
[53] S. Mizutani, Silica minerals in the early stage of diagenesis, Sedimentology 15 (1970) 419–436.
[54] M. Utada, Zeolitic zoning of the Neogene pyroclastic rocks in Japan, Scientific Papers of the College of General Education, University of Tokyo 21 (1971) 189–221.
[55] M. Utada, Wall rock alterations of ore deposits, in: T. Tatsumi (Ed.), Principles of modern ore geology, University of Tokyo Press, 1977, pp. 145–159, (in Japanese).
[56] K. Haga, M. Shibata, M. Hironaga, S. Tanaka, S. Nagasaki, Silicate anion structural change in calcium silicate hydrate gel on dissolution of hydrated cement, Journal of Nuclear Science and Technology 39 (2002) 540–547.

[57] A. Shayan, Expansion of AAR-affected concrete under aggressive marine conditions: a look at possible effects of complex interactions, in: B. Fournier (Ed.), Marc-André Bérubé Symposium on Alkali-Aggregate Reactivity in Concrete, 8th CANMET/ACI International Conference on Recent Advances in Concrete Technology, Montreal, Canada, 2006, pp. 369–389.
[58] L.D. Mitchell, P.E. Grattan-Bellew, J. Margeson, B. Fournier, The mechanistic differences between alkali silica and alkali carbonate reactions as studied by X-ray diffraction, in: M. Tang, M. Deng (Eds.), Proceedings of the 12th International Conference on Alkali-Aggregate Reaction in Concrete (ICAAR), Beijing, China, 2004, pp. 154–162.
[59] M.A. Bérubé, B. Fournier, The products of alkali-silica reaction in concrete: case study of Quebec region, Canadian Mineralogist 24 (1986) 271–288 (in French).
[60] W.F. Cole, C.J. Lancucki, M.J. Sandy, Products formed in an aged concrete, Cement and Concrete Research 11 (1981) 443–454.
[61] W.F. Cole, C.J. Lancucki, Products formed in an aged concrete, the occurrence of Okenite, Cement and Concrete Research 13 (1983) 611–618.
[62] A. Shayan, C.J. Lancucki, Alkali-aggregate reaction in the Causeway Bridge, Perth, western Australia, in: P.E. Grattan-Bellew (Ed.), Proceedings of the 7th International Conference on Alkali-Aggregate Reaction in Concrete (ICAAR), Ottawa, Canada (1986): Concrete Alkali-Aggregate Reactions, Noyes Publications, Park Ridge, New Jersey, USA, 1987, pp. 392–397.
[63] B. Durand, J. Berard, Use of gel composition as a criterion for diagnosis of alkali-aggregate reactivity in concrete containing siliceous limestone aggregate, Materials and Structures 20 (1987) 39–43.
[64] T. Katayama, T. Futagawa, Alkali-aggregate reaction in New Brunswick, eastern Canada — petrographic diagnosis of the deterioration, in: K. Okada, S. Nishibayashi, M. Kawamura (Eds.), Proceedings of the 8th International Conference on Alkali-Aggregate Reaction in Concrete (ICAAR), Kyoto, Japan, 1989, pp. 531–536.
[65] A.K. Mullick, G. Samuel, Reaction products of alkali-silica reaction — a microstructuural study, in: P.E. Grattan-Bellew (Ed.), Proceedings of the 7th International Conference on Alkali-Aggregate Reaction in Concrete (ICAAR), Ottawa, Canada (1986): Concrete Alkali-Aggregate Reactions, Noyes Publications, Park Ridge, New Jersey, USA, 1987, pp. 381–385.
[66] W. Wieker, C. Hübert, R. Ebert, Contribution to the chemical reaction mechanism of the alkali-aggregate reaction, in: A. Shayan (Ed.), Proceedings of the 10th International Conference on Alkali-Aggregate Reaction in Concrete (ICAAR), Melbourne, Australia, 1996, pp. 919–926.
[67] T. Katayama, M. Tagami, Y. Sarai, S. Izumi and T. Hira, Alkali-aggregate reaction under the influence of deicing salts in the Hokuriku district, Japan. Materials Characterization, Vol.53, nos.2–4 (2004), 105–122, Special Issue 29. Printed version of the Proceedings of the 9th Euroseminar on Microscopy Applied to Building Materials (EMABM), Trondheim, Norway (2003).
[68] ASTM C457-06, Standard test method for microscopic determination of parameters of air-void system in hardened concrete, Annual book of ASTM standards, West Conshoshocken, Pennsylvania, Concrete and aggregate, vol. 04.02, 2007, pp. 251–264.
[69] ASTM C856-04, Standard practice for petrographic examination of hardened concrete, Annual book of ASTM standards, West Conshoshocken, Pennsylvania, Concrete and aggregate, vol. 04.02, 2007, pp. 438–454.
[70] M. Tang, M. Deng, Z. Xu, Comparison between alkali-silica reaction and alkali-carbonate reaction, in: M.A. Bérubé, B. Fournier, B. Durand (Eds.), Proceedings of the 11th International Conference on Alkali-Aggregate Reaction in Concrete (ICAAR), Quebec, Canada, 2000, pp. 109–118.
[71] Personal communication, H. Sommer (2007).
[72] E.G. Swenson, A reactive aggregate undetected by ASTM tests, ASTM Bulletin TP239 (1957) 48–51.
[73] G. Davies, R.E. Oberholster, Alkali-silica reaction products and their development, Cement and Concrete Research 18 (1988) 621–635.
[74] M. Nomura, M. Aoyama, T. Hira, K. Torii, Case study on deterioration of concrete in road structures due to alkali-silica reaction (ASR) in Hokuriku Region and its evaluation methods, Concrete Research and Technology, Japan Concrete Institute 13 (3) (2002) 105–114 (in Japanese).
[75] D. Jana, Sample preparation techniques in petrographic examinations of construction materials: a state-of the art review, Proceedings of the 28th Conference on cement Microscopy, Denver, Colorado, USA, 2006, pp. 23–70.
[76] K. OKjellsen, A. Monsøy, K. Isachsen, R.J. Detwiler, Preparation of flat-polished specimens for SEM-backscattered electron imaging and X-ray micro-analysis — importance of epoxy impregnation, Cement and Concrete Research 22 (1992) 611–616.
[77] H. Insley, V.D. Fréchette, Microscopy of Ceramics and Cements, Academic Press, 1955 286 pp.
[78] J.H. Abbott, D.A. StJohn, The preparation of large area thin sections of concrete, Chemistry Division, Department of Scientific and Industrial Research, New Zealand, Report No.C.D.2311, 1981, 55 pp.
[79] JSCE-G574-2005, Area analysis method of elements distribution in concrete by using EPMA (tentative), Establishing a new JSCE standard to explore microscopic world of hardened concrete — mapping by EPMA and the leaching test for trace elements, Japan Society of Civil Engineers, Concrete Engineering Series, vol. 69, 2006, pp. 5–17, 106 pp. (in Japanese).
[80] N.V. Chukanov, S.V. Malinko, A.Y. Lisitsyn, V.T. Dubinchuk, O.V. Kuźmina, A.E. Zadov, Formicaite $Ca(HCO_2)_2$ — a new mineral, Memoirs of the All-Union Mineralogical Society Part 128 (2) (1999) 43–48 (in Russian).
[81] I. Sims, B. Hunt, B. Miglio, Quantifying microscopical examinations of concrete for alkali aggregate reactions (AAR) and other durability aspects, in: J. Holm, M. Geiker (Eds.), G.M.Idorn International Symposium on Concrete Durability. Toronto, Canada, 1992, pp. 267–288, ACI SP-131.
[82] P.E. Grattan-Bellew, L.D. Mitchell, Quantitative petrographic analysis of concrete — the damage rating index (DRI) method, a review, in: B. Fournier (Ed.), Marc-André Bérubé Symposium on Alkali-Aggregate Reactivity in Concrete, 8th CANMET/ACI International Conference on Recent Advances in Concrete Technology, Montreal, Canada, 2006, pp. 321–334.
[83] P. Rivard, B. Fournier, G. Ballivy, Quantitative assessment of concrete damage due to alkali-silica reaction (ASR) by petrographic analysis, in: M.A. Bérubé, B. Fournier, B. Durand (Eds.), Proceedings of the 11th International Conference on Alkali-Aggregate Reaction in Concrete (ICAAR), Quebec, Canada, 2000, pp. 889–898.
[84] D.A. StJohn, A.B. Pool and I. Sims, Concrete petrography, Arnold Publishers, London, 1998, 474 pp.
[85] D.A. StJohn, The use of large area thin sectioning in the petrographic examination of concrete, in: B. Erlin, D. Stark (Eds.), Petrography applied to concrete and concrete aggregates, American Society of Testing and Materials, Philadelphia, 1990, pp. 55–70, ASTM STP1061.
[86] Danish Standard DS 423.40 (2002): Concrete testing – hardened concrete – production of fluorescence-impregnated thin section (in Danish). 12 pp.
[87] B.F. Marshall, H.N. Walker, Evaluation and adaptation of the Dobrolubov and Romer method of microscopic examination of hardened concrete: methods and equipment used in preparing fluorescent ultrathin sections, Virginia Highway & Transportation Research Council, 78-R54, 1978, 23 pp.
[88] C. Famy, K.L. Scrivener, A.K. Crumbie, What causes differences of C–S–H gel gray levels in backscattered electron images? Cement and Concrete Research 32 (2002) 1465–1471.
[89] J.I. Goldstein, D.E. Newbury, P. Echlin, D.C. Joy, A.D. Romig Jr., C.E. Lyman, C. Fiori, E. Lifshin, Scanning electron microscopy and X-ray microanalysis, 2nd edition, Plenum Press, New York, 1992, 819 pp.
[90] P.J. Potts, J.F.W. Bowlers, S.J.B. Reed, M.R. Cave (Eds.), Microprobe techniques in the earth sciences, The Mineralogical Society Series, vol. 6, 1995, 419 pp.
[91] K. Torii, M. Nomura, A. Honda, Petrographic features of alkali-silica reactive aggregates in Hokuriku district and compatibility between various test methods determining alkali-silica reactivity of aggregate, Journal of Materials, Concrete Structures and Pavements, Japan Society of Civil Engineers, Part V vol. 64 (767) (2004) 185–197 (in Japanese).
[92] O. Çopuroğlu, Ö. Andiç-Çakir, M.A.T.M. Broekmans, R.A. Künel, Mineralogy, geochemistry and expansion testing of an alkali-reactive basalt from Western Anatoria, Turkey, in: I. Fernandes (Ed.), Proceedings of the 11th Euroseminar on Microscopy Applied to Building Materials, Elsevier, Porto, Portugal, 2007.
[93] A.B. Poole, P. Sotiropoulos, Reaction between dolomitic aggregate and alkali pore fluids in concrete, Quaternary Journal of Engineering Geology, London 13 (1980) 281–287.
[94] G.B. Morgan, D. London, Effect of current density on the electron microprobe analysis of alkali-aluminosilicate glasses, American Mineralogist 90 (2005) 1131–1138.
[95] R.E. Oberholster, Alkali reactivity of siliceous rock aggregates: diagnosis of the reaction, testing of cement and aggregate and prescription of preventive measures, in: G.M. Idorn (Ed.), Proceedings of the 6th International Conference on Alkali-Aggregate Reaction in Concrete (ICAAR), Copenhagen, Denmark, 1983, pp. 419–433.
[96] T. Fujii, K. Yamada, A. Imai, An Approach to evaluating alkali-silica reactivity from a petrological view point, Proceedings of Annual Conference of the Japan Cement Assotiation 59 (2005) 126–127 (in Japanese).
[97] D. Mori, Phase analysis, Establishing a new JSCE standard to explore microscopic world of hardened concrete — mapping by EPMA and the leaching test for trace elements, Japan Society of Civil Engineers, Concrete Engineering Series, vol. 69, 2006, pp. 99–100, (in Japanese).
[98] Y. Kawabata, K. Yamada, H. Matsushita, Petrological study on evaluation of alkali-silica reactivity and expansion analysis of andesite, Proceedings of Japan Society of Civil Engineers, Part E 63 (2007) 689–703 (in Japanese).
[99] Y. Kawabata, K. Yamada, H. Matsushita, Alkali-silica reactivity and expansion of mortar incorporating glassy andesite in alkaline solution, in: M.A.T.M. Broekmans, B.J. Wigum (Eds.), Proceedings of the 13th International Conference on Alkali-Aggregate Reaction in Concrete (ICAAR), Trondheim, Norway, 2008, pp. 874–883.
[100] D. Mori, K. Yamada, Y. Hosokawa, M. Yamamoto, Applications of electron probe microanalyzer for measurement of Cl concentration profile in concrete, Journal of Advanced Concrete Technology 4 (2006) 369–383.
[101] K. Yamamoto, How to discriminate cement paste fraction and examples of estimating chloride concentrations, Establishing a New JSCE Standard to Explore Microscopic World of Hardened Concrete — Mapping by EPMA and the Leaching Test for Trace Elements, Japan Society of Civil Engineers, Concrete Engineering Series, vol. 69, 2006, pp. 64–70, (in Japanese).
[102] K. Era, T. Mihara, T. Yamamoto, T. Miyagawa, Study on Controlling Effect of Lithium Ion on ASR Expansion, Journal of the Society of Materials Science, Japan vol. 58 (8) (2009) 697–702 (in Japanese).
[103] R. Matsumoto, A. Iijima, T. Katayama, Mixed-water and hydrothermal dolomitization of the Pliocene Shirahama Limestone, Izu Peninsula, central Japan, Sedimentology 35 (1988) 979–998.
[104] K. Mather, A.D. Buck, W.I. Luke, Alkali-silica and alkali-carbonate reactivity of some aggregates from South Dakota, Kansas, and Missouri. Symposium on Alkali-Carbonate Rock Reactions, Highway Research Board, No.45, 1964, pp. 72–109.
[105] G.M. Friedman, Identification of carbonate minerals by staining methods, Journal of Sedimentary Petrology 29 (1959) 87–97.
[106] S. Warne, A quick field or laboratory staining scheme for the differentiation of major carbonate minerals, Journal of Sedimentary Petrology 32 (1962) 29–38.